Daniel Isong Otu Egbe

Geochemical Modeling of Low Salinity Waterflooding and Surfactant Flooding in Heterogeneous Low-Permeability Carbonate Cores

Master's thesis in Petroleum Engineering
Supervisor: Dr. Ashkan Jahanbani Ghahfarokhi
June 2019

Master's thesis

◘ NTNU
Norwegian University of
Science and Technology

Daniel Isong Otu Egbe

Geochemical Modeling of Low Salinity Waterflooding and Surfactant Flooding in Heterogeneous Low-Permeability Carbonate Cores

NTNU

Norwegian University of
Science and Technology

Abstract

World energy consumption is projected to increase significantly by 2040 with fossil fuels remaining the main source of energy. About 60% and 40% of the world's oil and gas reserves, respectively, are found in carbonate reservoirs, however, on average only 30% of each is recovered during primary recovery. In addition, most of the large discoveries are in decline and newer discoveries are mostly smaller or satellite fields. The growing demand for energy and the lack of many new large discoveries underscores the need for maximising oil recovery from already mature fields. The low primary recovery also offers a huge potential for improved oil recovery (IOR).

Waterflooding has been the most widely used technique to improve recovery from oil reservoirs worldwide through pressure support. Recently, there has been a significant growth in interest in the chemistry and ionic composition of the injected water. Low salinity waterflooding (LSWF) is a relatively recent enhanced oil recovery (EOR) technique that has the ability to alter the crude oil/brine/rock (COBR) interactions and improve oil recovery in both clastics and carbonates. Combining low salinity waterflooding with other EOR methods such as surfactant flooding in a hybrid EOR process could also be beneficial for surfactants. In a low salinity environment, the phase behavior of surfactants is improved; making them more effective at mobilizing oil trapped by capillary forces.

This thesis models low salinity water and low salinity surfactant coreflood experiments based on the geochemical interactions that occur during the processes. An equation-of-state (EOS), compositional simulator GEM™ by CMG was used to perform numerical simulations. A history match of two coreflood experiments done on heterogeneous low-permeability carbonate cores has been performed, after which sensitivity analysis was conducted on many key parameters to investigate their effects on the results. A detailed analysis of the results has been done for all the modeling cases.

Wettability alteration was assumed to be the mechanism responsible for the increase in oil recovery during low salinity waterflooding, such that relative permeability interpolation based on the ion exchange equivalent fraction of magnesium ion was used for the history matching. The ability of surfactants to mobilize capillary trapped oil during surfactant flooding was modeled using capillary number-based relative permeability interpolation. Interpolations based on both the ion exchange equivalent fraction of magnesium and the capillary number were used to model the hybrid low salinity surfactant process. A successful history match of experimental oil recovery and pressure drop was obtained for low salinity waterflooding. The final oil recovery from the low salinity surfactant case was also found to match the experimental results. However, the desired effect was not observed for the individual processes in the case of low salinity surfactant flooding because the simulator currently lacks the ability to interpolate between rock regions. Nevertheless, the combined process resulted in a higher oil recovery than the individual processes.

A sensitivity study on the timing of low salinity water injection revealed that the earlier the onset of low salinity waterflooding, the higher the oil recovery. Significantly higher oil recovery was observed for secondary mode low salinity waterflooding compared to seawater flooding. A sensitivity study also revealed that the injection rate is a crucial

parameter in optimizing oil recovery. The injection temperature was found to have a notable effect on intra-aqueous, mineral reactions and pH, and should therefore be an integral part of all modeling and simulation studies. The use of different mechanistic modeling methods has been investigated, and it revealed that the modeling method used should be based on reservoir properties and experimental results. A decrease in the oil-water interfacial tension (IFT) resulted in a significant increase in oil recovery during surfactant flooding. Finally, a decrease in the adsorption revealed that the lower the surfactant adsorption, the earlier the effect of surfactant on oil recovery and pressure drop is observed.

Acknowledgements

First and foremost, I would like to thank the Almighty God for giving me the strength, wisdom and grace required to complete this thesis. Without Him, none of this would have been possible.

To my supervisor, Dr. Ashkan Jahanbani Ghahfarokhi, I express my deepest gratitude for his support and guidance throughout this project. It was a great experience working with him. I am truly grateful to him for the time and effort dedicated in overcoming the challenges faced while working on this thesis.

I would also like to thank the customer support at Computer Modelling Group Ltd. (CMG) for their constant assistance whenever I was faced with technical software issues.

I also extend my sincere gratitude to all my professors, fellow students and colleagues who made my years at the department of geosciences and petroleum, at NTNU memorable. Special thanks go out to Cleide Vieira, Alberto Bila, Adul Saboor Khan, and Salem Akarri, for all the good times.

Lastly, I express my highest of thanks to my family and friends, although no amount of thanks would be an equivalent appreciation for their unconditional love and support. I am forever indebted to my mum, Egbe Diana Eyere; who despite all the challenges, made sure that I got the best of everything.

Dedication

This thesis is dedicated to my beloved family; my mum, Egbe Diana Eyere, my brothers: Desmund Eyongkongho Egbe, Jovic Egbe, Konrad Egbe and Clovis Egbe, and my sisters: Ayuk Martha Nchong, Vydaline Egbe and Andreen Egbe. Your love and support made all of this possible

Table of Contents

List of Tables

List of Figures

Nomenclature

List of Abbreviations

Ca^{2+}	Calcium Ion
CH_3COO^-	Carboxylate Ion
Mg^{2+}	Magnesium Ion
SO_4^{2-}	Sulfate Ion
ADS	Adsorption
AN	Acid Number
ASP	Alkali-Surfactant-Polymer
BN	Base Number
BT	Breakthrough Time
CDC	Capillary Desaturation Curve
CEC	Cation Exchange Capacity
CMC	Critical Micelle Concentration
CMG	Computer Modelling Group
CO_2	Carbon Dioxide
COBR	Crude Oil/Brine/Rock
Conc	Concentration
EDL	Electrical Double Layer
EOR	Enhanced Oil Recovery
EOS	Equation of State
Eqv	Equivalent
Exch	Exchange
FW	Formation Water
HLB	Hydrophile-Lipophile Balance
IFT	Interfacial Tension
IOR	Improved Oil Recovery
KOH	Potassium Hydroxide
LPG	Liquefied Petroleum Gas
LS1	Low Salinity Water 1
LS2	Low Salinity Water 2
LS3	Low salinity water 3

LSE	Low Salinity Effect
LSS	Low Salinity Surfactant
LSWF	Low Salinity Waterflooding
MIE	Multicomponent Ionic Exchange
NaCl	Sodium Chloride
NaOH	Sodium Hydroxide
NGL	Natural Gas Liquids
OB	Oil/Brine
OOIP	Original Oil In Place
PDIs	Potential Determining Ions
PPM	Parts Per Million
PR	Peng-Robinson
PV	Pore Volume
PZC	Point of Zero Charge
RB	Rock/Brine
RF	Recovery Factor
SEM	Scanning Electron Microscope
SW	Seawater
SWCTT	Single Well Chemical Tracer Test
TDS	Total Dissolved Solids
US	United States
USBM	United States Bureau of Mines
USS	Unsteady State
VSWW	Very Strongly Water Wet
WAG	Water Alternating Gas

Subscripts / Superscripts

a, aq	Aqueous
b	Bulk
eff	Effective
eq	Equilibrium
g	Gas
h	Hydrocarbon
HS	High Salinity
i, l	Component (phase)

ineff	Ineffective
ir	Irreducible
LS	Low Salinity
m, mn	Mineral
max	Maximum
n	Normalized
nw	Non-wetting Phase
o	Oil
p	Pore
r	Residual
s	Solid
tot	Total
w	Water
w	Wetting Phase

List of Symbols

γ	Activity Coefficient
γ	Surface Tension
$\hat{A}$	Reactive Surface Area
κ	Total Interfacial Curvature
$\mathring{a}$	Ion Size
μ	Viscosity
ω	Moles of Adsorbed Component
ϕ	Porosity
ρ	Density
σ	Interfacial Tension
τ	Shear Stress
θ	Contact Angle
ζ	Ion Exchange Equivalent Fraction
A	Area
a	Activity
B	Langmuir Isotherm Parameter
c_{ϕ}	Rock Compressibility
E_a	Activation Energy
F	Gibbs Free Energy

I	Ionic Strength
I_{AH}	Amott-Harvey Index
K	Absolute Permeability
k	Effective Permeability
k	Reaction Rate Constant
K'	Selectivity Coefficient
k_r	Relative Permeability
K_{eq}	Equilibrium Constant
m	Molality
N	Number of Moles
n	Corey Exponent
N_c	Capillary Number
N_{cc}	Critical Capillary Number
N_T	Trapping Number
P, p	Pressure
P_c	Capillary Pressure
Q	Volumetric Flow Rate
q	Darcy Velocity
Q_α	Activity Product
R	Number of Reactions
R, r	Radius of Curvature
S	Saturation
T	Temperature
T_0	Reference Temperature
V	Volume
v	Stoichiometry Coefficient
v	Velocity
W	USBM Index
z	Valence Number

GEM Keywords

ADSORBTMAXA   Maximum Moles of Adsorbed Component

ADSTABA   Adsoprtion Table (surfactant mole fraction and corresponding adsorption)

AQIONS-IEX   Aqueous Ion Exchange Species

CEC-IEX   Cation Exchange Capacity

DTMAX   Maximum Time Step

DTMIN   Minimum Time Step

EQVFRIEX   Ion Exchange Equivalent Fraction

IFTTABLE   Interfacial Tension Table (surfactant mole fraction and corresponding IFT)

INTCOMP   Interpolation Component

KRINTRP   Interpolation Set Number

REACTION-IEX   Ion Exchange Reactions

RPT   Set of Relative Permeability Curves

SCOEFF-IEX   Selectivity Coefficients for Ion Exchange Reactions

SLT   Liquid-Gas Relative Permeability Table

SWT   Water-Oil Relative Permeability Table

1. Introduction

Carbonate reservoirs are estimated to hold about 60% and 40% of the world's oil and gas reserves, respectively[71]. Despite the significant amount of oil and gas in carbonates reservoirs, they have been very challenging to understand and develop due to their heterogeneous nature that results from the combination of depositional geometry and diagenesis. This, coupled with the fact that about 90% of carbonate rocks are either neutral or oil-wet has resulted in much lower primary recoveries (average of 30%) compared to sandstones[1,82].

The US Energy Information Administration projects a significant increase in the world energy consumption (about 28%) by 2040, with fossil fuels still leading the way (see fig. 1.1)[87]. Waterflooding has been and is currently the most widely used method to increase production from oil reservoirs worldwide because it is economical, easily accessible and reliable[27,30]. It is a secondary recovery mechanism that helps to increase and maintain reservoir pressure. Waterflooding has had significant effects in oil fields such as the Ekofisk field in the North Sea and the Wilmington field in California, US, where voidage replacement (water replacing oil in the pore space) has helped to mitigate further surface subsidence that resulted from significant compaction due to high pressure drop during primary production.
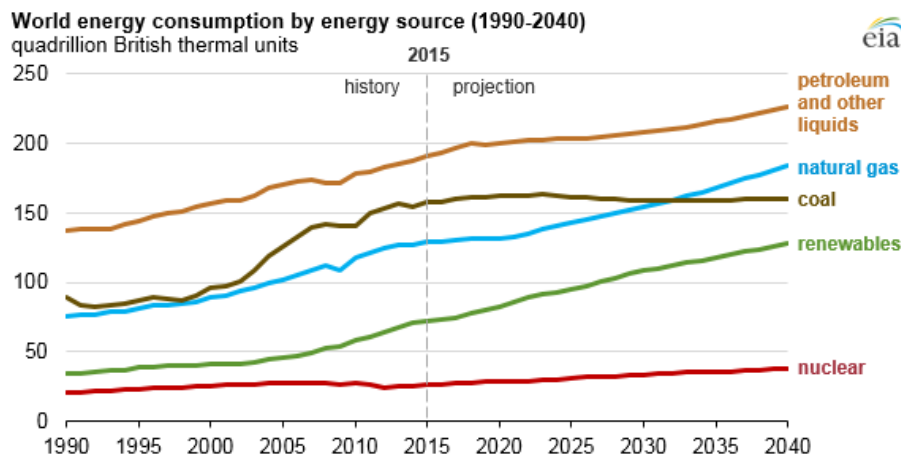
Figure 1.1: Projected world energy consumption[87]

The history of waterflooding dates back to the 1920s, with the first reported field implementation in the Bradford oil field in Pennsylvania, US[27]. Since then, several large scale water injection projects have been implemented in many oil reservoirs in many locations around world, ranging from the North Sea to the Arctic regions. The injection water used in most waterflooding projects especially in offshore oil fields is selected based on the compatibility of the injection water with the reservoir brine (formation water) and economic considerations[30]. Despite the increase in waterflooding projects, more than half of the total resources of the fields in the Norwegian Continental Shelf (NCS) and worldwide are still left behind after the application of secondary recovery mechanisms[65]. Additionally, most of the large discoveries are in decline and newer discoveries are mostly smaller or satellite fields.

1

Initially, less attention was dedicated to the effects of the chemistry and ionic composition of injected brine. However, it has recently been reported by many researchers that modifying the chemistry of the injected brine either by changing the ionic composition or the salinity by dilution can lead to significant increases in the oil recovery both in sandstones and carbonates, compared to conventional high salinity waterflooding. This is known as low salinity waterflooding (LSWF) or smart waterflooding. The concept of low salinity waterflooding was first reported by Bernard in the late 1960s, where he compared the recovery from flooding natural and synthetic cores containing hydratable clays with brine and fresh water[19]. A higher oil recovery was observed when the cores were flooded with fresh water compared with brine.

In the 1990s, a lot of effort was dedicated to understanding the interactions and effects of brine composition on wettability and oil recovery, by Morrow and his colleagues at the University of Wyoming[59,60]. Subsequently, many laboratory and field implementations have confirmed the potential of low salinity waterflooding to increase oil recovery. Other reasons for the recent increase in research dedicated to low salinity waterflooding include: lower cost, it is relatively simpler compared to other recovery mechanisms such as chemical flooding, and can be implemented either in secondary or tertiary mode or combined with other enhanced oil recovery (EOR) mechanisms such as surfactant or polymer flooding.

Despite the growing interest in LSWF, the principal mechanism(s) responsible for the increase in oil recovery is still not fully understood, making it difficult to optimize the process. Furthermore, considerably less research on the process has been done on carbonates compared to sandstones. Some studies[8,34,51,79] have also revealed the potential of combining low salinity water and surfactants (LSS) in a hybrid EOR process. The effectiveness of surfactants in increasing oil recovery is optimized in low salinity environments[8,79].

1.1. Motivation

The growing demand for petroleum and other liquids and the low primary recovery from carbonates offers a huge potential for EOR. Although the petroleum industry in Norway was somewhat pioneered by the chalk (carbonate) fields in the North Sea, more focus has been placed on sandstone fields in the last few decades. In late 2018, the FORCE Carbonate and Chalk Reservoirs network was formed, with the aim of facilitating the continued advancements, for the sustainable development of Norwegian carbonate reservoirs; signifying growing interests in carbonate reservoirs[66]. This, the lack of understanding on the main mechanism(s), and the few research in carbonates prompted work on this topic; to provide more insights into the geochemical modeling of LSWF and LSS in carbonates.

1.2. Scope of Work

This thesis begins by conducting a comprehensive literature review on the relevant processes. An in-depth knowledge of low salinity waterflooding and surfactant flooding, and their associated mechanisms associated with increase in oil recovery in carbonates is

obtained, and provides the foundation for the work done in the thesis. Afterwards, insights into how the geochemical interactions that occur during the processes can be modeled is acquired, as well as other relevant knowledge on the physics of the reservoir simulator.

Two coreflood models are then built to model the geochemical interactions occurring during LSWF, and history match results (oil recovery and pressure drop) from experiments done on heterogeneous low-permeability carbonate cores. During the modeling process, sensitivity is done on the grid size (number of gridblocks) and the time steps (maximum and minimum) to optimize the run time while also ensuring that the physics of the process is properly captured. After history matching the experimental results for the two corefloods, they are considered as the base cases.

Some modifications are done to the base cases in order to evaluate the potential of combining seawater and surfactant flooding on oil recovery from the cores. Afterwards, the two processes are combined to model the combination of seawater, low salinity water and surfactant flooding for one of the cores, similar to what was done in the experiments. Finally, a sensitivity analysis is done to investigate the effects of key parameters such as the timing of low salinity waterflooding, injection temperature, injection rate, mechanistic modeling method, interfacial tension and adsorption on the results obtained.

This thesis is divided into eight chapters. Chapter 2 provides a theoretical background of some relevant petrophysical and interfacial properties such as porosity, absolute permeability, wettability, interfacial tension, capillary pressure, and effective and relative permeability, as well as processes such as drainage and imbibition that are relevant to fluid migration. In chapter 3, the concept of enhanced oil recovery is discussed alongside some literature review on laboratory and field studies of LSWF, surfactant flooding and low salinity surfactant (LSS). A detailed description of the numerical modeling approach and considerations is provided in chapter 4. The results obtained from the modeling studies are provided and discussed in chapter 5. Chapter 6 describes the results of the sensitivity analysis, and the conclusions are provided in chapter 7. The thesis is completed by providing some recommendations for future work in chapter 8.

2. Theoretical Background

The initial contents, reserves, production potential and behavior of a hydrocarbon reservoir is controlled by four fundamental properties. They include: rock properties such as porosity, permeability, compressibility, which depend on the packing and arrangements of the solid grain/particle, reservoir fluid properties and the composition of the phases, interfacial properties such as wettability, capillary pressure, relative permeability and phase saturation, and the initial hydrocarbon fluid migration into the reservoir and the resulting thermodynamics associated with the mixture. In this chapter, some of the aforementioned fundamental rock and fluid properties are discussed.

2.1. Porosity

Porosity, ϕ is one of the essential features of every reservoir rock and can be defined as the fraction of the total rock that is void space. The porosity of a reservoir rock can be as a result of the depositional process; known as primary porosity or due to post-depositional processes that alter the rock; referred to as secondary porosity[38,67]. It can also be generated due to tectonic stress that causes the development of fractures, and this type of porosity is known as fracture porosity. In hydrocarbon reservoirs, the porous material can be divided into two main groups: clastics and carbonates; both of which are sedimentary rocks. The different groups arise from the origin of the rock. Clastic sedimentary rocks are typically deposited in riverbeds and consists of fine grains while carbonates are formed from biological processes[88]. These processes (deposition and biological) take place over long geological periods, during which the rocks undergo compression. Figure 2.1 is a schematic image and an actual photograph showing the solid grains in a sandstone rock.
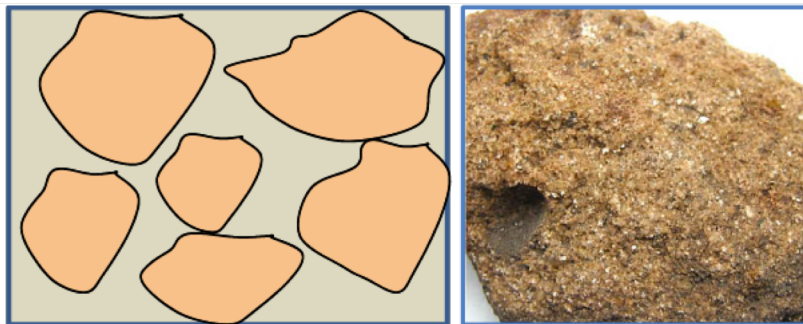
Figure 2.1: Solid grains in a porous rock (Left: schematic image, right: sandstone photograph)[88].

The porosity of a reservoir rock is estimated as:

$$\phi = \frac{V_p}{V_b} \tag{2.1}$$

where V_p and V_b represent the pore and bulk volume, respectively.

The porosity of interest to reservoir engineers is the effective porosity, because it represents the interconnected pore volume and is what contributes to fluid flow in the reservoir. The isolated pores form the ineffective porosity. The sum of the effective porosity, ϕ_{eff} and ineffective porosity, ϕ_{ineff} is the total porosity of the rock:

$$\phi_{tot} = \phi_{eff} + \phi_{ineff} \tag{2.2}$$

The two methods used to measure porosity are from laboratory measurements or downhole tools such as wireline logs. The porosity obtained from logs is usually the total porosity. Empirical data from nearby formations or core plugs from formations with similar geological properties are typically used to calculate the effective porosity[67]. The porosities determined from laboratory measurements are more accurate than porosities from logs, although they suffer from sampling problems[38]. Using the porosities from the two methods together helps to optimize accuracy.

2.2.   Absolute Permeability

Permeability refers to the ability of a rock to transmit fluids through its network of interconnected pores[38]. There are three types of permeability: absolute, effective and relative permeability. The absolute permeability is a property of the rock while effective and relative permeabilities are properties of the fluids, and are discussed later in this chapter.

Absolute permeability refers to the permeability of a rock when only a single phase is flowing through it. An empirical correlation that relates fluid flow to the pressure gradient and gravitational forces was derived by Henry Darcy based on certain simplifying assumptions. They include: single phase flow, incompressible flow, laminar flow, horizontal flow, and no chemical reaction between the rock and fluid[62]. The correlation is known as Darcy law and is the standard correlation used to calculate permeability in the oil and gas industry today.

The absolute permeability of a reservoir rock is determined from coreflooding experiments, whereby the pressure difference (P_1 and P_2) across a core is measured for a given fluid flow rate as shown in fig. 2.2.
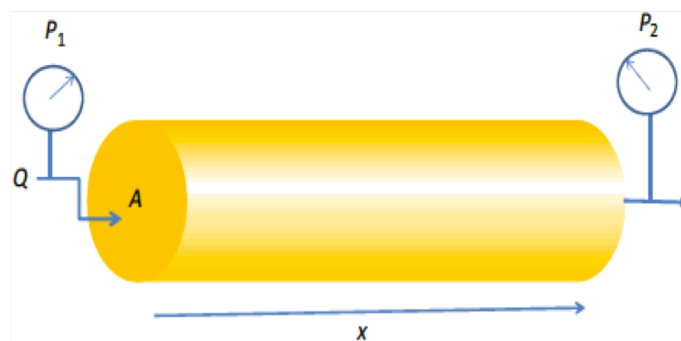
Figure 2.2: Schematic of absolute permeability measurement[88].

For an incompressible fluid of viscosity, μ (cp), flowing through a horizontal core of area, A (cm^2) and length, x (cm) at volumetric flow rate, Q (cm^3/s), Darcy's law is expressed as:

$$Q = \frac{KA(P_1 - P_2)}{\mu x} \qquad (2.3)$$

The unit for pressure, P in the above equation is atm. The absolute permeability, K can then be calculated from eq. (2.3), and is expressed in the units Darcy (D).

2.3. Fluid Saturation

It refers to the volume of the pore space occupied by hydrocarbon fluids; typically oil, water and gas. The saturation of a given phase is expressed as:

$$S_i = \frac{V_i}{V_p} \quad i = o, w, g \qquad (2.4)$$

where V_i is the fluid volume

The saturation of the hydrocarbon phases in the reservoir at any time is dependent on three forces: interfacial forces between the fluids and between the fluids and the solid matrix, gravitational(buoyancy) forces that cause the segregation of the fluids in the reservoir according to density, and external hydrodynamic forces such as flow from an aquifer[38]. The total saturation of fluids in a reservoir rock is therefore given by:

$$S_o + S_w + S_g = 1 \qquad (2.5)$$

2.4. Surface and Interfacial Tension

Interfacial tension (IFT), σ is the change in Gibbs free energy, F for a change in area, A (or the change in energy per unit area of the surface between phases) while surface tension, γ is the energy per unit area between a fluid or solid and its vapor phase that is in thermodynamic equilibrium[21]. Sometimes, surface tension and IFT are erroneously used interchangeable. However, it should noted that although the two are similar due to the cohesive forces that exist between the molecules, adhesive forces between the liquid phase of a substance and the solid, liquid or gas phase of another substance are the dominant forces in IFT[64]. Mathematically, IFT can be expressed as:

$$\sigma = \frac{dF}{dA} \qquad (2.6)$$

IFT originates from the imbalance of attractive forces that exists at the interface between the molecules of two immiscible or poorly miscible fluids. Figure 2.3 is a schematic of the forces at the interface between oil and water. The inter-molecular forces between the oil molecules are weak Van der Waal forces of attraction (represented by the dotted arrows)

compared to the strong hydrogen bonding between water molecules, represented by the solid arrows. At the surface between the two fluids, some of the hydrogen bonds between water molecules are replaced by Van der Waal forces; thereby creating an imbalance of forces.
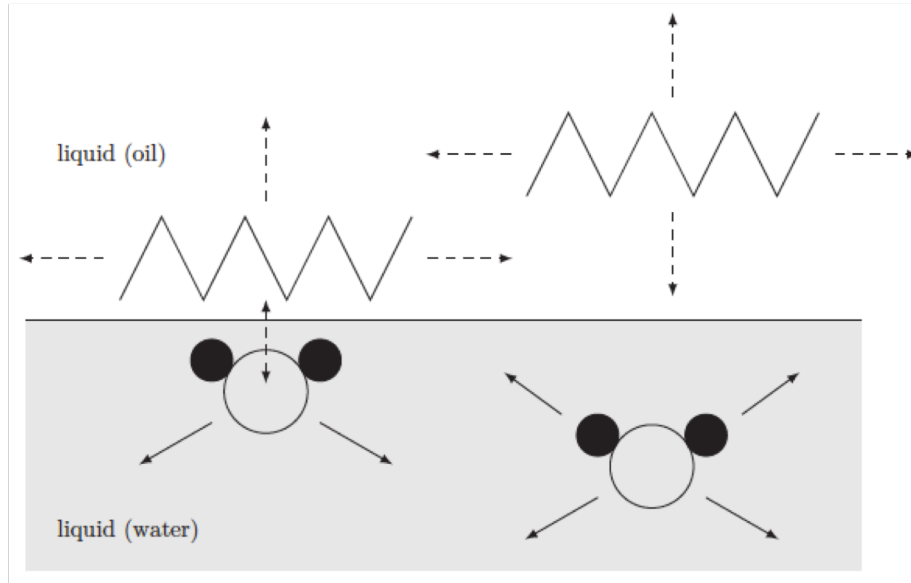
Figure 2.3: Schematic of interfacial forces between oil and water[21]

2.5.   Capillary Pressure

The arrangement of fluids in the pore space of a reservoir is controlled by an energy balance, and the displacement of one fluid by another from the pore space only occurs if the process is energetically favorable[21]. If two fluids (water and oil) are in contact with each other and a solid surface, one of the phases is usually referred to as the non-wetting phase (nw) whereas the other is the wetting phase (w). The solid surface has a high preference for the wetting phase, and therefore coats the surface while the non-wetting phase is repelled. This results in the formation of a curvature at the interface between the two fluid phases.

The curved interface gives rise to a pressure difference between the phases. The non-wetting phase pressure is usually the higher of the two because it requires a higher pressure for it to be displaced from the porous medium[21]. A relationship between the pressure difference and the interfacial curvature can be derived by applying an energy balance that relates the work done against the pressure difference to the change in the surface energy. The energy balance gives rise to the Young-Laplace equation:

$$(P_{nw} - P_w)dV = \sigma \, dA \tag{2.7}$$

where dV and dA are the infinitesimal change in volume and the corresponding change in area, respectively. $P_{nw} - P_n$ in the above equation is known as the local capillary pressure,

P_c and the equation simplifies to:

$$P_c = \sigma \frac{dA}{dV} \tag{2.8}$$

The interface between two fluids can be curved in two directions; with different radii of curvature. In that case, the capillary pressure is expressed as:

$$P_c = \sigma \left(\frac{1}{R_1} + \frac{1}{R_2} \right) = \kappa \sigma \tag{2.9}$$

Where κ is the total curvature of the interface between the two fluids. The pore channels in a porous medium are typically treated as capillary tubes. In a capillary tube of radius r, the interfacial curvature between two fluids is given as:

$$R_1 = R_2 = \frac{r}{\cos \theta} \tag{2.10}$$

where θ is the contact angle. Equation (2.9) then simplifies to:

$$P_c = \frac{2\sigma \cos \theta}{r} \tag{2.11}$$

The above equation shows that the capillary pressure is a function of the pore-size distribution, fluid-fluid IFT, wettability as well as the saturation history; as will be explained in the next section.

2.6. Drainage and Imbibition

Drainage is a process whereby the wetting phase is displaced from the porous medium by the non-wetting phase. It can also be defined as an increase in the saturation of the non-wetting phase. The process is divided into primary and secondary drainage. A primary drainage process refers to the first time the non-wetting phase is invading the pores, such as the migration of oil and gas from a source rock to a hydrocarbon reservoir during accumulation[21]. Secondary drainage occurs when the non-wetting phase is invading a porous medium that had already been invaded by a non-wetting phase, such as during gas injection processes.

Imbibition refers to the displacement of the non-wetting phase by the wetting phase. Similarly, imbibition can be classified as primary or secondary imbibition. In primary imbibition, a wetting phase invades a porous medium that is initially saturated with the non-wetting phase while secondary imbibition is the invasion of the wetting phase into a porous medium where some wetting phase is already present[21]. Secondary imbibition is the most common type of imbibition encountered in petroleum reservoirs, such as during waterflooding of an oil reservoir.

The increase in the non-wetting phase saturation during drainage results in a gradual increase in the non-wetting phase pressure, and a corresponding increase in the local

capillary pressure. The porous medium consists of pores and throats; of which the pores are wider and therefore would have larger radii of curvature of the interface between the fluids. Equation (2.11) therefore implies that the order of filling during drainage would be the pores first because require less non-wetting phase pressure due to their larger sizes and then the throats. The filling sequence in imbibition is the reverse; with the throats being filled first. This difference in the pore/throat filling sequence gives rise to differences in the change in the non-wetting phase saturation (S_{nw}) for the same pressure change during the two processes, which results in what is known as capillary pressure hysteresis[49]:

$$\left[\frac{dS_{nw}}{dP_c} \right]_{drainage} > \left[\frac{dS_{nw}}{dP_c} \right]_{imbibition} \tag{2.12}$$

Figure 2.4 shows a typical drainage and imbibition capillary pressure curves. It can be seen that the change in the capillary pressure with the wetting phase saturation is different for drainage and imbibition.
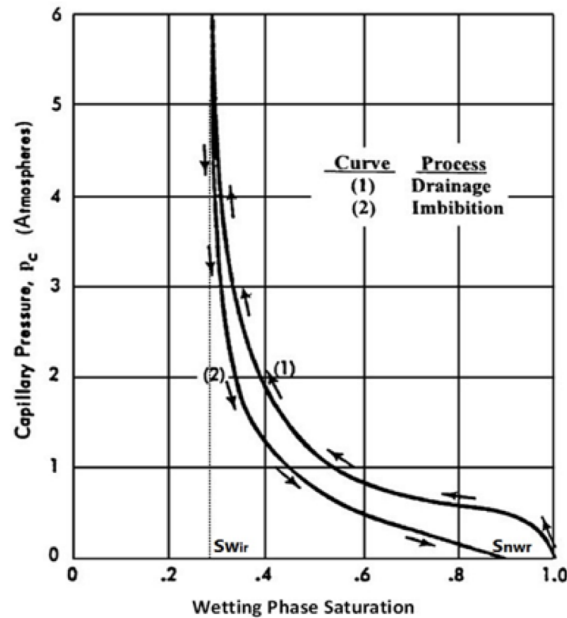
Figure 2.4: Capillary pressure curves for drainage and imbibition[49].

2.7. Wettability

Wettability refers to the tendency of a fluid to adhere to a solid surface in the presence of other immiscible fluids[3]. The most universal measure of the wettability of a system is the contact angle[59]. Wettability can therefore be alternatively defined as the distribution of contact angles throughout the porous medium[21]. The fundamental expression used to determine contact angle is the Young's equation (eq. (2.13)), which expresses the contact angle in terms of the fluid/fluid and fluid/solid IFT. It is derived by treating the interfacial

tensions as forces and applying a horizontal force balance to the system in fig. 2.5.

$$\cos\theta = \frac{\sigma_{nws} - \sigma_{ws}}{\sigma} \tag{2.13}$$

where σ is the fluid/fluid IFT, σ_{nws} is the IFT between the non-wetting phase and the solid and σ_{ws} is the IFT between the wetting phase and the solid.
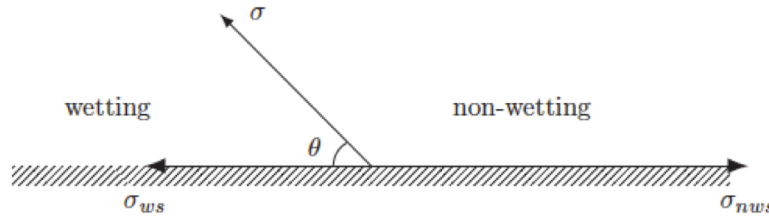
Figure 2.5: Schematic of wetting and non-wetting phases in contact with a solid[21]

Based on contact angle, the wettability can be classified as shown in table 2.1[44]. The wettability of reservoir rocks is a very important parameter because it controls the distribution of fluids in the porous media[3,13]. In addition, wettability affects other important flow properties such as relative permeability, capillary pressure and residual saturations[12,13]. The attractive forces between the rock and the wetting phase causes the wetting phase to occupy the smaller pores, forming thin films in contact with the rock surface while the non-wetting phase occupies the larger pores.

Several studies have investigated the effect of wettability on oil recovery[2,35,50,59,69]. Kennedy et al.[50] investigated the effect of wettability on oil recovery for two cases: constant IFT and varying IFT. Oil recovery was plotted against sessile drop ratio (ratio of the height to the width of an oil droplet on a solid surface) and they found that the highest recovery was obtained for a ratio of 0.5; representing a mixed-wet state. Varying results were reported by Morrow[59] from his study on the effect of wettability on oil recovery during waterflooding. In some cases, higher recovery was obtained from less water-wet compared to very strongly water-wet (VSWW) whereas in other cases, the reverse was observed. There is currently no consensus on the optimum wetting condition for maximum oil recovery from waterflooding. Some reasons for the contrasting results from different studies include: lack of a unified standard method for recovering cores and handling and storing the cores, difficulty of reproducing the wetting state and the method used to characterize the wetting state[2].

Table 2.1: Wettability classification based on contact angle measurements[44]

Wettability state	Contact angles (degrees)
Complete wetting or spreading of water	0
Strongly water-wet	0 – 50
Weakly water-wet	50 – 70
Neutrally wet	70 – 110
Weakly non-wetting to water	110 – 130
Strongly non-wetting to water	130 – 180
Completely non-wetting to water	180

Figure 2.6 shows water displacing oil from the pore space for two different wettability states: strongly water-wet and strongly oil-wet. In the strongly water-wet case, the water advances along the pore walls due to the rock surface having a higher preference for water. As the water advances, it displaces the oil that lies ahead of it until the oil phase becomes disconnected and immobile giving rise to 'residual oil'. Similarly, in the strongly oil-wet case, the oil resides in the small pores and close to the rock surface while the water occupies the larger pores. During waterflooding, the water forms continuous channels and displaces the oil in front of it. As more water is injected, the water starts invading the smaller pores and forms more continuous channels until no more water can invade the smaller pore space[13]. This prevents the flow of oil and oil production ceases despite the fact that there are still continuous thin films of oil in the cracks and crevices of the pores.

Wettability depends on the chemical composition of the fluids that gives rise to the molecular attraction between the water molecules and/or the oil molecules[2]. The degree of wetness is strongly affected by the rock mineralogy, adsorption and desorption of the components in the oil, and the film deposition and spreading ability of the oleic phase. Generally, most reservoirs are initially water-wet in nature. As oil migrates into the reservoir, a wettability change might occur due to the adsorption of polar components such as asphaltenes present in the oil onto the rock surface. Other factors that may cause an alteration of the wettability include: reservoir rock type, connate water salinity, the presence of film forming components, and the type and distribution of the minerals present[2].
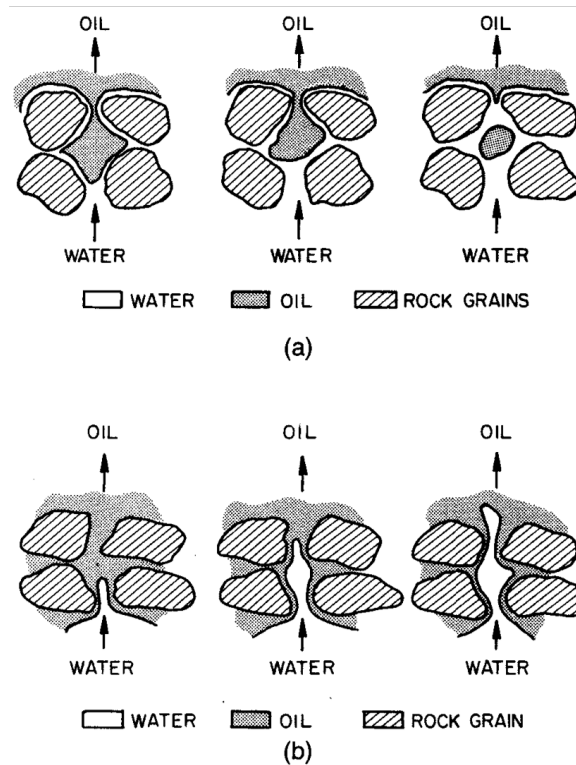
Figure 2.6: Illustration of oil displacement by water during waterflooding for (a) strongly water-wet and (b) strongly oil-wet[69]

Other common methods used to measure wettability include: the Amott method and the USBM (United States Bureau of Mines) method. The Amott method involves measuring the amount of oil and water imbibed by rock sample spontaneously and forcibly, and is expressed as the Amott-Harvey index (I_{AH}). Although the USBM method is similar to the Amott method, it only considers the work required for forced fluid displacement, and is denoted by the USBM wettability index, W[11,33,38]. The range of values for I_{AH} and W for different wettability conditions is shown in table 2.2

Table 2.2: Amott-Harvey and USBM index values for different wettability conditions[11,33]

Wettability Index	Water Wet	Neutral Wet	Oil Wet
I_{AH}	0.3 to 1.0	-0.3 to 0.3	-1.0 to -0.3
W	near 1	near 0	near -1

2.8.   Effective and Relative Permeability

Effective permeability refers to the ability of a porous system to conduct one fluid in the presence of other immiscible fluids[13]. It is a function of the relative fluid saturations, and the rock wettability. Relative permeability is typically defined as the ratio of the effective permeability of a given fluid to its absolute permeability. It depends on many factors such

as pore geometry, wettability, capillary number, saturation history, fluid distribution and viscosity ratio[21,27]. The expression for the relative permeability of phase i is given as:

$$k_{ri} = \frac{k_i}{K} \quad i = o, w, g \tag{2.14}$$

where k_i is the effective permeability of the rock to fluid phase i. Darcy's law presented in eq. (2.3) can then be modified to account for the flow of each phase by taking into account its effective permeability:

$$q_i = \frac{Kk_{ri}(P_1 - P_2)}{\mu_i x} \tag{2.15}$$

where q_i is the Darcy velocity and μ_i is the phase viscosity.

Relative permeability is a very important parameter for history matching of both experimental and field production data. Several empirical correlations have been developed for estimating relative permeability. One of the earliest correlations was the Kozeny-Carman equation, which expresses the permeability as a function of the fluid effective path length and the mean hydraulic radius of the channel through which the fluid flows[43]. Purcell used the assumption that the porous medium can be represented as a bundle of capillary tubes with varying sizes to obtain an equation for permeability in terms of the porosity and capillary pressure desaturation curve (CDC) of the system[43]. The two correlations have been modified by many authors to obtain new correlations for estimating relative permeability. Today, the most common empirical correlation used for relative permeability estimation is the Brooks-Corey model, which expresses relative permeability as a power law in the normalized water saturation[23]:

$$k_{rw}(s_w) = k_{rw}^o s_{wn}^{n_w} \tag{2.16}$$

$$k_{ro}(s_w) = k_{ro}^o (1 - s_{wn})^{n_o} \tag{2.17}$$

$$s_{wn} = \frac{s_w - s_{wir}}{1 - s_{wir} - s_{or}} \tag{2.18}$$

where k_{ro}^o and k_{rw}^o are the end-point relative permeabilities, s_{wn} is the normalized water saturation, s_{wir} is the irreducible water saturation, s_{or} is the residual oil saturation and n_o and n_w are the power law parameters for oil and water, respectively, and are known as Corey exponents. This correlation was used to estimate relative permeabilities for all the simulations done in this thesis.

As mentioned in section 2.7, the wettability of a system has a significant effect on the relative permeability of the fluids because it controls the distribution of fluids in the pore space[13]. Figure 2.7 shows the oil-water relative permeability curves for a water-wet rock and an oil-wet rock. The two figures show that the relative permeability of oil is higher for the water-wet case than for the oil-wet case for the same set of saturations. Similarly, the relative permeability of water is higher for the oil-wet case than for the water-wet case for the same set of saturations. This is because the water is confined to the smaller pores while the oil occupies the larger pores in the water-wet rock, making it easier for oil to be displaced. The reverse is true for the oil-wet rock.
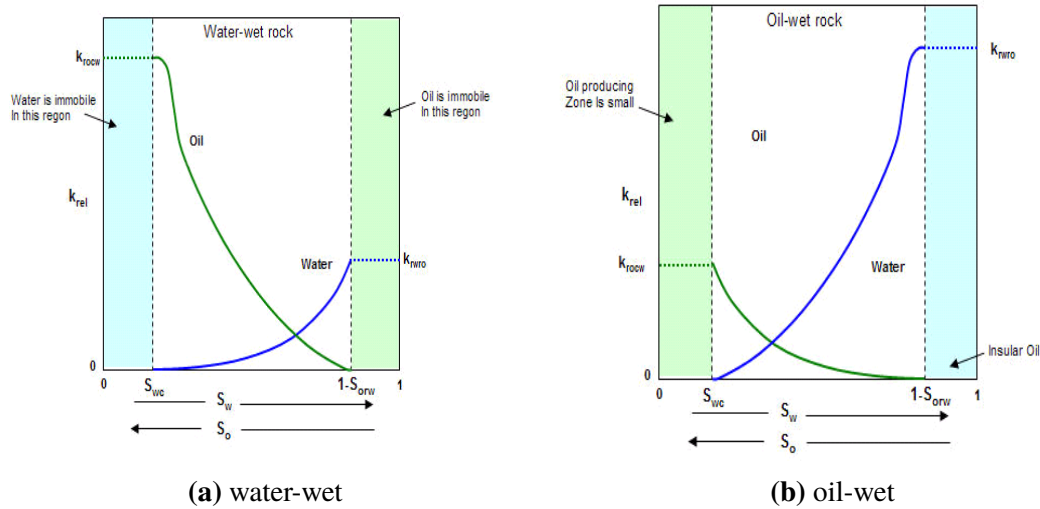
(a) water-wet   **(b)** oil-wet

Figure 2.7: Relative permeability curves for water-wet and oil-wet rocks

2.9. Carbonate Rocks

Carbonate rocks show significant differences from clastic sedimentary rocks such as sandstones. As previously discussed in section 2.1, most carbonate rocks are formed from biological activity such as reef building and accumulation of sediments on the seafloor, while others are formed as precipitates from seawater or as water evaporates from onshore shallow basins[4]. The formation and deposition of the rocks takes place in situ[37]. After the sediments are deposited, the rock structure is altered by chemical and physicals processes; known as diagenesis. These processes change the fundamental characteristics of the rock such as porosity and permeability, and as a result induce reservoir heterogeneity, which makes modeling and prediction of production performance difficult[82]. Carbonate sedimentary rocks are also susceptible to mineral dissolution and precipitation due to the presence of metastable minerals such as aragonite and magnesium[4]. Mineral dissolution and precipitation varies with temperature, pressure and chemistry of the pore-fluid.

The three main types of carbonate rocks are limestone, dolomite and chalk[22]. Limestones are primarily made up of calcium carbonate (also known as calcite, $CaCO_3$). They usually contain varying amounts of other minerals such as quartz, clay minerals, pyrite, siderite and feldspar. Limestone is converted into dolomite or dolostone [$(CaMgCO_3)_2$], with an increase in the concentration of magnesium (Mg). Dolomite is typically not formed on the earth's surface. The rocks are originally deposited as calcite, and then converted into dolomite during the process of diagenesis. Chalk is a type of very fine-grained limestone[22] and therefore consists predominantly of $CaCO_3$ as well. Both chalk and limestone are relatively soft, although chalk is the softer of the two. The soft nature of chalk makes it susceptible to fracturing. As such, most chalk reservoirs exists as naturally fractured reservoirs such as those in the Ekofisk field.

2.10. Chapter Summary

A review on some of the properties and processes that play an important role in the accumulation, production and behavior of hydrocarbon reservoirs has been provided in this chapter. The wettability of a reservoir rock is one of the most important parameters because it governs the distribution in the pore space, and therefore has an effect on other important properties such as capillary pressure, relative permeability, and residual saturation. Relative permeability and capillary pressure are known as effective transport coefficients and play an important role in history matching and upscaling from pore-scale to field-scale. Relative permeability depends on many factors such as wettability, pore geometry, saturation history and fluid distribution. Other properties such as porosity which refers to the storage capacity of the reservoir rock, phase saturation, and interfacial tension have been discussed.

The differences between carbonates and clastic sedimentary rocks have been discussed. These differences arise due to a difference in the depositional environments and the processes that alter the rocks after deposition. Clastic sedimentary rocks are deposited in riverbeds while carbonates are formed from biological processes, as precipitates from seawater or as water evaporates from shallow onshore basins. After deposition, rock properties are altered during diagenesis; inducing the heterogeneity observed in most carbonate reservoirs. Limestone, dolomite and chalk; which are the three main types of carbonate rocks have also been briefly discussed. Calcite is the dominant mineral in both limestone and chalk while dolomite (or dolostone) consists mainly of $(CaMgCO_3)_2$ and is formed during the process of diagenesis.

3. Enhanced Oil Recovery (EOR)

The production of oil and gas from a hydrocarbon reservoir typically begins with the natural energy of the reservoir as the driving force. The process is known as depletion and the energy comes from the expansion of the fluids initially in place, rock expansion or aquifer influx[74]. Recovery from this mechanism is typically in the range of 30-35%, and there is therefore need for an intervention when the natural energy is no longer able to drive fluids out of the reservoir. The injection of water in the aquifer or gas in the gas cap for pressure maintenance and volumetric sweep efficiency is usually the next step[51,74]. This is called secondary recovery, and is followed by the injection of fluids into the reservoir to alter the crude oil/brine/rock (COBR) interactions[56,74]; known as enhanced oil recovery. EOR and improved oil recovery (IOR) are sometimes used interchangeably. However, Sheng[74] asserts that EOR should strictly be used only for processes that alter the COBR interactions whereas IOR refers to all reservoir processes that improve oil recovery but for depletion.

EOR is aimed at improving the microscopic displacement efficiency and the volumetric sweep efficiency, and ultimately, oil recovery. The four main categories of EOR methods include: thermal recovery, miscible gas injection, chemical injection and microbial flooding[32,36,74,86]. Thermal recovery processes involve the introduction of heat into the reservoir, such as the injection of steam; to lower the oil viscosity thereby improving the ability of the oil to flow. This is mostly applicable to heavy viscous oils. In miscible gas injection, rich gases such as natural gas liquids (NGL), liquefied petroleum gas (LPG) and carbon dioxide (CO_2) that have the ability to dissolve in the oil and improve its ability to flow by reducing its viscosity are injected into the reservoir[86].

EOR by chemical injection is subdivided into four categories: polymer flooding, surfactant flooding, alkali flooding and low salinity waterflooding (LSWF). Polymer flooding involves the injection of polymers in the aqueous phase, to increase the viscosity of the displacing phase and reduce the mobility ratio between the displacing and the displaced phases[51,74,86]. This reduces the degree of fingering and channeling of the displacing phase through the porous medium. In Surfactant flooding, surfactants are injected to mobilize trapped oil by reducing the IFT between oil and the displacing phase or by changing the rock wettability. The reduction in the IFT is associated with an increase in the capillary number (discussed later in the chapter) and a decrease in capillary forces. Alkali flooding is characterized by the injection an alkali such as sodium hydroxide (NaOH), which reacts with the naphthenic acids in the oil, generating in situ surfactants that reduce the IFT and cause wettability alteration[74]. The alkali also prevents the other chemicals (surfactant and polymer) from adsorbing onto the rock surface. LSWF is the most recent among the chemical EOR methods. It involves modifying the salinity and composition of the injected water, as discussed in the next section.

Microbial flooding involves the injection of microbes to improve oil recovery through biological and biochemical effects[36]. The application of the different EOR methods depends on reservoir conditions such as rock permeability, oil viscosity, brine salinity and reservoir temperature[32]. Recently, a common approach has been to use a combination of the different methods such as alkali-surfactant-polymer (ASP) flooding, low-salinity

surfactant polymer flooding (LSSP), or low salinity surfactant-CO_2. This is referred to as a hybrid EOR process.

3.1. Low Salinity Waterflooding

Low salinity waterflooding (LSWF) is an EOR technique whereby the ionic concentration and composition of the injected brine is controlled[24,32,45]. The technique is also known in literature as smart waterflooding, advanced ion management, designer waterflood and LoSal. It is a relatively new EOR method that has been subject to a lot of research due to the low operating and capital costs associated with the technique, its environmentally friendly nature and the fact that it can be implemented either in secondary or tertiary modes, unlike the other EOR methods[32,72].

Many laboratory studies have reported an increase in oil recovery in carbonates from LSWF as well as a few field studies[5,41,54,55,61,70,89]. Despite the growing interest in the process, there is currently no consensus on the mechanisms responsible for the increase in oil recovery. Wettability alteration is however the widely accepted mechanism. A summary of laboratory and field studies, and the proposed mechanisms in carbonates is presented in this section.

3.1.1. Spontaneous imbibition and coreflood experiments

coreflood experiments are crucial to understanding the mechanisms behind wettability alteration during LSWF[32]. Several coreflooding tests have been done on carbonate cores, and a description of some of the most recent studies follows. Nasralla et al.[61] conducted spontaneous imbibition tests, and qualitative and quantitative unsteady state (USS) experiments on limestone cores aged in crude oil for 28 days at 100 °C, to investigate the effect of low salinity brines. The spontaneous imbibition tests were conducted in both secondary and tertiary modes at a temperature of 70 °C and the purpose was to provide a qualitative indication of the wettability of the low salinity brines relative to the formation brine. The qualitative tests were intentionally conducted at low rates (0.025 cc/min or 0.05 cc/min) so that the effects of low salinity water (LSW) on relative permeability could be examined, while the flow rate was increased in steps in the quantitative tests from 0.05cc/min in order to minimize capillary end effect. Little production was observed in the spontaneous imbibition tests after formation water (FW) was injected, but an increase in oil recovery was observed during seawater and 10-times diluted seawater injection, respectively, indicating a change in wettability. A similar trend was observed in the quantitative USS tests, where an increase of 6-7% of OOIP was observed for the 10-times diluted seawater.

Hamouda and Gupta[41] investigated the role of some ions on the increase in oil recovery from chalk reservoirs through laboratory experiments. The Steven Klint (Denmark) Chalk, which is stratigraphically similar to the interval between the uppermost Tor formation and the lower Ekofisk formation in the North Sea was used for the experiments. Both crude oil and model oil (n-decane + stearic acid) were used for the coreflood experiments. The acid number (AN) and base number (BN) of the crude oil were 0.06 KOH/g and 0.60 KOH/g, respectively. The cores were initially saturated with synthetic seawater (SSW); which was

also used during the primary injection stage. Different low salinity brines were used in the secondary injection stage. It was observed that the ion dilution factor had an effect on the oil recovery response time of LSWF. An earlier response was observed for the 1:10 LSW dilution compared to the 1:50. Divalent cations such as Mg^{2+}, Ca^{2+} and SO_4^{2-} were also identified as the main wettability modifiers and multi-ion exchange was observed as the primary mechanism for wettability alteration. Fines migration and dissolution were also identified as possible additional mechanisms.

A significant issue in some coreflood experiments is the impact of capillary end effects on the flow and production of oil. They cause an overestimation of the residual saturation, and suppress the end point relative permeability of water[57]. Shehata et al.[73] used long outcrop limestone cores in their coreflood experiments, in order to minimize capillary end effects. Ageing of the cores was done at a temperature of 195°F for 20 days with a crude oil of acid number (0.18 mg KOH/g oil). The effect of salinity as well as the concentration of important ions (Mg^{2+}, Ca^{2+} and SO_4^{2-}) on oil recovery was investigated. They found that a change in the salinity from seawater to deionized water and from deionized water to seawater had a significant effect on oil recovery. In addition, Mg^{2+}, Ca^{2+} and SO_4^{2-} ions were observed to be crucial in the mobilization of trapped oil in the cores.

3.1.2. Field studies

There are very few reports on the field scale implementation of LSWF in carbonate reservoirs. Sylte et al.[40,83] designed and implemented a pilot waterflood in the Ekofisk field; which is made up of two naturally fractured chalk formations (Ekofisk and Tor). A dramatic increase of over 50% in the total oil production was observed over 3 years. This stimulated more research on the potential of advanced waterflooding in carbonates[77].

However, the first ever field application of LSWF in a carbonate reservoir was reported by Yousef et al.[89]. Two field trials were performed and a single well chemical tracer test (SWCTT) was designed to evaluate the change in residual oil saturation during LSWF. In both trials, a reduction in the residual oil saturation of about 7 saturation units was observed, confirming the potential of LSWF to increase oil recovery in carbonate reservoirs. The increase in oil recovery was attributed to a change in wettability to a more water-wet state. It was also observed that temperature strongly affects the change in the wettability and the efficiency of LSWF in carbonate reservoirs.

3.1.3. Proposed mechanisms

Several mechanisms have been proposed as the reasons for the increase in oil recovery during LSWF. These mechanisms depend on many factors such as the formation brine chemistry, crude oil type and reservoir parameters such as temperature, pressure, porosity and permeability. Wettability alteration is widely accepted to be the main reason for the improved oil recovery from the process, although there is currently no consensus on the optimum wettability state. Some studies have observed improved oil recovery due to a change to more water-wet state[25,89] while others reported a change to more intermediate state[2,5,7]. In addition, different wettability alteration mechanisms have been observed in different studies. The different mechanisms are described below:

Multicomponent ionic exchange

Multicomponent ionic exchange (MIE) has been proposed as a dominant wettability alter-ation mechanism during LSWF[16,17,81,91,92]. The proposed mechanism by Zhang et al.[91,92] involves an anion exchange process that occurs between the potential determining ions, PDIs (Mg^{2+}, Ca^{2+}, and SO_4^{2-}) in the brine and the carbonate rock surface. The SO_4^{2-} ions are adsorbed unto the positively charged carbonate surface, reducing the electrostatic repulsion. Ca^{2+} ions are then adsorbed and they react with the carboxylic group bonded to the carbonate rock surface. This results in the release of some carboxylic materials from the rock surface and a subsequent change in wettability. They also investigated the effect of temperature on the process and observed that the adsorption of SO_4^{2-} and co-adsorption of Ca^{2+} increases with temperature as well as the substitution of Ca^{2+} by Mg^{2+} at the rock surface.

The MIE mechanism was observed in fractured limestone cores, although the rate of substitution of Ca^{2+} by Mg^{2+} was slower as temperature increased, due to the lower surface reactivity of limestone[81]. Ravari[68] however did not observe any MIE or substitution of Ca^{2+} by Mg^{2+}, using outcrop limestone even at high temperatures. The mechanism of MIE is therefore dependent on rock mineralogy and might not be valid for all carbonate rock types[32].

A new mechanism for the MIE process was recently proposed by Adegbite et al.[1]. They suggested that the positive charge of the carbonate surface is reduced by the negatively charged sulfate ion, which causes the divalent cations (Ca^{2+} and Mg^{2+}) to be attracted to the carbonate surface. The positive ions then form a complex with the carboxylic ion, causing it to be completely released from the carbonate surface. The schematic of the proposed MIE mechanisms by Zhang et al. and Adegbite et al. is shown in fig. 3.1.
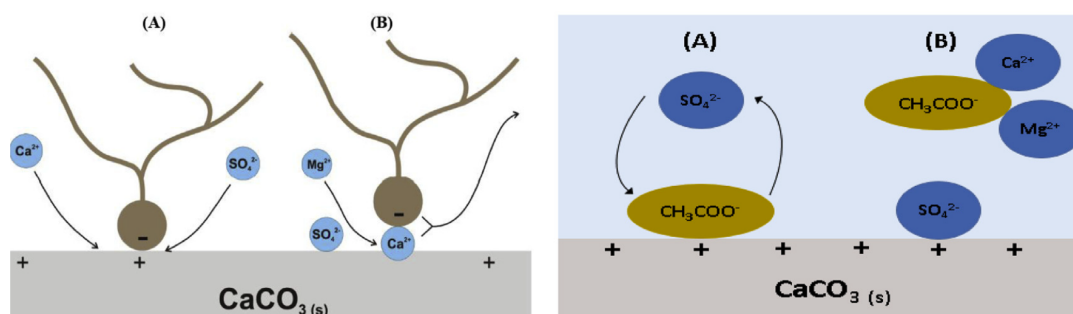
Figure 3.1: Mechanism of MIE in carbonate rocks: a) Proposed by Zhang et al.[92] b) Proposed by Adegbite et al.[1].

Expansion of electric double layer

Expansion of the electric double layer (EDL) has also been suggested as a wettability alteration mechanism. The thickness of the water film that separates the oil/brine (OB) interface and the rock/brine (RB) interface is inversely proportional to the ionic strength[77]. In a high salinity brine environment, there is competition between the PDIs for surface sites. As the multivalent cations interact with the negatively charged oil surfaces, there is a decrease in the electrostatic repulsive forces resulting in the compression of the EDL and a possible change in the wettability to oil-wet[77]. During LSWF, an expansion of

the EDL occurs, which increases the electrostatic repulsive forces between OB and RB interfaces resulting in a thicker and more stable water film and a change in wettability to more water-wet. In addition, the charge of the RB interface is changed from positive to negative if there is an increase in pH above the carbonate point of zero charge (PZC) density. PZC refers to a condition when a surface's electrical charge density is zero. This results in an expansion of the EDL, due to repulsive electrostatic forces between the RB and OB interfaces (both negatively charged). The mechanism of wettability alteration by EDL expansion as suggested by many researchers is shown in fig. 3.2.
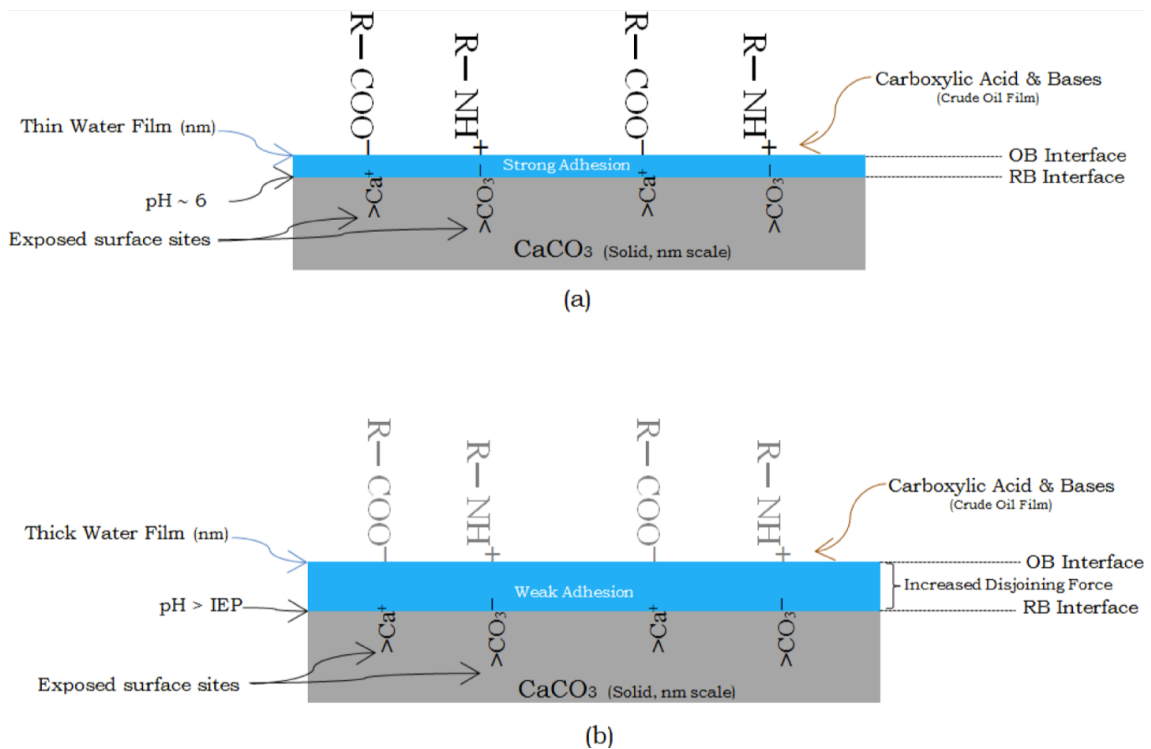
Figure 3.2: Schematic of the EDL expansion mechanism: a) Original wetting condition b) Wetting condition in low salinity brine.[77].

Rock dissolution

Hiorth et al.[42] proposed the dissolution of calcite as the main wettability alteration mechanism. A geochemical model was developed and tested using experimental results. They believed that if a change in surface potential was responsible for low salinity effects, then the change should be observed at both high and low temperatures. This was however not the case based on the results from their model. In addition, they suggested that the adsorption of oil components onto the carbonate rock surface is a strong and irreversibly process, and therefore the equilibrium between the rock surface and oil should not be affected by a change in water chemistry. Based on the observations, they proposed rock dissolution as a mechanism for wettability alteration in carbonates.

Altahir et al.[10] developed an innovative approach to investigate dissolution and dissolution induced fines migration using a heterogeneous limestone core. Scanning electron microscope (SEM) images were taken before and after coreflood experiments, to investigate the potential of dissolution to alter the rock geometry, and for comparison purposes. Ionic

chromatography was also used to quantify the concentrations of anions and cations produced in the effluent. Fines migration was observed in all the images, and they proposed dissolution as the mechanism for fines migration. Also, no pressure drop was observed, and this was attributed to the coexistence of both dissolution and fines migration. Finally, an increase in pH was observed, which they believed is further confirmation of the dissolution of calcite.

Fines migration

Fines migration has also been suggested as a mechanism that can increase the water-wetness of a rock. It can cause the partial or full blockage of high permeability channels, thereby diverting the flow to unswept zones and increasing the volumetric sweep efficiency[10,41]. However, RezaeiDoust et al.[70] pointed out that improved microscopic sweep efficiency is responsible for the improvement in oil recovery during fines migration, and not wettability alteration.

Interfacial tension and pH

A decrease in IFT and an increase in pH can improve oil recovery by lowering the residual oil saturation. The residual oil saturation is determined by the capillary number; discussed in section 3.2.1. During LSWF, there is a negligible change in the injected fluid viscosity. A decrease in the IFT would therefore increase the capillary number and lower the residual oil saturation. However, it is not clearly established in literature whether LSWF affects IFT (fluid/fluid interactions), contact angle (rock/fluid interactions) or both. Wettability alteration and reduction in IFT was proposed as the two dominant mechanisms in carbonates by Meng et al.[58]. Brine salinity was however found to have negligible effect on IFT (fluid/fluid interactions) but a significant effect on contact angle (rock/fluid interactions)[90]. It is therefore believed that although a decrease in IFT and an increase in pH during LSWF could contribute to the improved recovery during LSWF, they are not the dominant mechanisms.

Formation of micro-dispersions

The role of COBR interactions and the formation of micelles were investigated by Sohrabi et al.[78]. Significant additional oil recovery was observed in clay-free porous medium, which they believed was due to the formation of micelles[78]. It is believed that micro-dispersions are formed in the oil-phase when low salinity water comes in contact with crude oil, and the micro-dispersions deplete the surface-active components at the oil/brine interface. This changes the balance of forces at the rock/brine and oil/brine interfaces and results in wettability alteration.

3.2. Surfactant Flooding

As discussed above, oil trapped by capillary forces is mobilized during surfactant flooding due to a reduction in the IFT between oil and water phases (increase in capillary number) or a change in the system wettability. This increases the microscopic displacement efficiency, and thereby results in higher oil recovery. The different aspects of surfactants such as surfactant types, characterization, phase behavior, capillary number (N_c) and capillary

desaturation curve (CDC), and surfactant retention are discussed in this section.

3.2.1. Capillary number and capillary desaturation curve

The capillary number is an important parameter that determines the mobilization of capillary trapped oil during immiscible displacements[48]. It is the dimensionless ratio of viscous forces to capillary forces expressed as:

$$N_c = \frac{\mu q}{\sigma} \tag{3.1}$$

where μ and q are the injected phase viscosity and Darcy velocity, respectively, and σ is the fluid/fluid IFT.

Capillary forces; represented by the interfacial tension are responsible for the trapping of the non-wetting phase (oil) during immiscible displacements in porous media. By increasing the viscous forces, the trapped oil may be mobilized. The viscous forces required for the mobilization of trapped oil is determined by the fluid dynamics of the displacing phase[48]. The relationship between capillary number and residual oil saturation is typically shown through a capillary desaturation curve (CDC):
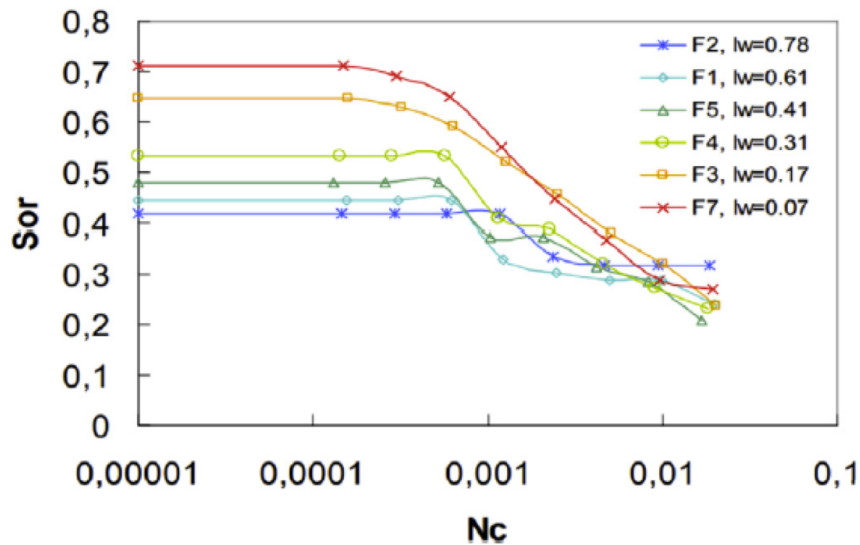
Figure 3.3: Capillary Desaturation Curves at various wettabilities[48]

Figure 3.3 shows that the initial S_{or} is strongly is function of the rock wettability. The pore geometry (pore size distribution) also has a significant effect on the initial S_{or}[67]. The wider the pore size distribution, the larger the initial S_{or}. At low capillary number, a residual oil saturation plateau region is seen in the curve. As the N_c increases above a critical value known as the critical capillary number (N_{cc}), a decrease in the S_{or} is observed. The critical capillary number depends on the rock wettability, rock structure, permeability, and fluid types[48].

3.2.2. Types of surfactants

Surfactants, also known as surface active agents, are organic compounds made up of both hydrophobic and hydrophilic groups (that is they are amphiphilic). The hydrophobic group forms the tail of the surfactant and is composed of a hydrocarbon chain while the hydrophilic group forms the head. The amphiphilic nature of surfactants prevents them from thriving in either a pure water or oil phase. They therefore adsorb at the interface between the two fluids, with the hydrophilic head in the water phase and the hydrophobic tail in the oil phase. This changes the interfacial properties of the system resulting in a reduction in the IFT[74]. Based on the ionic nature of the head group, surfactants are divided into four classes:

Anionic surfactants are characterized by a negatively charged hydrophilic group. They are the most commonly used surfactants in chemical EOR processes because they are effective at reducing IFT, cheap, thermally stable and have a relatively rate of adsorption on sandstone rocks[74]. Their negatively charged nature implies that they are mostly used only in sandstone reservoirs whose surface charge is also negative. Common examples include: sulfates, carboxylates and sulfonates. Cationic surfactants are the direct opposite of anionic surfactants. They have a positively charged head, which limits their applicability to carbonate reservoirs only. An example of cationic surfactants is alkyltrimethylammonium salts. They are both known as ionic surfactants.

Non-ionic surfactants carry no charge in their hydrophilic head. They are more tolerant to a high salinity environment than the ionic surfactants. However, they are less effective at reducing IFT. As such, they are mostly used as cosurfactants, in order to improve the phase behavior of the system. Fatty alcohols and alkylphenol ethoxylates are typical examples of non-ionic surfactants. The last class of surfactants consists of two active groups and they are called zwitterionic or amphoteric surfactants. The two groups can either be cationic-non-ionic, cationic-anionic or anionic-non-ionic. Zwitterionic surfactants are both temperature and salinity-tolerant, but they are also expensive and are therefore rarely used[74].

3.2.3. Characterization of surfactants

There are many methods used to characterize surfactants; some of which are discussed below:

Hydrophile-lipophile balance (HLB)

The hydrophile-lipophile balance is an indication of the tendency of surfactants to solubilize in water or oil, thereby forming water-in-oil or oil-in-water emulsions[74]. A low HLB implies the surfactant is more soluble in oil, and forms water-in-oil emulsions. Surfactants of low HLB have the ability to form middle phase emulsions in a low salinity environment, while surfactants of high HLB can form middle phase emulsions when the formation salinity is high. They should therefore be selected accordingly[74].

Critical micelle concentration (CMC)

CMC refers to the surfactant concentration above which micelles spontaneously form. When surfactants are introduced into a system, they reduce the system free energy (surface

tension) by initially partitioning into the interface; reducing the interfacial energy and shielding the hydrophobic parts from having contact with water. As the amount of surfactants at the interface increases, the surfactants adsorb at the interface. When the interface becomes saturated, the surfactants start aggregating into micelles to prevent contact between the hydrophobic parts and water as shown in fig. 3.4. After the CMC is reached, the addition of surfactants results in no further decrease in the surface tension (or IFT)[74].
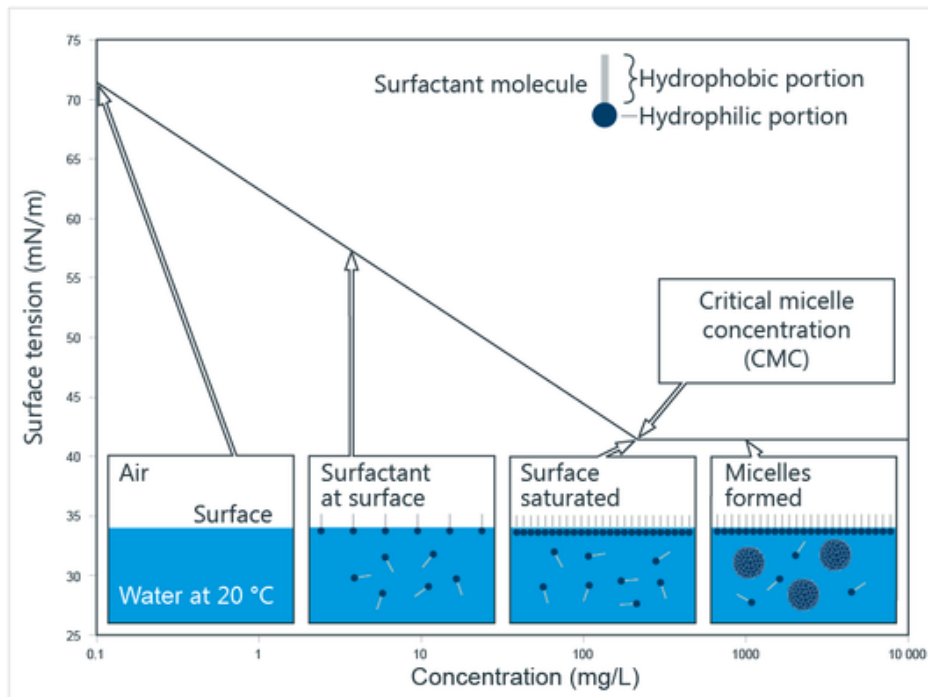
Figure 3.4: Surface tension of a surfactant solution below and above the CMC[53].

Solubilization ratio

The solubilization ratio of oil or water is the ratio of the volume of solubilized oil or water to the volume of surfactant in the microemulsion phase. It is closely related to the interfacial tension. The minimum value of IFT between water and oil is reached when their solubilization ratios are equal, which also corresponds to the optimal salinity[74,79].

3.2.4. Surfactant phase behavior

The salinity of brine has a strong effect on the phase behavior of surfactants. If the brine salinity is high, the surfactant moves from the aqueous phase to the oil phase due to an increase in the aqueous phase electrolytic concentration. This results in the formation of a water-in-oil microemulsion; also known as Upper-phase or Winsor Type II microemulsion. At low brine salinities, the surfactant solubilizes in the aqueous phase forming an oil-in-water emulsion (Lower-phase or Winsor Type I microemulsion). A middle-phase microemulsion (Winsor Type III microemulsion) is formed at intermediate salinity levels, where the surfactant separates into a separate phase from oil and water[74].

The three types of microemulsions and the effect of brine salinity on surfactant phase behavior is shown in fig. 3.5. A ternary diagram is conventionally used to illustrate the surfactant-brine-oil phase behavior as shown in fig. 3.5, with the surfactant pseudo-component at the apex and oil and water at the lower left and right, respectively. In the case of lower-phase microemulsion, it can be seen that the slope of the tie lines is negative; which is why it is also called type II(-) microemulsion. A similar naming convention applies to the intermediate and upper-phase microemulsions.
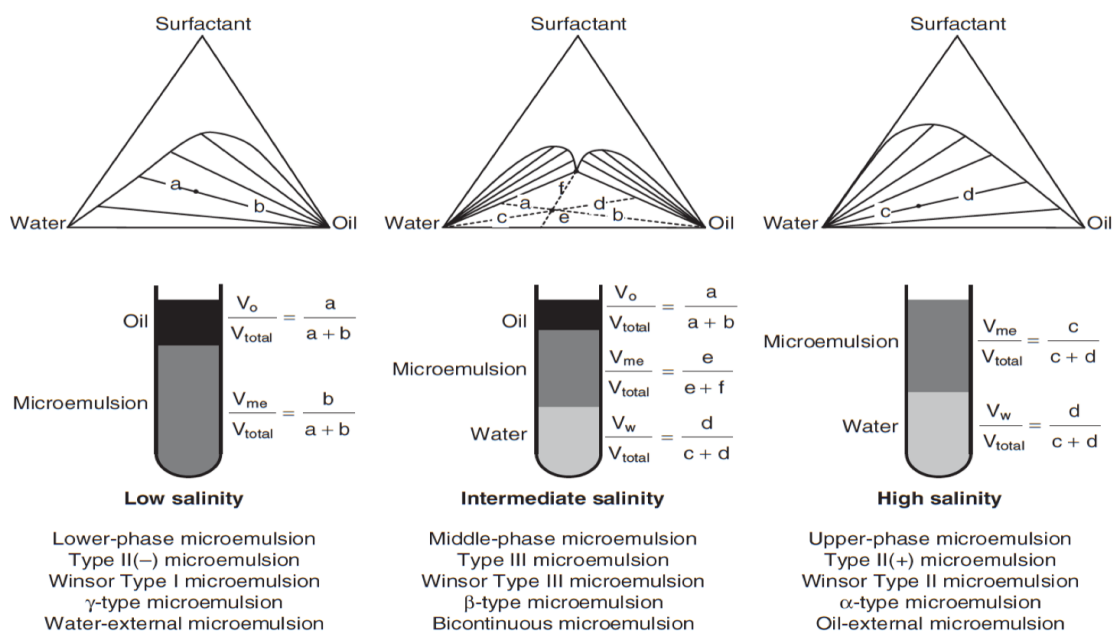
Figure 3.5: The effect of brine salinity on surfactant phase behavior and the types of microemulsion formed[74]

3.2.5. Surfactant retention

The success or failure of a surfactant flooding project is determined by the degree of surfactant retention in the porous media[74]. Four different mechanisms contribute to surfactant retention and they include: precipitation, adsorption, phase trapping and ion exchange. In this thesis however, surfactant retention was modeled only as a function of adsorption, as will be further discussed in the next chapter. The different mechanisms are described below:

Precipitation

As discussed above, surfactant solubility decreases with salinity. At some salinity, the aggregation or precipitation of surfactant starts. In the presence of divalent or multivalent cations such as Ca^{2+} and Mg^{2+}, a divalent complex with limited solubility in water is formed. This causes the precipitation of surfactant from the solution. As the surfactant concentration is increased, the precipitates redissolve. A further increase in the surfactant concentration results in re-precipitation[74]. This implies that a reversible reaction occurs with increasing surfactant concentration:

$$2\,(R-SO_3) + M^{2+} \longleftrightarrow M(R-SO_3)_2 \downarrow \qquad \text{(R1)}$$
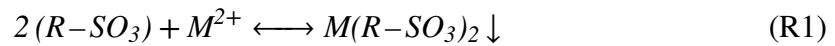
Where R-SO$_3$ and M represent a surfactant and divalent ion, respectively.

Adsorption

Surfactant adsorption varies with rock type and surfactant type. Anionic surfactants have much less adsorption in sandstones compared to non-ionic surfactants, whereas the reverse is true for carbonates[74]. From an adsorption standpoint, non-ionic surfactants are therefore a better option for carbonates. The degree of surfactant adsorption typically increases with surfactant concentration. At some very high concentration, a plateau is reached; which represents the CMC for pure surfactants.

Phase trapping

It is strongly related to the type of microemulsion formed. For a Winsor Type I microemulsion, very little phase trapping is observed because the microemulsion is the water-external phase and can therefore be miscibly displaced by the chase water. For a Winsor Type II microemulsion, the microemulsion is an oil-external phase while the chase water is an aqueous phase. The viscosity of the microemulsion could be much higher than that of the chase water. Also, a very high IFT behind the microemulsion slug could make the microemulsion and chase water immiscible, such that the microemulsion phase is easily bypassed by the chase water resulting in phase trapping[74].

Ion exchange

Ion exchange between the clay surface (in sandstones) or rock surface (in carbonates) and the brine/surfactant system could occur in brines with a high concentration of multivalent cations such as Ca^{2+} and Mg^{2+}, resulting in the surfactant retention[67].

3.3. Low Salinity Surfactant Flooding

Despite the lack of consensus on the main mechanisms responsible for the observed low salinity effects, recent studies have shown that combining LSWF with other chemical EOR methods such surfactant or polymer flooding helps to improve the performance of the chemicals through more favorable phase behavior such as improved solubility and reduced adsorption or retention[8,74]. In a low salinity environment, surfactants form Winsor Type I microemulsion and the surfactant tends to remain in the aqueous phase whereas a Winsor Type II microemulsion is formed at high salinity, and the surfactant is trapped in the oleic phase[8]. In addition, surfactants designed to cope in a high salinity environment are usually more expensive that those that operate in low salinity environments.

The main objective of a hybrid EOR process such as LSS is to combine the benefits from the individual processes such that the overall recovery is higher than the recovery from the individual processes. The addition of surfactants helps to prevent the retrapping of oil mobilized during LSWF[84]. To investigate the combined effect of LSS, Alagic and Skauge[8] performed coreflooding experiments involving a combination LSWF and

surfactant flooding using four outcrop Berea sandstone cores. The cores were aged in crude oil to establish a non water-wet state. Synthetic seawater with total dissolved solids of 36,321 ppm was used to saturate the cores. Low salinity water was made with distilled water containing 0.50 wt% NaCl. The surfactant used was an anionic surfactant; internal olefin sulfonate.

The low salinity brines were used in secondary modes whereas the surfactant was used in tertiary mode during the displacement tests. In one of the tests, seawater (high salinity) was used in secondary mode to investigate the effect of salinity on oil recovery. A higher oil recovery was observed for the cases where LSW was used in secondary mode compared to SW. Water breakthrough was also observed to occur earlier in the case of SW injection, and plateau production was reached earlier in the cases of LSWF. Higher tertiary oil recovery was observed for all the cases. However, significantly higher tertiary recovery was obtained in a low salinity environment than in the high salinity environment because the presence of divalent cations (Ca^{2+} and Mg^{2+}) in the high salinity brine reduces the effectiveness of the surfactant[8]. Alameri et al.[9] also performed LSS displacement experiments on heterogeneous low permeability carbonate cores using a non-ionic surfactant; described further in section 4.2.

3.4.   Chapter Summary

This chapter presents a review of literature and important features of enhanced oil recovery, with a focus on chemical EOR. Many laboratory and a few field studies have revealed that LSWF yields a better oil recovery than the conventional high salinity waterflooding. In addition, LSWF is more advantageous than other chemical EOR methods because of its low operating and capital costs, environmentally friendly nature and the fact that it can be implemented in both secondary and tertiary modes. Several mechanisms have been proposed to be responsible for the low salinity effect (LSE) in carbonates including: multicomponent ionic exchange, expansion of the electric double layer, rock dissolution, fines migration, reduction in IFT, increased in pH and the formation of micro-dispersions, although some of the mechanisms have been identified to be related to each other. Conflicting results from experiments have also led to a lack of consensus on the main mechanism(s) for the observed LSE. Wettability alteration is agreed by many authors and researchers to be the main mechanism, although the mechanism responsible for the wettability alteration is still subject to research.

The use of surfactants as a tertiary method of improving oil recovery has also been a frequently used chemical EOR method. Surfactants have the ability to mobilize oil trapped by capillary forces during secondary recovery through a reduction in IFT (increase in capillary number) and wettability alteration. The four types of surfactants based on the ionic nature of the head group include: anionic, cationic, non-ionic and zwitterionic/amphoteric. Many different methods are used to characterize surfactants such as the hydrophile-lipophile balance, the critical micelle concentration, and the solubilization ratio. The three different types of microemulsions formed by surfactants depending on the salinity of the brine include: Winsor Type I, II or III microemulsions. Four mechanisms contribute to the retention of surfactants in porous media, and therefore determine the degree of success or failure of any surfactant flooding project. They are: precipitation, adsorption, phase trapping and ion exchange.

The combination of LSWF and other chemical EOR methods in a hybrid EOR process has recently been gaining a lot of attention. This is because the low salinity environment helps to improve the performance of the chemicals through favorable phase behavior. A few laboratory studies have shown that the combined benefits from a hybrid EOR process could be higher than the benefits from the individual processes.

4. Numerical Modeling

Reservoir modeling is a very valuable tool for the verification and validation of experimental results, and also for predictions at conditions beyond the scope of experimental work[32]. However, the number of modeling studies on LSWF and LSS in carbonates are relatively much fewer than in sandstones. This is because more time has been dedicated to understanding the mechanisms responsible for the incremental oil recovery in carbonates through laboratory studies. In addition, modeling based on the geochemical reactions that occur between the carbonate rock surface and the aqueous phases was further delayed by the complex nature of the COBR interactions and heterogeneity in carbonates[1].

Jerauld et al.[46,47] presented one of the earliest models on LSWF; which considered salt as an additional component lumped in the aqueous phase. Relative permeability, capillary pressure, and aqueous phase density and viscosity were all modeled as functions of salinity. In the model, however, residual oil saturation was assumed to be linearly dependent on salinity. The model equations for relative permeability and capillary pressure are presented below:

$$k_{rw} = \theta k_{rw}^{HS}(S^*) + (1 - \theta)k_{rw}^{LS}(S^*) \tag{4.1}$$

$$k_{row} = \theta k_{row}^{HS}(S^*) + (1 - \theta)k_{row}^{LS}(S^*) \tag{4.2}$$

$$P_{cow} = \theta P_{cow}^{HS}(S^*) + (1 - \theta)P_{cow}^{LS}(S^*) \tag{4.3}$$

$$\theta = (S_{orw} - S_{orw}^{LS})/(S_{orw}^{HS} - S_{orw}^{LS}) \tag{4.4}$$

$$S^* = (S_o - S_{orw})/(1 - S_{wr} - S_{orw}) \tag{4.5}$$

Although the same scaling factor proposed by Jerauld et al. is currently used by most LSWF models, Al-Shalabi et al.[6] pointed out the need to use different scaling parameters for handling the relative permeability and capillary pressure of oil and water, respectively. They used UTCHEM; an in-house simulator at the University of Texas at Austin to simulate and history match coreflood experiments done on composite carbonate cores. It was observed that LSWF had negligible effect on the endpoint water relative permeability and Corey water exponent[6]. They also highlighted the need for geochemical modeling of LSWF to investigate the change in surface charge and expansion of the EDL.

Dang et al.[29] developed a comprehensive ion exchange model that captures the geochemical reactions occurring during LSWF. The model was coupled with the compositional simulator; GEM from CMG and was validated with the ion exchange model of PHREEQC and two coreflood experiments for a North Sea reservoir and a heterogeneous sandstone Texas reservoir. The geochemistry model was also used to evaluate LSWF optimization through well placement, and they investigated the potential of a hybrid EOR process that involved combining LSWF and CO_2 injection in a miscible WAG process[28,30].

A geochemical model that uses the equivalent fraction of divalent cations (Ca^{2+} and Mg^{2+}) was proposed by Awolayo et al.[18]. The model was used to history match several carbonate coreflood experiments. Based on the simulation results, they concluded that the interplay

between surface charge alteration and mineral dissolution was key to the improved oil recovery at core-scale.

Tavassoli et al.[84] proposed a multi-mechanistic approach for modeling LSS flooding, which incorporates wettability alteration mechanism associated with LSWF and IFT reduction associated with surfactant flooding. The model was implemented in UTCHEM-IPHREEQC and used to match LSS flooding experimental results by Alagic and Skauge[8]. In their model, EDL expansion was assumed to be the main mechanism responsible for wettability alteration, and thus they used total ionic strength as the interpolation parameter for relative permeability. Multiphase relative permeabilities were modeled using Corey-type equations as a function of trapping number (N_T) to account for the effect of gravity and viscous forces on the mobilization of trapped oil[84]. The relationship between residual oil saturation and IFT was also modeled as a function of N_T. Surfactant adsorption was modeled using a Langmuir-type isotherm that takes into account salinity, rock permeability and surfactant concentration. An excellent match was obtained between simulation and experimental results.

To the best of my knowledge, very few geochemical modeling study has been done on low salinity surfactant flooding in carbonates so far. This thesis describes the geochemical modeling of LSWF and LSS in heterogeneous low-permeability carbonates cores using the geochemistry model embedded in the CMG-GEM reservoir simulator. First of all, the models are built and simulations are done to history match the LSWF coreflood experimental results. Then, some modifications are made to the models to simulate surfactant flooding in tertiary mode with SW injection in secondary mode. Finally, one of the models is modified to simulate LSS flooding; to investigate the combined benefits from the process. Sensitivity analysis is then performed to investigate the effects of key parameters on the results obtained.

This chapter begins by providing a brief description of the reservoir simulator used for modeling and numerical simulations in this thesis, after which a discussion of the experimental data is provided. A comprehensive description of the geochemistry model follows, and the chapter is concluded by a description of the simulation models.

4.1. Reservoir Simulator

The CMG-GEM 2018.10 reservoir simulator was used in this thesis for modeling LSWF and LSS in carbonates cores. It is an efficient, multidimensional, equation-of-state (EOS) compositional simulator developed by the Computer Modelling Group (CMG)[26]. GEM™ is suitable for modeling LSWF and LSS because it captures most the important chemical and physical phenomena that occur during the two processes, which include intra-aqueous reactions, mineral dissolution/precipitation, IFT reduction and wettability alteration[26,29]. It utilizes either the Peng-Robinson (PR) or the Soave-Redlich-Kwong (SRK) EOS for phase equilibrium calculations and for predicting the density and viscosity of the oil and gas phases[26]. The PR EOS was used in this thesis for all the simulations.

The first step to running a simulation in GEM™ is the creation of an input file (data file) in which reservoir parameters, fluid properties and the desired recovery mechanism are

defined. After the simulation is run, the initial input file is used by GEM™ to create three new files; an output restart file (RST), an output simulation results file (SRF), and an output file. After the simulation run is complete, the results can be opened using the Results software by CMG for visualization and analyses of the results. Results™ consists of two components: Plots; where well, field, and special history data, and block properties can be plotted over time and distance, and Reservoir; where changes in reservoir properties can be visualized overtime either in two or three-dimensions (2D or 3D).

4.2.   Experimental Data

Two coreflood experiments were performed by Alameri et al.[9] on heterogeneous low permeability carbonate cores. The carbonate cores used for the experiments were from two facies; Facies 5 and 6 of a Middle Eastern carbonate reservoir. The experiments were aimed at investigating the viability of a hybrid of low salinity water-surfactant EOR process.

The cores were first flooded with formation water at a rate of 0.1 ml/min so that the core is initially 100% saturated with brine. Oil was then injected into the cores at the same flow rate until irreducible water saturation was reached (S_{wi}). The carbonate cores were then aged for eight weeks at reservoir temperature (195°F) and pressure, for restoration of the wettability. After ageing, the cores were flooded with synthetic seawater at a flow rate of 0.1 ml/min until residual oil saturation. Brines of different salinities (LS1, LS2 and LS3) were then injected to study the effect of low salinity brine on wettability alteration and oil recovery[9].

LS1, LS2 and LS3 brines were made by diluting SW twice, four times and fifty times, respectively. 5 pore volumes (PV) were injected for each set of low salinity water. After low salinity waterflooding, the cores were flooded with a non-ionic, ethoxylated alcohol surfactant. For the first coreflood experiment, 10 PV were injected with 5000 ppm surfactant diluted in LS2 brine, while 5 PV were injected with 1000 ppm of surfactant diluted in LS2 brine for the second coreflood experiment. The same injection rate of 0.1 ml/min was used for both cases. Oil recovery and pressure drop for all the flooding experiments were measured and recorded and are shown in figs. A.1 and A.2. More information about the experimental work can be found in Alameri et al.[9] and Teklu et al.[85].

4.3.   Geochemistry

During low salinity waterflooding, the initial thermodynamic equilibrium of the system is disrupted through the geochemical reactions that occur at the rock/brine interface[1,28,45]. The geochemical reactions can be divided into homogeneous and heterogeneous reactions. The homogeneous reactions occur between the aqueous phase components, and are also known as intra-aqueous reactions whereas the heterogeneous reactions occur between the aqueous components and mineral species such as mineral dissolution/precipitation and

ion exchange reactions[26]. The two types of reactions are typically represented as chemical equilibrium reactions and rate-dependent reactions, respectively, because the intra-aqueous reactions are relatively faster than the mineral dissolution/precipitation reactions.

4.3.1. Governing equations

Fluid flow in the reservoir or any porous medium is governed by Darcy's law. The diffusion and dispersion of components in the aqueous phase also contributes to the movement of the aqueous phase components[26,63]. The three different species involved in the geochemical reactions during LSWF and LSS include: hydrocarbon components (n_h) that may be soluble in the aqueous phase, aqueous phase components (n_a) and mineral components (n_m). The conservation equations for the different species are given in eqs. (4.6) to (4.8):

$$\psi_i \equiv \sum_{\alpha=o,g,w} \Delta T_\alpha^u y_{i\alpha}^u \left(\Delta P^{n+1} + \Delta P_{c\alpha}^u - \tilde{\rho}_\alpha^u g \Delta d \right) + \sum_{q=g,o,w} \Delta D_{iq}^u \Delta y_{iq}^u +$$

$$V\sigma_{i,aq}^{n+1} + q_i^{n+1} - \frac{V}{\Delta t} \left(N_i^{n+1} - N_i^n \right) = 0, \quad i = 1, ..., n_h \quad (4.6)$$

$$\psi_j \equiv \Delta T_w^u y_{jw}^u \left(\Delta P^{n+1} - \tilde{\rho}_w^u g \Delta d \right) + \Delta D_{iw}^u \Delta y_{iw}^u + V\sigma_{j,aq}^{n+1} +$$

$$V\sigma_{j,mn}^{n+1} + q_j^{n+1} - \frac{V}{\Delta t} \left(N_{ja}^{n+1} - N_{ja}^n \right) = 0, \quad j = 1, ..., n_a \quad (4.7)$$

$$\psi_k \equiv V\sigma_{k,mn}^{n+1} - \frac{V}{\Delta t} \left(N_k^{n+1} - N_k^n \right) = 0, \quad k = 1, ..., n_m \quad (4.8)$$

The superscripts n and n+1 in the above equations denote the old and new time levels, respectively. The discretization of the equations is done in an adaptive implicit manner where explicit and implicit gridblocks are respectively denoted by the superscript u = n or u = n+1. The intra-aqueous reaction rates and mineral dissolution/precipitation rates are represented by the terms $V\sigma_{i,aq}^{n+1}$ and $V\sigma_{k,mn}^{n+1}$, respectively. A discussion on intra-aqueous reactions and mineral dissolution/precipitation reactions is provided in the next subsections.

4.3.2. Intra-aqueous reactions

According to Bethke[20], equilibrium constants are used in modeling chemical equilibrium reactions. For a chemical reaction to be in thermodynamic equilibrium, the rate of the forward and backward reactions must be equal; implying that the activity product of the reaction must be equal to its equilibrium constant. This concept gives rise to the governing equations for chemical equilibrium reactions:

$$Q_\alpha - K_{eq,\alpha} = 0, \quad \alpha = 1, ..., R_{aq} \quad (4.9)$$

$$Q_\alpha = \prod_{i=1}^{n_{aq}} a_i^{v_{i\alpha}} \quad (4.10)$$

where $K_{eq,\alpha}$ is the equilibrium constant for aqueous reaction α, R_{aq} is the number of aqueous phase reactions, Q_α is the activity product, and a_i and $v_{i\alpha}$ are the activity of component

k and the stoichiometry coefficients, respectively. The aqueous phase components consists of both components that only exist in the aqueous phase (n_a components) and gaseous components that are soluble in the aqueous phase, n_c. The total number of components in the aqueous phase, n_{aq} is the sum of the two. The aqueous species can also be divided into independent (primary) and dependent (secondary) aqueous species.

Tables of values of the equilibrium constants for many reactions as a function of temperature can be found in the works by Delaney and Lundeen[31] and Kharaka et al.[52]. The relationship between the activities of a species i, a_i and its molality, m_i is given in eq. (4.11). The molality of a species is its moles per kilogram (mol/kg) of water, and is expressed in units molal (M).

$$a_i = \gamma_i m_i, \quad i = 1, ..., n_{aq} \tag{4.11}$$

γ_i in the above equation is the activity coefficient. The activity of an ideal solution is equal to its molality because $\gamma_i = 1$. However, most solutions are non-ideal and a value other than one is required for γ_i. Many models exists for calculating the activity coefficients of electrolytic solutions such as the Debye-Hückel equation, the Davies equation and the B-Dot model[20]. An activity coefficient model describes the relation between a species' activity coefficient and the ionic strength (I) of the solution. The Davies and B-Dot models are variants of the Debye-Hückel equation developed by Debye and Hückel in 1923[20]. In GEM™, computations of the ionic activity coefficients are done using the B-Dot model. The model is widely applied in many geochemical models because it can accurately predict the activity coefficients of species over a wide range of temperature (0-300°C) and molality (up to 3M ionic strength of a solution with NaCl as the dominant solute), compared to the other models[20]. The expressions for the B-Dot equation and ionic strength are given in eqs. (4.12) and (4.13):

$$\log \gamma_i = -\frac{A_\gamma z_i^2 \sqrt{I}}{1 + \mathring{a}_i B_\gamma \sqrt{I}} + \dot{B} \tag{4.12}$$

$$I = \frac{1}{2} \sum_{i=1}^{n_{aq}} m_i z_i^2 \tag{4.13}$$

A_γ, B_γ and $\dot{B}$ are temperature dependent coefficients, $\mathring{a}_i$ is the ion size parameter (constant), z_i is the valence number of species i, and m_i is its molality[20,26].

4.3.3. Mineral dissolution and precipitation reactions

Reactions involving minerals and aqueous species are slower than aqueous reactions, and are modeled using kinetic rate laws[20,26]. The expression for the rate law for mineral dissolution and precipitation is given in eq. (4.14):

$$r_\beta = \hat{A}_\beta k_\beta \left(1 - \frac{Q_\beta}{K_{eq,\beta}}\right), \quad \beta = 1, ... R_{mn} \tag{4.14}$$

where r_β is the reaction rate, $\hat{A}_\beta$ is the reactive surface area for mineral β, and k_β, $K_{eq,\beta}$ and Q_β are the rate constant, equilibrium constant and activity product for mineral reaction

β, respectively. Q_β is similar to the activity product for aqueous chemical equilibrium reactions given in eq. (4.10):

$$Q_\beta = \prod_{i=1}^{n_{aq}} a_i^{v_{i\alpha}} \tag{4.15}$$

The activities of minerals are equal to unity and are therefore not included in the above equation. The ratio $(Q_\beta/K_{eq,\beta})$ in eq. (4.14) is called the saturation index. Mineral dissolution occurs if $\log(Q_\beta/K_{eq,\beta})<0$ while mineral precipitation occurs if $\log(Q_\beta/K_{eq,\beta})>0$. If $\log(Q_\beta/K_{eq,\beta})=0$, the mineral is in equilibrium with the aqueous phase and no reaction occurs ($r_\beta = 0$). Equation (4.14) applies to minerals only. The rate of formation/consumption of different aqueous species is obtained by multiplying r_β by the respective stoichiometry coefficient[26,63]:

$$r_{k\beta} = v_{k\beta} \cdot r_\beta \tag{4.16}$$

Reaction rate constant for different reactions are normally reported in literature at a reference temperature, T_0 (usually 298.15K or 25°C). The temperature of petroleum reservoirs is typically higher than T_0. To calculate the rate constant at a different temperature T, eq. (4.17) is used:

$$k_\beta = k_{0\beta} \exp\left[-\frac{E_{a\beta}}{R}\left(\frac{1}{T} - \frac{1}{T_0}\right)\right] \tag{4.17}$$

where $E_{a\beta}$ and $k_{0\beta}$ are the activation energy for reaction β (J/mol) and the rate constant for reaction β at the reference temperature, T_0, R is the universal gas constant (8.314J/mol-K). Both T and T_0 are in Kelvin (K). The activation energy (E_a) needed for the chemical reactions that result in wettability modification during LSWF is very important because if the reaction rate is slow, no new equilibrium would be established during the LSWF interval and thus no low salinity effects would be observed[70]. The activation energy is related to how strongly the polar oil components are bonded to the mineral surface, the solvency of the polar components in the actual phases and the reactivity of the ions in the injected water. The bonding energy between polar compounds in oil and carbonates is generally higher than that between the oil and clays in sandstones[70].

The equilibrium constants for aqueous and mineral reactions can alternatively be calculated using a fourth order polynomial expression as a function of reservoir temperature, T:

$$\log(K_{eq}) = a_0 + a_1 T + a_2 T^2 + a_3 T^3 + a_4 T^4 \tag{4.18}$$

The default values of a_0, a_1, a_2, a_3 and a_4 for the different reactions are specified GEM's internal library and the reservoir temperature, T is 90.6°C. In this thesis, eq. (4.18) is used to calculate the equilibrium constants for all the aqueous and mineral reactions used in the modeling studies.

As mineral dissolution/precipitation occurs, the surface area available for reactions also changes, and therefore the reactive surface area is an important parameter when calculating the reaction rate. The change in the reactive surface area as minerals dissolve/precipitate is calculated using eq. (4.19)[26,63]:

$$\hat{A}_\beta = \hat{A}_\beta^0 \cdot \frac{N_\beta}{N_\beta^0} \tag{4.19}$$

where $\hat{A}_\beta^0$ and N_β^0 are the reactive surface area and the number of moles of mineral β per unit gridblock bulk volume at time 0 and N_β is the number of moles of mineral β per unit gridblock bulk volume at current time.

In addition, both the void volume (porosity) and permeability of the porous medium are altered as a result of mineral dissolution and precipitation. Equations (4.20) and (4.21) are the expressions used in calculating the change in porosity:

$$\hat{\phi}^* = \phi^* - \sum_{\beta=1}^{n_m} \left(\frac{N_\beta}{\rho_\beta} - \frac{N_\beta^0}{\rho_\beta} \right) \tag{4.20}$$

$$\phi = \hat{\phi}^*[1 + c_\phi(p - p*)] \tag{4.21}$$

where ϕ is the new porosity, ϕ^* is the reference porosity with no mineral dissolution/precipitation, $\hat{\phi}^*$ is the porosity with dissolution/precipitation, ρ_β is the mineral's molar density, c_ϕ is the rock compressibility, p and p^* are the current and reference pressures, respectively.

To calculate the change in permeability, the Kozeny-Carman equation is used:

$$\frac{k}{k^0} = \left(\frac{\phi}{\phi^0} \right)^3 \cdot \left(\frac{1 - \phi^0}{1 - \phi} \right)^2 \tag{4.22}$$

where k^0 is the initial permeability and ϕ^0 is the initial porosity.

4.3.4. Ion exchange reactions

When water with a different ionic composition to the formation water is injected, multiple ion exchange and geochemical reactions occur between the ions in the aqueous phase and the rock surface. The exchange reactions are fast and homogeneous, and are therefore modeled as chemical equilibrium reactions[18,26]. The multiple ion exchange and geochemical reactions are key to the increase in oil recovery during LSWF. However, they differ with the reservoir rock type. As earlier discussed in section 3.1.3, sulfate ions are adsorbed from the aqueous phase during LSWF in carbonates, which reduces the surface charge allowing the adsorption of cations from the aqueous phase.

In this thesis, multicomponent ion exchange and the resulting wettability alteration during low salinity waterflooding is modeled using the exchange of divalent cations; Ca^{2+} and Mg^{2+}. The ion exchange reactions are shown in table 4.2. The X in the reactions represents the ion exchanger on the carbonate rock surface. During low salinity waterflooding, Ca^{2+} and Mg^{2+} are taken up by the exchanger, while Na^+ is released. The reverse process occurs during high salinity waterflooding[26]. Ion exchange reactions are characterized by equilibrium constants, like chemical equilibrium reactions:

$$K_{Na/Ca} = \frac{[a(Ca^{2+})]^{1/2}a(Na - X)}{a(Na^+)[a(Ca - X_2)]^{1/2}} \tag{4.23}$$

$$K_{Na/Mg} = \frac{[a(Mg^{2+}]^{1/2}a(Na-X)}{a(Na^+)[a(Mg-X_2)]^{1/2}} \tag{4.24}$$

where a is the activity. It is however difficult to evaluate the activity coefficients of Na-X, Ca-X_2 and Mg-X_2, and thus, selectivity coefficients are used in the place of equilibrium constants according to the Thomas-Gaines convention[14]. Rewriting eqs. (4.23) and (4.24) in terms of the selectivity coefficients results in the expressions in eqs. (4.25) and (4.26):

$$K'_{Na/Ca} = \frac{\zeta(Na-X)[m(Ca^{2+})]^{0.5}}{[\zeta(Ca-X_2)]^{0.5}m(Na^+)} \cdot \frac{[\gamma(Ca^{2+})]^{0.5}}{\gamma(Na^+)} \tag{4.25}$$

$$K'_{Na/Mg} = \frac{\zeta(Na-X)[m(Mg^{2+})]^{0.5}}{[\zeta(Mg-X_2)]^{0.5}m(Na^+)} \cdot \frac{[\gamma(Mg^{2+})]^{0.5}}{\gamma(Na^+)} \tag{4.26}$$

where $\zeta[i-X_a]$ $(i = Na^+, Ca^{2+} or Mg^{2+}$ and a is the valency) is the ion exchange equivalent fraction on the exchanger, m is the molality and γ is the activity coefficient. An important property of the exchanger is its cation exchanger capacity (CEC), which describes the amount of ions that can be adsorbed on its surface. The moles of all components in GEM™ are expressed as moles per gridblock bulk volume, N. Thus, if V is the bulk volume of the rock, the total moles of the exchangeable species (Na-X, Mg-X_2 and Ca-X_2) would be $VN_{(i-X_a)}$. Equation (4.27) must therefore be satisfied for a given value of CEC in the gridblock:

$$VN_{Na-X_2} + 2VN_{Ca-X_2} + 2VN_{Mg-X_2} = V\phi(CEC) \tag{4.27}$$

The equivalent fractions of the exchangeable species is calculated by:

$$\zeta(Na-X) = \frac{N_{Na-X}}{\phi CEC} \tag{4.28}$$

$$\zeta(Ca-X_2) = \frac{N_{Ca-X_2}}{\phi CEC} \tag{4.29}$$

$$\zeta(Mg-X_2) = \frac{N_{Mg-X_2}}{\phi CEC} \tag{4.30}$$

where $\phi CEC = N_{Na-X} + 2N_{Ca-X_2} + 2N_{Mg-X_2}$

Table 4.1 shows the various species used in the simulations done in this thesis. All the intra-aqueous, mineral and ion-exchange reactions used in the modeling of low salinity waterflooding and low salinity surfactant flooding are provided in table 4.2.

Table 4.1: List of the aqueous, solid and exchange species used in coreflood simulations

Species	Elements
Independent aqueous species	H^+, OH^-, HCO_3^-, Ca^{2+}, CH_3COO^-, SO_4^{2-}, Mg^{2+}, Na^+, Cl^-
Dependent aqueous species	$CaCH_3COO^+$, $CaSO_4$, $MgSO_4$, $NaCl$, H_2O, CO_2
Solid species	Calcite ($CaCO_3$), Dolomite ($CaMg(CO_3)_2$)
Exchange species	Na^+, Ca^{2+}, Mg^{2+}

Table 4.2: List of aqueous, mineral and ion exchange reactions used in simulations

Aqueous Reactions	Equilibrium Constants
$CO_2 + H_2O \longleftrightarrow H^+ + HCO_3^-$	$K_1^{eq} = 10^{-6.39}$
$H^+ + OH^- \longleftrightarrow H_2O$	$K_2^{eq} = 10^{12.39}$
$CaCH_3COO^+ \longleftrightarrow CH_3COO^- + Ca^{2+}$	$K_3^{eq} = 10^{0.38}$
$CaHCO^{3+} \longleftrightarrow Ca^{2+} + HCO_3^-$	$K_4^{eq} = 10^{-1.51}$
$CaSO_4 \longleftrightarrow Ca^{2+} + SO_4^{2-}$	$K_5^{eq} = 10^{-2.69}$
$MgSO_4 \longleftrightarrow Mg^{2+} + SO_4^{2-}$	$K_6^{eq} = 10^{-2.54}$
$HSO_4^- \longleftrightarrow H^+ + SO_4^{2-}$	$K_7^{eq} = 10^{-3.06}$
$NaCl \longleftrightarrow Cl^- + Na^+$	$K_8^{eq} = 10^{1.06}$
Mineral Reactions	**Solubility Product**
$(CaCO_3) + H^+ \longleftrightarrow Ca^{2+} + HCO_3^-$	$K_1^{sp} = 10^{6.41}$
$(CaMg(CO_3)_2) + 2H^+ \longleftrightarrow Ca^{2+} + Mg^{2+} + 2HCO_3^-$	$K_2^{sp} = 10^{2.53}$
Ion Exchange Reactions	**Selectivity Coefficient**
$Na^+ + \frac{1}{2}Ca{-}X_2 \longleftrightarrow \frac{1}{2}Ca^{2+} + Na{-}X$	$K_1' = 10^{0.67}$
$Na^+ + \frac{1}{2}Mg{-}X_2 \longleftrightarrow \frac{1}{2}Mg^{2+} + Na{-}X$	$K_2' = 10^{0.58}$

4.4. Wettability Alteration Modeling

The change in wettability from more oil-wet to intermediate wet during low salinity waterflooding was proposed as the reason behind the observed increase in oil recovery from the coreflood experiments. Wettability alteration is modeled in terms of a change in the relative permeability where two separate relative permeability curves are defined; one for seawater (high salinity) and the other for low salinity water. The Brooks-Corey relative permeability functions defined in eqs. (2.16) to (2.18) were used to obtain the oil and water relative permeability curves. The relative permeability tables in the model are defined under the ROCKFLUID section, which begins with RPT keyword; denoting

the designated rock type. This is followed by a definition of the interpolant used for interpolation between the different sets of relative permeability curves.

In this thesis, multicomponent ion exchange is assumed to be the main mechanism responsible for the change in wettability, and is modeled using the ion exchange equivalent fraction of Mg^{2+} ($\zeta[Mg-X_2]$) as the interpolant for the relative permeability curves. $\zeta[Mg-X_2]$ represents the amount of Mg^{2+} that is adsorbed on the carbonate surface during the process. Zhang et al.[91,92] reported that there is a high tendency of Mg^{2+} to substitute Ca^{2+} on the rock surface at high temperatures (usually 90°C-110°C). The reservoir temperature in this case is 90.6°C, thus using $\zeta[Mg-X_2]$ as the interpolant is a reasonable assumption.

Relative permeability interpolation based on $\zeta[Mg-X_2]$ is activated in the model through the keyword INTCOMP EQVFRIEX 'Mg'. INTCOMP defines the parameter used for interpolation, which in this case is $\zeta[Mg-X_2]$. The values of the interpolant have to also be defined for the interpolation to occur. This is done using the keyword INTCOMP_VAL after the INTCOMP EQVFRIEX 'Mg' keyword. Calculations of the equivalent fractions for the ions involved in the ion exchange process are done during the simulations and based on the values calculated and the values defined in the relative permeability tables, the interpolations are performed. The modeling done in this thesis assumes that if $\zeta[Mg-X_2]$ is less than or equal to 0.33, the oil-wet relative permeability curves are used whereas the less oil-wet curves are used when $\zeta[Mg-X_2]$ is greater than or equal to 0.43. For $\zeta[Mg-X_2]$ values between 0.33 and 0.43, interpolation is done between the two curves. After specifying the values of the interpolant, the beginning of the oil-water relative permeability table is indicated by the SWT keyword, after which all the lines are treated as rows until a new keyword is encountered.

During surfactant flooding, relative permeability interpolation is based on the oil-water capillary number (N_c). This is activated through the keyword INTCOMP CAPNOW. Interpolation based on capillary number requires that a table consisting of surfactant mole fractions and the corresponding IFT is defined. This is done through the IFTTABLE keyword; which consists of values of the mole fraction of surfactant in the first column versus the respective oil-water IFT in the second column. When the table is defined, the interpolation values can either be based on a linear or logarithmic interpolation of the values in IFTTABLE. Logarithmic interpolation of N_c was used in this thesis, and this was initiated through the INTLOG keyword (that is, INTCOMP_VAL = $\log_{10}(N_c)$). The table requires at least two entries to be able to do the interpolation based on the capillary number, and each entry begins on a new line.

Modeling of wettability alteration for a hybrid EOR process such as the combination of low salinity water and surfactant (LSS) requires the use of two different interpolation routines due to a difference in the mechanism of wettability alteration for the two processes. The definition of two different interpolation routines requires that two separate rock types are defined, using the keywords RPT 1 and RPT 2. For the rock type containing low salinity water curves, the interpolation is based on $\zeta[Mg-X2]$ whereas interpolation is based on the capillary number for the rock type containing surfactant curves. The IFTTABLE used in the simulations was based on experimental measurements of oil-water IFT values in the absence and presence of the surfactant with some minor modifications, and is given in table 4.3.

Table 4.3: Surfactant mole fraction versus oil-water interfacial tension values

cift	sigft
0	20.75
0.00004224	4.54
0.00021121	0.5

$cift$ is the surfactant mole fraction, $sigft$ is the oil-water IFT.

The capillary number in GEM™ is computed using eq. (4.31):

$$N_c = \frac{\mu_o v_o}{\sigma_{ow}} \tag{4.31}$$

where σ_{ow} is the oil-water IFT, μ_o is the oil viscosity, and v_o is the oil phase velocity. The relative permeability for oil and water at any time is obtained using an equation similar to that proposed by Jerauld et al.[46]:

$$k_{rl}^{altered} = \omega k_{rl}^{initial} + (1 - \omega)k_{rl}^{final} \tag{4.32}$$

where ω is a function of the interpolant. When no ion-exchange has occured (no wettability alteration), $\omega = 1$ and $k_{rl}^{altered} = k_{rl}^{initial}$. Similarly, when the ion-exchange process is complete, $\omega = 0$ and $k_{rl}^{altered} = k_{rl}^{final}$ representing the new less oil-wet state. Values for ω at any time during the simulations are computed using eq. (4.33):

$$\omega(\zeta_{Mg-X_2}) = \frac{\zeta_{(Mg-X_2)}^{initial} - \zeta_{(Mg-X_2)}(x, t)}{\zeta_{(Mg-X_2)}^{initial} - \zeta_{(Mg-X_2)}^{final}} \tag{4.33}$$

where $\zeta_{(Mg-X_2)}^{initial}$, $\zeta_{(Mg-X_2)}(x, t)$ and $\zeta_{(Mg-X_2)}^{final}$ are the equivalent fractions at the start of the injection, at any time during the injection, and at the end of the injection process. For interpolation based on capillary number, eq. (4.34) is used:

$$\omega(N_c) = \frac{\log_{10} N_c^{initial} - \log_{10} N_c}{\log_{10} N_c^{initial} - \log_{10} N_c^{final}} \tag{4.34}$$

Similarly, $\log_{10} N_c^{initial}$ is the logarithm of the capillary number at the start of surfactant injection, $\log_{10} N_c$ is the logarithm of the capillary number at any time during surfactant injection and $\log_{10} N_c^{final}$ is the logarithm of the capillary number at the end of surfactant injection. It should however be noted although the interpolation is based on $\log_{10} N_c$, the assumption of an "extreme process" is used to calculate the water and oil relative permeabilities, resulting in straight line curves and a residual oil saturation of zero. The endpoint water relative permeabilities were calculated from the reported pressure drop using Darcy's law. However, some tuning was done to the endpoint values to match the oil recovery and pressure drop. The relative permeability curves used in the coreflood simulations are shown in figs. 4.1 and 4.2.

(a) Coreflood 1   **(b)** Coreflood 2
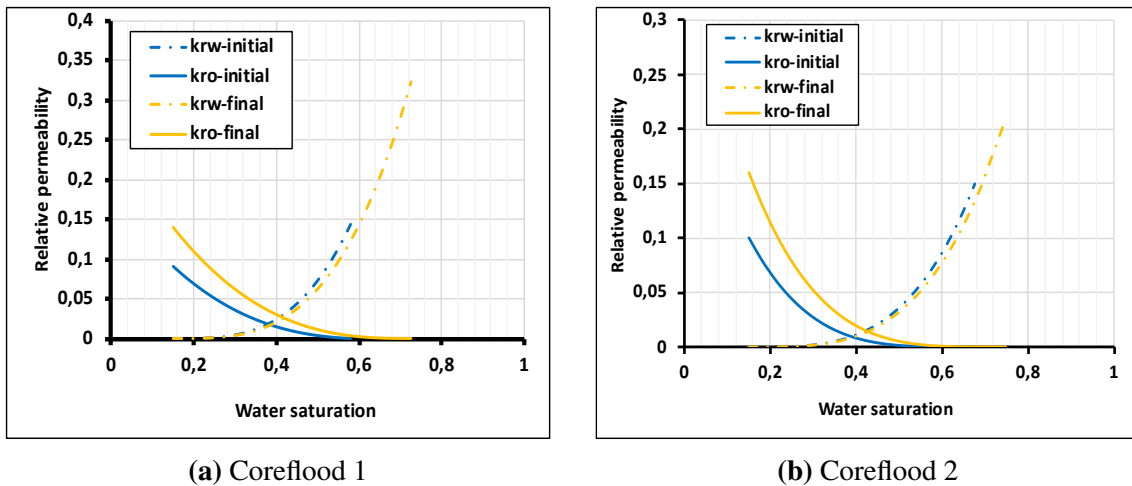
Figure 4.1: Low salinity waterflooding relative permeability curves

(a) Coreflood 1   **(b)** Coreflood 2
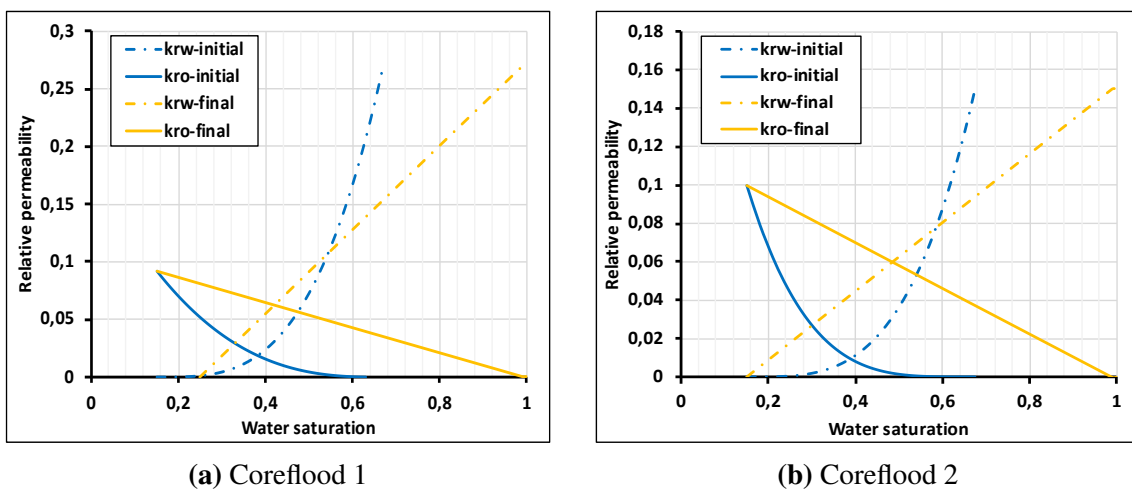
Figure 4.2: Surfactant flooding relative permeability curves

4.5. Capillary Pressure

The effect of capillary pressure on the simulation results and history matching of coreflood data was also taken into account for low salinity waterflooding but was neglected for surfactant injection. Initially, a constant pressure and saturation is defined for all gridblocks. As the different fluids are injected, both the pressure and saturation change. The Skjaeveland capillary pressure correlation was used to model capillary pressure effects on the history match results[76]. The correlation is given in eqs. (4.35) and (4.36) for oil-wet and mixed-wet conditions, respectively:

$$P_c = \frac{C_o}{\left(\frac{S_o - S_{oR}}{1 - S_{oR}}\right)^{a_o}} \tag{4.35}$$

$$P_c = \frac{c_w}{\left(\frac{S_w - S_{wR}}{1 - S_{wR}}\right)^{a_w}} + \frac{c_o}{\left(\frac{S_o - S_{oR}}{1 - S_{oR}}\right)^{a_o}} \tag{4.36}$$

where c_w, c_o, a_w and a_o are all constants for water and oil. c_w and c_o represent the entry pressures whereas a_w and a_o account for the pore size distribution. S_{wR} and S_{oR} are the irreducible water and residual oil saturations, respectively. Figures 4.3 and 4.4 show the imbibition capillary pressure curves used in the two coreflood simulations.
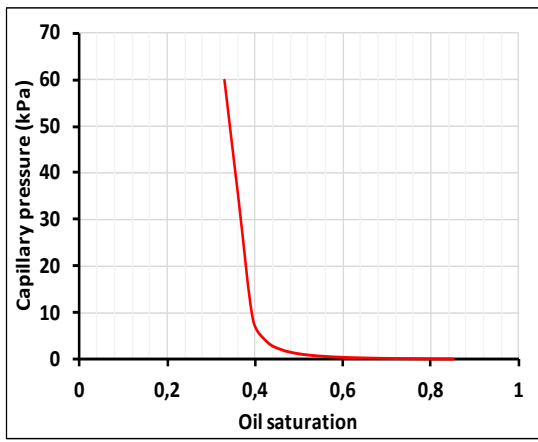
(a) Initial imbibition capillary pressure curve
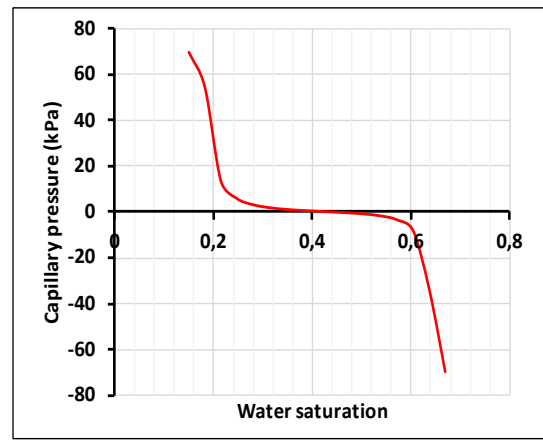
(b) Final imbibition capillary pressure curve

Figure 4.3: Coreflood 1 imbibition capillary pressure curves
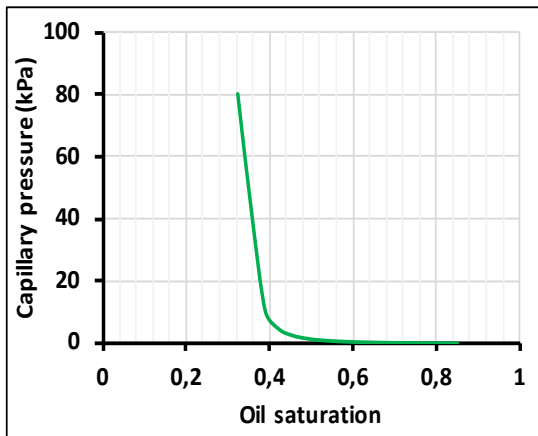
(a) Initial imbibition capillary pressure curve
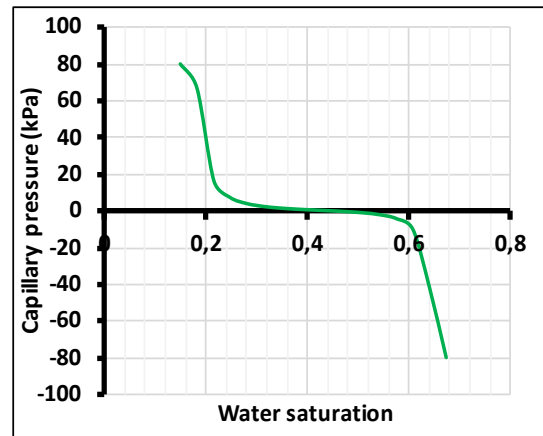
(b) Final imbibition capillary pressure curve

Figure 4.4: Coreflood 2 Imbibition capillary pressure curves

4.6. Surfactant Adsorption

Adsorption is a very important aspect of chemical flooding, and therefore must be considered when modeling the process. The adsorption of components from the aqueous in GEM™ is defined using either an adsorption table for each component in the aqueous phase or using the Langmuir adsorption model. If the former is used, a mixing rule based on the extended multicomponent Langmuir model is used to predict multicomponent adsorption. The former method models surfactant adsorption as a function of surfactant concentration and salinity, and was used in this thesis. Equation (4.37) is the extended Langmuir isotherm for multicomponent adsorption[15,39]:

$$\omega_i = \frac{\omega_{i,max} B_i y_{i\_aqu}}{1 + \sum_j B_j y_{j\_aqu}} \tag{4.37}$$

where B_i is the parameter for Langmuir isotherm relation, ω_i and $\omega_{i,max}$ are the moles and maximum moles of the adsorbed component, respectively, and y_{i_aqu} is the mole fraction of component i in the aqueous phase. The mixing rule used to predict rate of adsorption of each component in a multicomponent mixture is given in eq. (4.38).

$$\omega_i/\omega_{i,max} = \chi_i = \frac{\Gamma_i(y_{i\_aqu})}{1 + \sum_j \Gamma_j(y_{j\_aqu})} \tag{4.38}$$

The above equation can be rearranged to give eq. (4.39), for a single adsorbing species:

$$\Gamma_i(y_{i\_aqu}) = \frac{\chi_i}{1 - \chi_i} \tag{4.39}$$

In the model, adsorption is included through the keywords ADSORBTMAXA and ADSTABA. ADSORBTMAXA defines the maximum adsorption of the component whereas ABSTABA defines a table containing values of the mole fractions of the component on one column and the corresponding adsorption values on the second column. The maximum adsorption of a component, $\omega_{i,max}$ and the adsorption values for each mole fraction, ω_i are used to calculate Γ_i using eq. (4.39), and a table of Γ_i versus mole fractions of the component is created and stored internally. ω_i is then eventually obtained from Γ_i and $\omega_{i,max}$ using eq. (4.38). The keywords activating adsorption should also be in the ROCKFLUID section, just below the relative permeability curves, and the ADSORBTMAXA keyword should come before the ABSTABA keyword. The values used to model surfactant adsorption in this thesis are given in table 4.4. For mole fractions that lie between the values defined in the table, linear interpolation is done whereas the first or the last entry on the table is chosen if the mole fraction lies out of the range in the table.

Table 4.4: Values used to model surfactant adsorption from the aqueous phase

ADSORBTMAXA 'Surfact' ($\omega_{i,max}$)	0.006762
ADSTABA 'Surfact'	
Mole Fraction	Adsorption
0	0
4.224E-05	0.000644
2.112E-05	0.003220

4.7.   Simulation Model

Two one dimensional (1D) Cartesian grid systems consisting of 30 x 1 x 1 and 40 x 1 x 1 gridblocks have been used to model the two coreflood experiments by Alameri et al.[9]. The composite of four cores from Facies 5 was discretized into 40 gridblocks whereas that from Facies 6 (three composite cores) was discretized into 30 gridblocks. 10 gridblocks were used to represent each part of the composite cores and the dimensions were chosen such that experimental measurements are honored. The 40-gridblock and 30-gridblock models are known as corefloods 1 and 2, respectively. Heterogeneity in porosity and permeability is captured by the composite nature of the cores that was used for the experiments. Based on X-Ray Diffraction (XRD), the predominant mineral is Calcite, with minor occurrences of Dolomite. A volume fraction 95% and 5% was therefore used for Calcite and Dolomite, respectively. The petrophysical properties of the cores and the properties of the models used for the coreflood simulations are given in tables 4.5 and 4.6, respectively. The properties and compositions of the fluids are given in tables A.1 and A.2. Figure 4.5 shows the porosity and permeability distribution for the two coreflood models.

A horizontal configuration was used for the simulation models, similar to the configurations used in the experiments, with two vertical wells; an injector and a producer. Rate control was used for the injection well and a constant injection rate of 0.1 ml/min (1.44e-4 m^3/min) was set for the injection well in both cases. Based on the dimensions of the cores used in the simulation runs, one PV is equivalent to 0.34 and 0.23 day of injection time for corefloods 1 and 2, respectively. The producer was controlled using a minimum bottomhole pressure, which was set at 1200 kPa. A sensitivity study was done on the number of gridblocks and the maximum and minimum time steps represented in the models as DTMAX and DTMIN; to ensure that the physics of the process is properly captured. This can be observed from the material balance error reported during the simulation runs.

Table 4.5: Petrophysical properties of reservoir cores (Adapted from Alameri et al. [9])

Core properties	Facies 5 cores	Facies 6 cores
Length, L (in)	1.643 3.255 1.82 1.896	1.95 1.81 1.51
Diameter, D (cm)	3.81	
Cross-sectional Area (cm^2)	11.401	

Note: The diameter, D and cross-sectional area, A are the same for both cases

Table 4.6: Properties of simulation models

Model Description	Coreflood 1	Coreflood 2
Model Dimensions (1D)	40 x 1 x 1	30 x 1 x 1
Gridblock sizes	$\Delta x_1 = 0.00417$m $\Delta x_2 = 0.00827$m $\Delta x_3 = 0.00462$m $\Delta x_4 = 0.00482$m $\Delta y = 0.03195$m $\Delta z = 0.03195$m	$\Delta x_1 = 0.00495$m $\Delta x_3 = 0.00460$m $\Delta x_3 = 0.00384$m $\Delta y = 0.03355$m $\Delta z = 0.03355$m
Pore Volume (cm^3)	49.3163	32.4875
Porosity (ϕ)	$\phi_1 = 0.2694$ $\phi_2 = 0.2460$ $\phi_3 = 0.2070$ $\phi_4 = 0.1454$	$\phi_1 = 0.2375$ $\phi_2 = 0.2271$ $\phi_3 = 0.1736$
Permeability ($K_x = K_y = K_z$), mD	$K_{x1} = 3.380$ $K_{x2} = 2.250$ $K_{x3} = 1.160$ $K_{x4} = 0.696$	$K_{x1} = 3.380$ $K_{x2} = 1.810$ $K_{x3} = 0.696$
Initial water saturation	0.18	0.20
Reservoir Temperature (°C)	90.6	90.6
Initial pressure (kPa)	1200	1200
Mineral volume fraction	75% Calcite 5% Dolomite	75% Calcite 5% Dolomite

(a) Permeability distribution for model 1
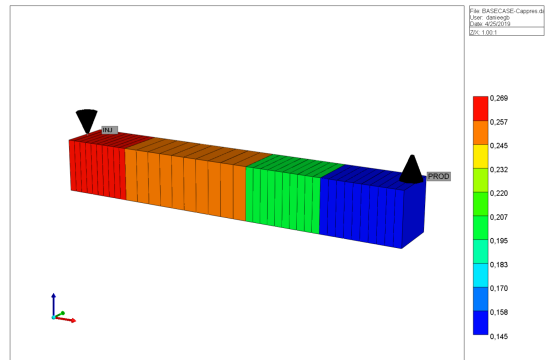
(b) Porosity distribution for model 1
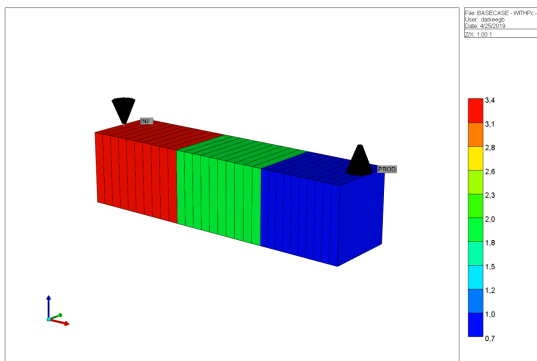
(c) Permeability distribution for model 2
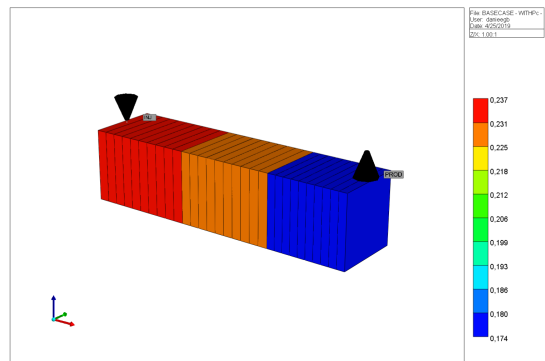
(d) Porosity distribution for model 2

Figure 4.5: Simulation models with heterogeneous porosity and permeability.

4.8.   Chapter Summary

Wettability alteration is the widely accepted mechanism during low salinity waterflooding. The change in wettability results from the geochemical reactions that occur between the rock and the aqueous phases. The geochemical reactions are divided into homogeneous and heterogeneous reactions. The homogeneous reactions occur between the aqueous phase components, are fast and are represented as chemical equilibrium reactions. They are also known as intra-aqueous reactions. The heterogeneous reactions occur between components in the aqueous phase and mineral species. They are slower than the homogeneous reactions and are represented as rate-dependent reactions. Mineral dissolution/precipitation and ion exchange reactions are two examples of heterogeneous reactions. In this chapter, a comprehensive discussion on the different geochemical reactions has been provided.

Modeling of wettability alteration during LSWF and surfactant flooding based on the geochemical interactions between the aqueous phases and the rock has been described in this chapter. The change in wettability was modeled in terms of a change in relative permeability. The Brooks-Corey relative permeability model was used to obtain all the relative permeability curves. Multicomponent ion exchange involving the exchange of SO_4^{2-}, CH_3COO^-, Ca^{2+} and Mg^{2+} was assumed as the main wettability alteration mechanism during LSWF, and thus used to model the process. Wettability alteration during surfactant flooding was assumed to be a result of a reduction in IFT and a change in wettability. Surfactant retention was modeled based on the adsorption of surfactants as they move through the porous media; using an extended multicomponent Langmuir adsorption model. Capillary pressure was also modeled using the correlation by Skjaeveland et al.[76]. All the simulations were done using the EOS compositional simulator GEM™ by CMG.

The two coreflood models have been described. A horizontal configuration has been used for both models to honor the configurations used in the experiments. A sensitivity study on the number of gridblocks and time step was done to ensure that the physics of the processes were properly captured during the simulations. The injection well was controlled using a maximum injection rate of 0.1 ml/min, whereas a minimum bottomhole pressure of 1200 kPa was used to control the producer well. A summary of the model properties has also been presented.

5. Results and Discussions

Several modeling cases (data files) were built, and simulations were performed to history match the experimental results of oil recovery and pressure drop from the two coreflood experiments. The relative permeability and capillary pressure curves shown in figs. 4.1 to 4.4 depict a change a wettability from oil-wet during seawater injection to intermediate wet after LSWF and finally to water-wet after surfactant flooding. The crossover point changes from 0.39 during seawater injection to 0.44 and 0.43, respectively after low salinity waterflooding. In this chapter, the results of the history match are presented and discussed including the oil recovery, pressure drop, ion exchange equivalent fractions of exchange species (Ca^{2+} and Mg^{2+}), effluent ions concentration and pH. The results of surfactant flooding and low salinity surfactant flooding are also presented.

5.1. Low Salinity Waterflooding

Figures 5.1 and 5.2 show the results of the best history match obtained for oil recovery and pressure drop for the two coreflood simulations. It can be seen that the simulations results are in very good agreement with the experimental results, especially when capillary pressure is included in the model. The figures also show that capillary pressure has a greater effect on the pressure drop than the oil recovery, which is in line with the observations of Adegbite et al.[1]. The history match parameters for relative permeability and capillary pressure are given in table 5.1 whereas the geochemical history match parameters are summarized in table 5.2.

Table 5.1: Relative permeability and capillary pressure parameters used for history matching

Relative permeability	Coreflood 1	Coreflood 2
k_{rw}^*	0.27	0.15
k_{ro}^*	0.092	0.1
n_w	3.3	3.5
n_o	2.7	3.9
Capillary pressure		
C_w (kPa)	0.08	0.1
C_o (kPa)	-0.08	-0.1
$a_w = a_o$	2	2

Table 5.2: Geochemistry parameters used for history matching

Ion exchange reactions parameters	
CEC	80
$K'_{Na/Ca}$	0.67
$K'_{Na/Mg}$	0.58
Interpolation parameter 1	0.33
Interpolation parameter 2	0.43
Mineral reactions	
Reactive surface area (m^2/m^3)	100
Activation energy (J/mol)	41870
Reaction rate Calcite (mol/m^2s)	-6.8
Reaction rate Dolomite (mol/m^2s)	-10.8
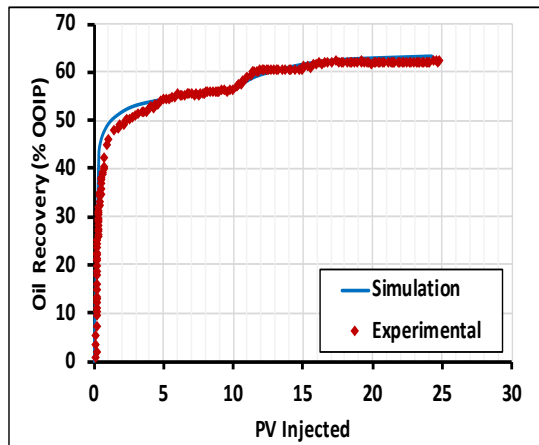
(a) Oil recovery with no Pc
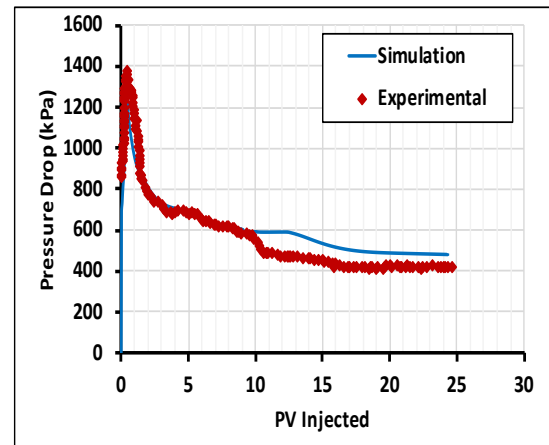
(b) Pressure drop with no Pc
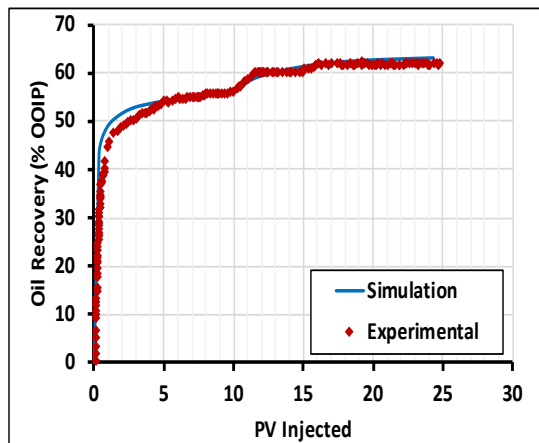
(c) Oil recovery with Pc
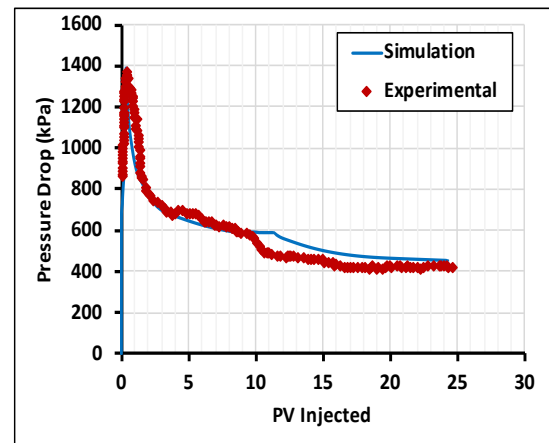
(d) Pressure drop with Pc

Figure 5.1: History match of oil recovery and pressure drop for coreflood 1, with and without capillary pressure

(a) Oil recovery with no Pc

(b) Pressure drop with no Pc

(c) Oil recovery with Pc

(d) Pressure drop with Pc
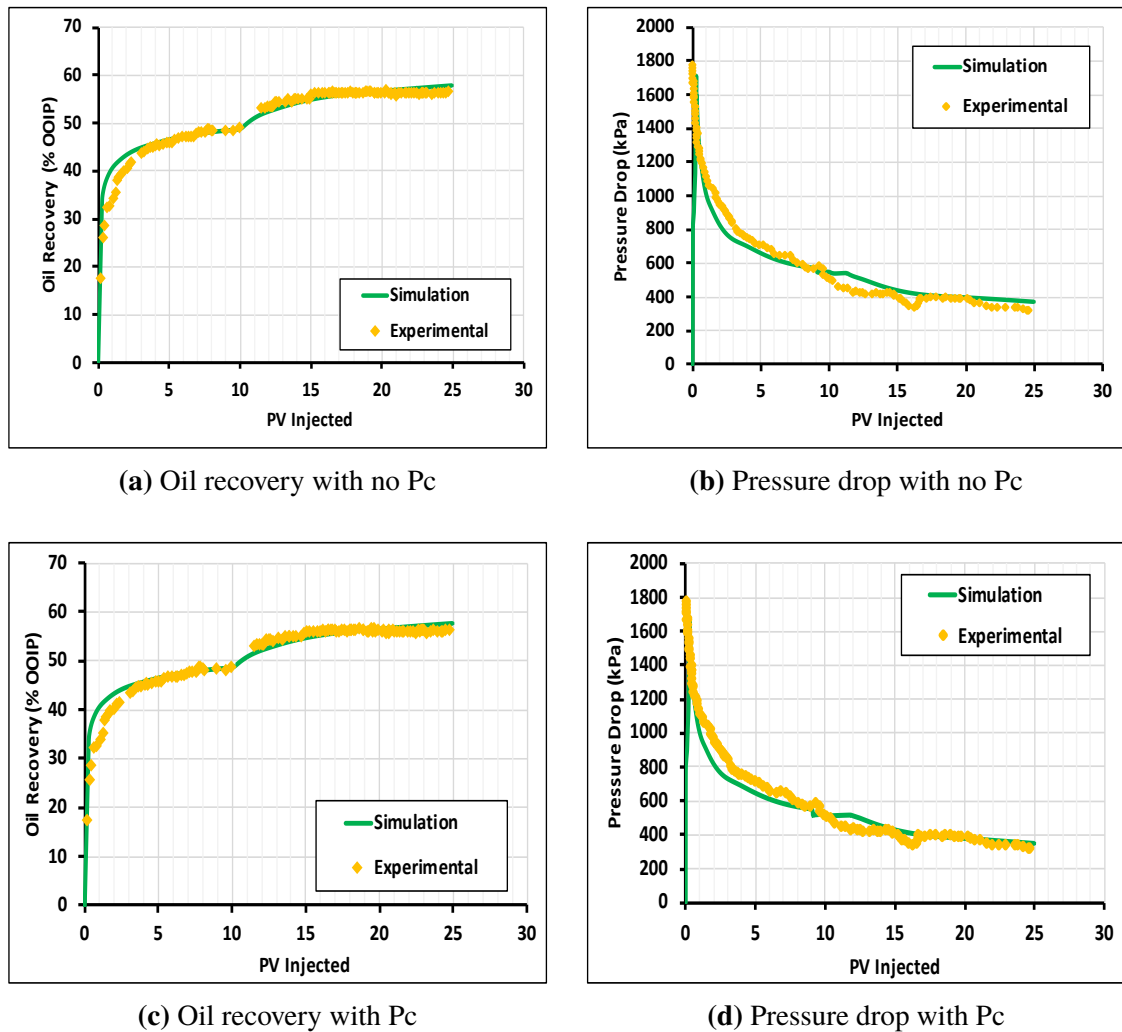
Figure 5.2: History match of oil recovery and pressure drop for coreflood 2, with and without capillary pressure

The concentration of SO_4^{2-} in SW is about 5 times its concentration in the initial formation water (FW) (see table A.2). The higher concentration increased the amount of SO_4^{2-} adsorbed on the exchanger on the carbonate surface during SW injection , and this resulted in the desorption of oil from the rock surface. This also increased the cation exchange capacity (CEC) of the rock and subsequently led to the co-adsorption of Mg^{2+} as shown in fig. 5.3. Mg^{2+} was exchanged during SW injection until equilibrium was reached. That is, when the ion exchange equivalent fraction of Mg^{2+} remained constant. During LSWF, no further adsorption of SO_4^{2-} occured because of the high SO_4^{2-} adsorption that had previously occured during SW injection. However, the carbonate surface site was still open to more cation exchange, and thus the exchange of Mg^{2+} and Ca^{2+} continued until equilibrium was reached at each injection stage.

The ion exchange equivalent fractions for different gridblocks are shown in fig. 5.3. This figure shows that the amount of Mg^{2+} exchanged on the surface site is higher than that of Ca^{2+}, and this could be the reason for the improved recovery. Additionally, it can also be seen that when LS3 brine is injected, further adsorption of Mg^{2+} occurs only in the

49

injector gridblock. In the other gridblocks, the desorption of Mg^{2+} from carbonate surface takes place. On the other hand, there is high adsorption of Ca^{2+} for all the gridblocks. This desorption of Mg^{2+}, and adsorption of Ca^{2+} is most likely the reason why no further increase in oil recovery was observed from the experiments, after the injection of LS3 brine.
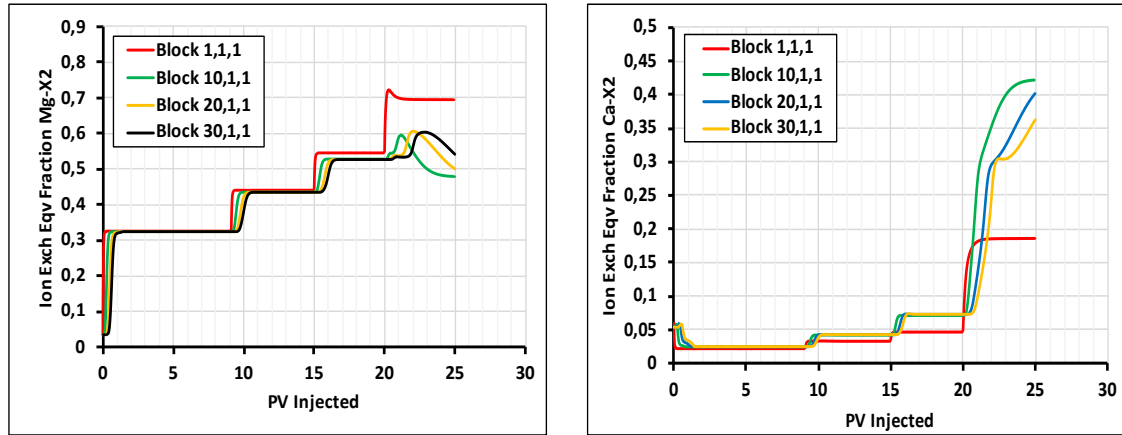
Figure 5.3: Ion exchange equivalent fractions for different gridblocks

The adsorption of Mg^{2+} and Ca^{2+} decreases the amounts of the ions present in the aqueous phase and this results in the dissolution of calcite. The dissolution of calcite increases the amount of Ca^{2+} in solution, and causes the precipitation of dolomite as shown in fig. 5.4. However, it can be seen that calcite dissolution is about one order of magnitude higher than dolomite precipitation. A decrease in the effluent concentrations of Mg^{2+}, Ca^{2+}, SO_4^{2-}, Na^+ and Cl^- was reported from the experimental work, and the same trend was observed from the simulations as shown in fig. 5.5. The increase in the effluent concentration of Ca^{2+} towards the end of the injection cycle is because of an increase in Ca^{2+} adsorption during the period of LS3 brine flooding, as previously discussed. The increase in Ca^{2+} adsorption increases the rate of calcite dissolution, resulting in an increase in the effluent concentration of Ca^{2+}. The effluent concentration of Mg^{2+} also increased towards the end because of a decrease in dolomite precipitation.
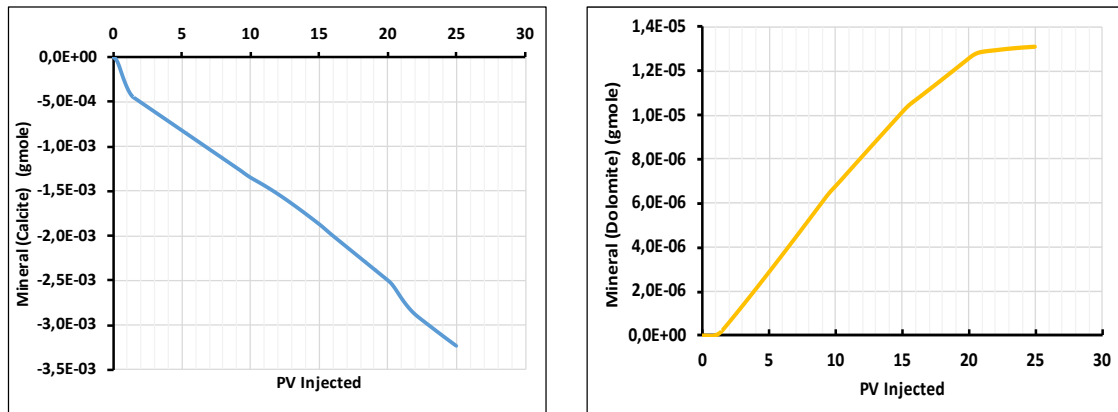
Figure 5.4: Changes in mineral moles of calcite and dolomite

It is also worth noting that Na^+ and Cl^- are considered as non-active ions and are not expected to play a role in the process[18]. Since Na^+ and Cl^- were neither present in seawater nor in any of the low salinity brines, the Na^+ and Cl^- in the effluent is from the formation water. The small dips at the start of each injection stage is because of the ion exchange taking place between the injected brine and exchanger on the carbonate surface. Figure 5.6 shows an increase in pH during the process. There is a sharp rise in the pH at the start of LS3 brine injection, after which the pH decreases to an equilibrium value. This is most likely due to the increased Ca^{2+} adsorption, and calcite dissolution during LS3 brine injection.
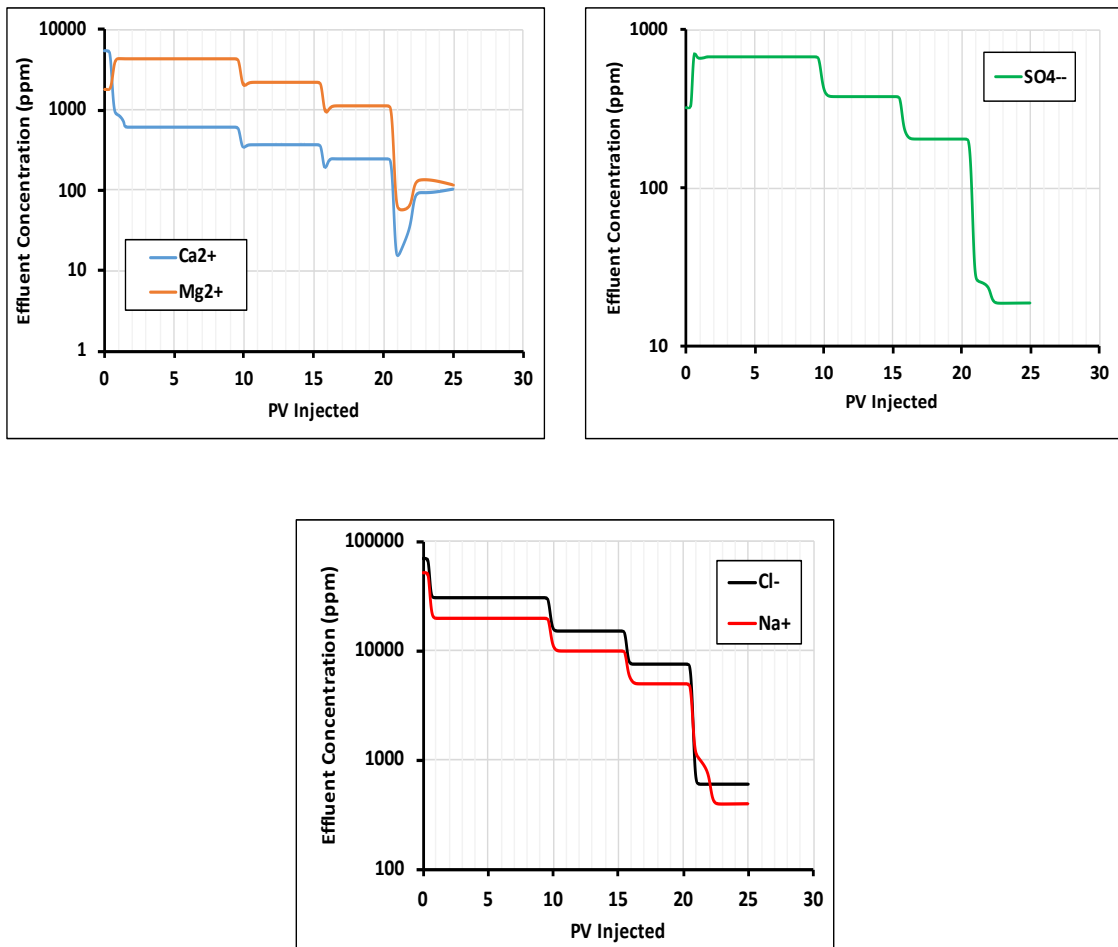
Figure 5.5: Effluent ions concentration

(a) Coreflood 1

(b) Coreflood 2
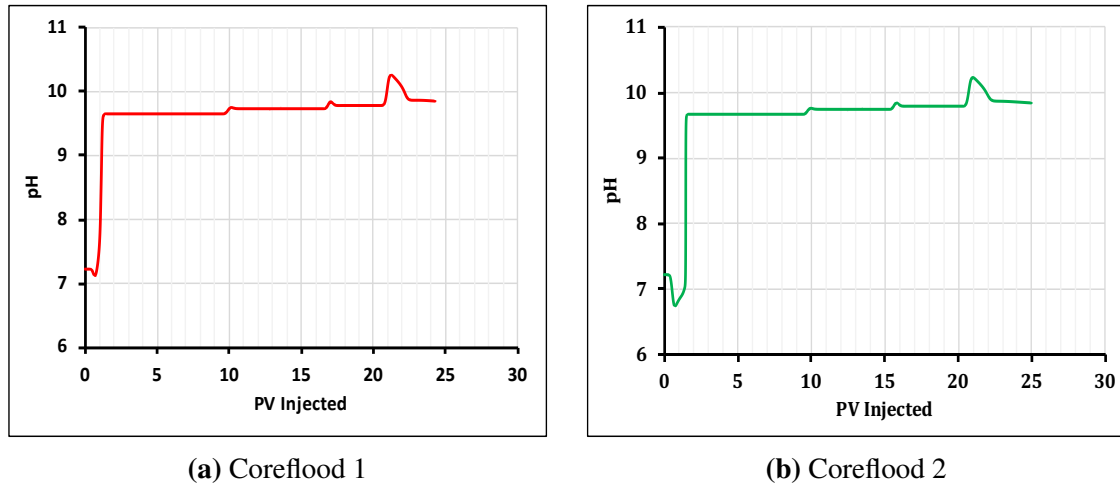
Figure 5.6: Effluent pH

5.2. Surfactant Flooding

As previously mentioned, a non-ionic ethoxylated alcohol surfactant was used during the experiments to evaluate its potential to increase oil recovery after low salinity waterflooding. In this section, the results of the modeling studies involving seawater injection and surfactant flooding are presented. For both coreflood simulations, 10 PV were flooded with seawater, after which another 10 PV were flooded with surfactant dissolved in LS2 brine. The concentration of surfactant used for the simulations was the same as that in the experiments (1000 ppm for coreflood 1 and 5000 ppm for coreflood 2).

Figures 5.7 and 5.8 show the oil recovery and pressure drop obtained from the simulations. The effect of the surfactant on oil recovery and pressure drop is visible only for the second coreflood simulation. In order for the residual oil after waterflooding to be mobilized, the capillary number has to be increased by several orders of magnitude[8]. In the first coreflood, the increase in the capillary number is less than one order of magnitude, and therefore no increase in oil recovery is observed after the surfactant is injected. The surfactant is unable to mobilize the oil trapped by capillary forces after waterflooding. The higher concentration of surfactant used in the second coreflood results in a higher reduction in IFT, and an increase in the capillary number that is about two orders of magnitude. Thus, the surfactant was able to mobilize residual oil and increase the oil recovery. The oil-water capillary number for different gridblocks is shown in fig. 5.9. The results of the oil recovery for the two coreflood simulations are summarized in table 5.3.

From the second coreflood, it can be seen that the increase in oil recovery corresponds to a simultaneous increase in the pressure. Tavassoli et al.[84] suggested that the increase in pressure might be due to the two-phase flow of oil and water in front of the surfactant slug. Based on the modeling results, it is possible that surfactant adsorption also plays a role in the pressure increase because no increase was observed for first coreflood simulation; where there is a lower rate of surfactant adsorption. After the increase, there is a sharp decline in the pressure due to the mobilization of oil by the surfactant. As expected, surfactant adsorption increases with concentration as shown in fig. 5.10. However, the

adsorption is small compared to the amount of surfactant injected; which is a unique characteristic of non-ionic surfactants in carbonate reservoirs[74]. It should be noted that the same geochemical reactions used during the modeling of low salinity waterflooding were used in these simulation studies. The ion exchange equivalent fractions of Mg^{2+} and Ca^{2+} are shown in fig. 5.11.
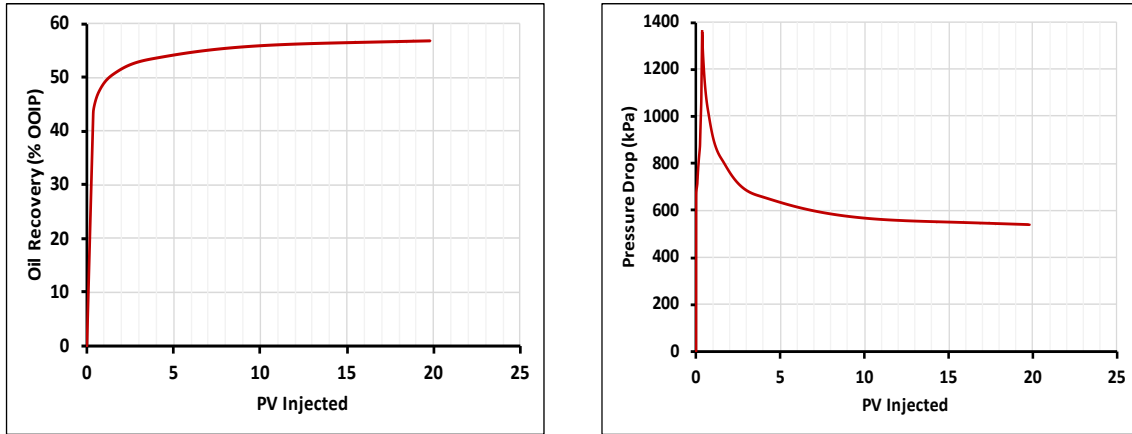
Figure 5.7: Oil recovery and pressure drop for coreflood 1
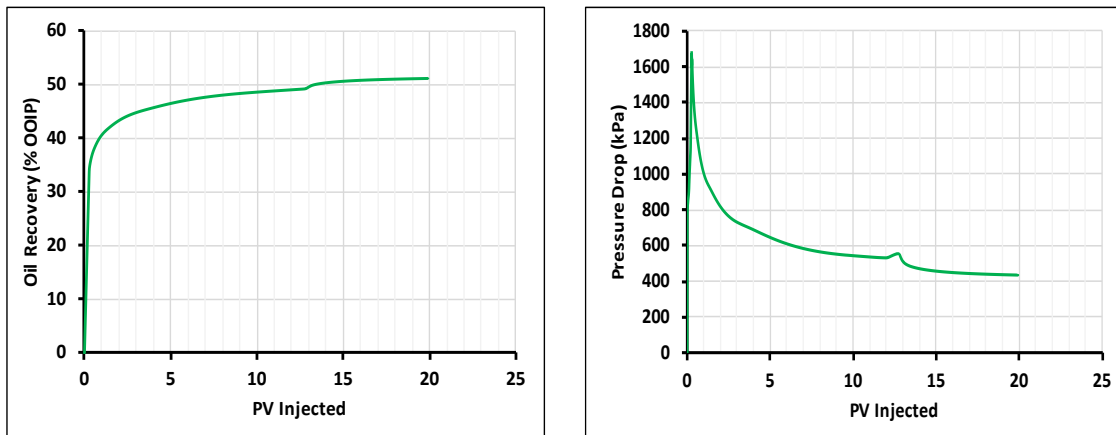
Figure 5.8: Oil recovery and pressure drop for coreflood 2

Table 5.3: Summary of oil recovery from seawater and surfactant floods for coreflood simulations

Injection fluid	Oil Recovery (% OOIP)	
	Coreflood 1	**Coreflood 2**
Seawater	55.95	48.66
Surfactant	56.77	51.17
Δ RF	0.82	2.51
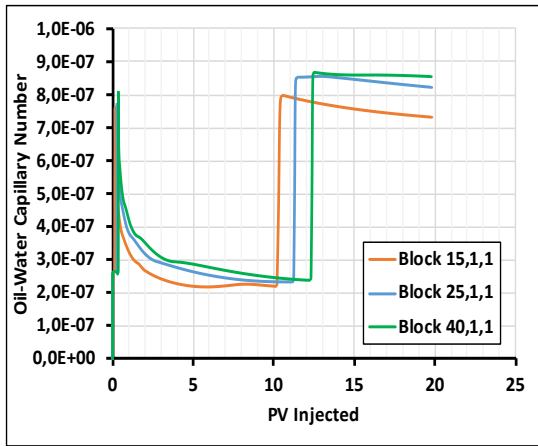
(a) Coreflood 1
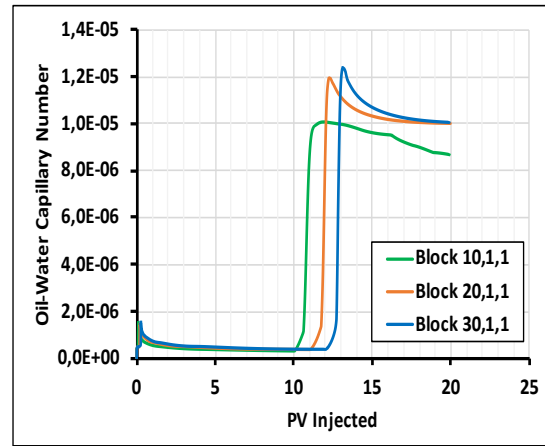
(b) Coreflood 2

Figure 5.9: Oil-Water capillary number for different gridblocks
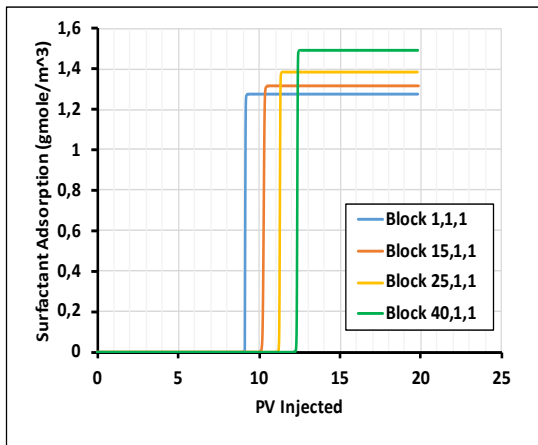
(a) Coreflood 1
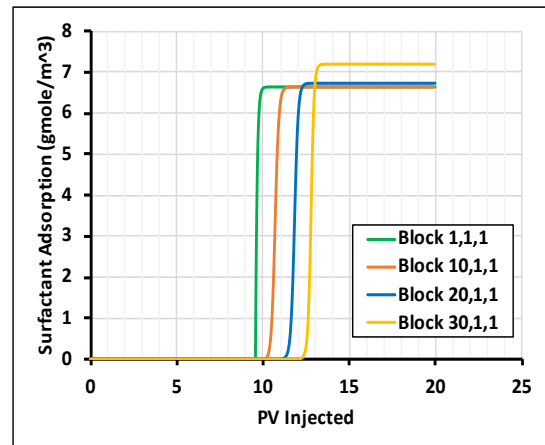
(b) Coreflood 2

Figure 5.10: Surfactant adsorption for different gridblocks
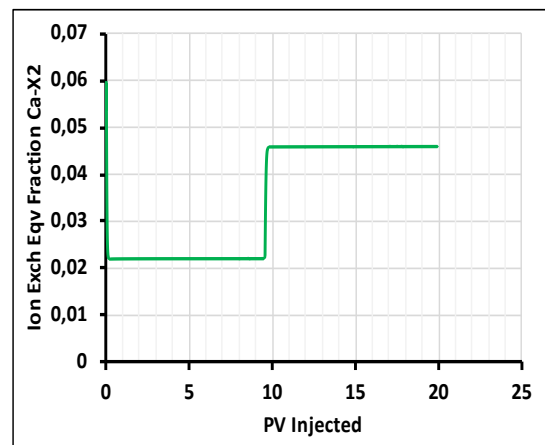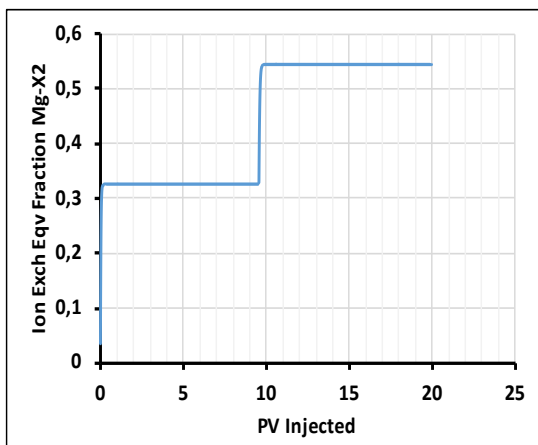
Figure 5.11: Ion exchange equivalent fractions of Mg^{2+} and Ca^{2+}

5.3. Low Salinity Surfactant Flooding

After modeling the two previous cases, an attempt was made to model the combination of seawater, low salinity water and surfactant injection, similar to the experimental procedure. However, this was done only for the first coreflood. As discussed in section 4.4, modeling such a process requires the definition of two rock regions where interpolations are based on the equivalent fraction of Mg^{2+} and the capillary number for low salinity waterflooding and surfactant injection, respectively. This was implemented in the coreflood model. It was however observed that although the overall recovery from the simulation matches that from the experiment, the change in oil recovery at the different injection stages was not observed. This is because although the simulator takes into account the different processes and mechanisms of wettability alteration, it does not interpolate between the rock types. The fact that the final recovery is almost the same as what is obtained from the experiment, and greater than the two previously modeled cases is an indication that although the process has been modeled correctly, the simulator currently lacks the ability to interpolate between rock types. Figure 5.12 shows the oil recovery from the simulation.

The ion exchange equivalent fractions of Mg^{2+} and Ca^{2+} in fig. 5.13 show a decrease in the amount of Mg^{2+} and Ca^{2+} on the carbonate surface during surfactant flooding. This is because as the surfactant dissolved in LS2 brine is injected, the concentration of Mg^{2+} and Ca^{2+} in the injected fluid is lower than their respective concentrations on the carbonate surface. This led to the release of the divalent cations from the rock surface and a corresponding decrease in the ion exchange equivalent fractions of the two cations. The oil-water capillary number and surfactant adsorption profiles in fig. 5.14 also show an increase in both the capillary number and surfactant adsorption at the beginning of surfactant injection, as expected. One interesting observation from the simulation was that the concentration of surfactant in the effluent was slightly higher than in the injection fluid. This might be due to in-situ generation of surfactant during LSWF, as a result of the increase in pH. This however requires further investigation.
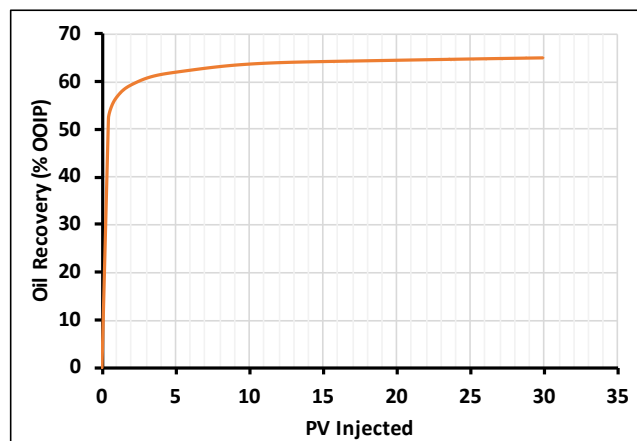
Figure 5.12: Oil recovery for LSS coreflood simulation
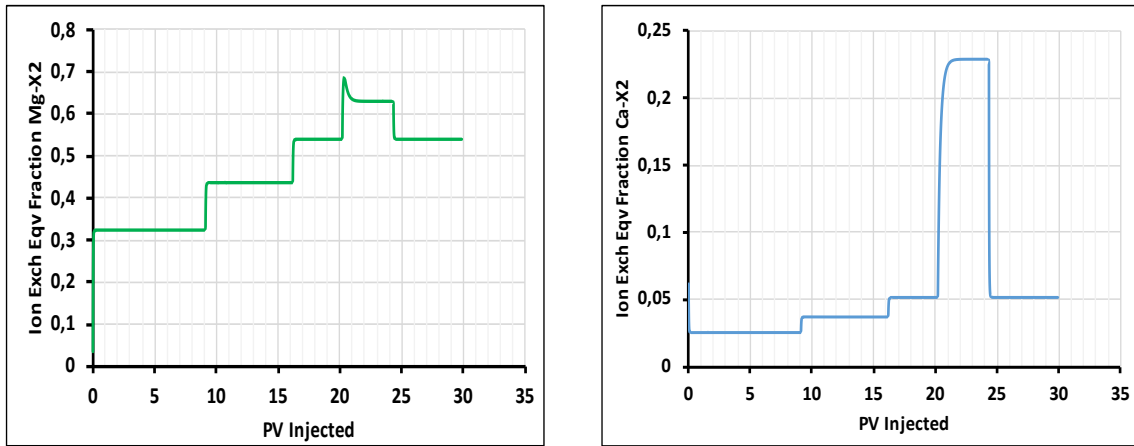
Figure 5.13: Ion exchange equivalent fractions of Mg^{2+} and Ca^{2+}, Block 1,1,1
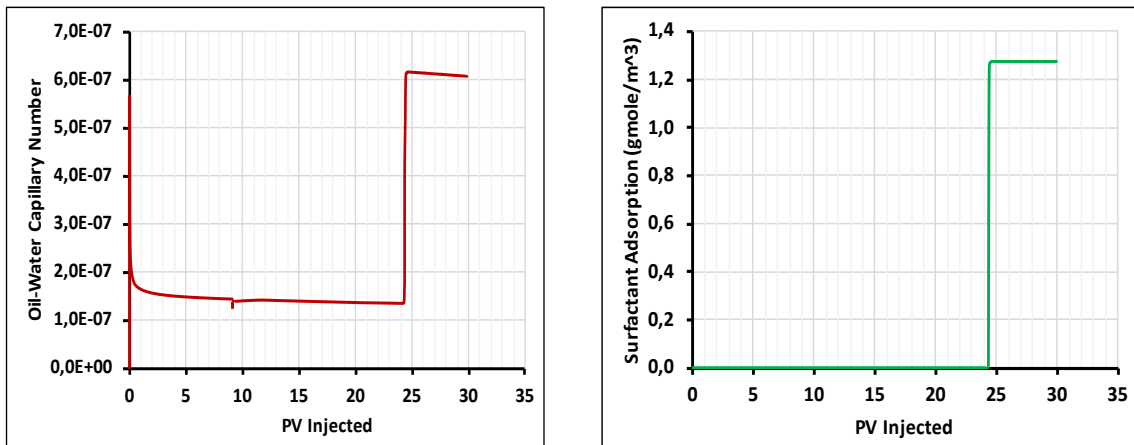
(a) Oil-water capillary number

(b) Surfactant adsorption

Figure 5.14: Oil-Water capillary number and surfactant adsorption, Block 1,1,1

5.4.   Chapter Summary

This chapter presents results of coreflood simulations of low salinity waterflooding, surfactant flooding and low salinity surfactant flooding. First, results of the history match of oil recovery and pressure drop for the two coreflood simulations are presented. A good match between experimental and simulated oil recovery and pressure drop was obtained. The ion exchange equivalent fractions of Ca^{2+} and Mg^{2+}, changes in mineral moles of calcite and dolomite, effluent ion concentrations and pH have all been presented, and they show that the physical and chemical mechanisms occurring during the processes are properly captured.

Multicomponent ion exchange was the main wettability alteration mechanism during LSWF for both corefloods. The adsorption of sulfate during SW injection increased the cation exchange capacity of the rock and led to the co-adsorption of Ca^{2+} and Mg^{2+} during LSWF. This led to the desorption of oil from the rock, and an increase in oil recovery. The exchange of Mg^{2+} was however higher than the exchange of Ca^{2+}; implying that the improved recovery is most likely due to the exchange of Mg^{2+}.

The increase in oil recovery during surfactant flooding was due to a decrease in the oil-water interfacial tension (increase in capillary number) and a change in wettability. The corresponding increase in pressure as oil recovery increased was probably because of the two-phase flow of oil and water ahead of the surfactant slug and surfactant adsorption. The surfactant adsorption profiles show an increase in adsorption with surfactant concentration. The higher oil recovery from low salinity surfactant flooding is due to a combination of both wettability alteration during LSWF and surfactant flooding, and a reduction in the oil-water interfacial tension during surfactant flooding. The higher concentration of surfactant in the effluent than in the injection fluid is mostly likely because of the in-situ generation of surfactant as a result of the increase in pH during LSWF, although it is subject to further investigations.

6. Sensitivity Analysis

Sensitivity analysis is a crucial part of every modeling study. It is aimed at investigating how results and conclusions change when some of the model's parameters and assumptions are changed. In this thesis, sensitivity analysis has been done on many key parameters. The sensitivity analysis was focused separately on low salinity waterflooding and surfactant flooding, due to the current limitation of the reservoir simulator in modeling the combined low salinity water and surfactant process. For the sensitivity study on LSWF, emphasis was placed on the oil recovery and ion exchange equivalent fractions whereas for surfactant flooding, oil recovery and pressure drop were the main parameters.

6.1. Low Salinity Waterflooding

6.1.1. Timing of low salinity water injection

The effect of injecting low salinity water in secondary mode compared to seawater injection has been investigated by some researchers[75,93]. A comparison of oil recovery from LSWF in secondary and tertiary modes was done by Zhang and Morrow[93], based on their experiments done on Berea sandstone cores. They concluded that improvement in oil recovery by LSWF is usually observed for both secondary or tertiary modes, but sometimes only for one or the other. Shiran and Skauge[75] also reported a positive response from injecting low salinity water in secondary mode for water-wet and intermediate-wet Berea sandstone cores. They suggested that the high oil recovery observed in secondary mode compared to tertiary mode by LSWF might be a result of effective trapping. The injection of low salinity water at an early time might lead to more effective mobilization of oil by maintaining a continuous oil phase[75]. In this thesis, the effect of injecting low salinity water in secondary and tertiary modes has been investigated and the results are discussed.

Secondary-mode low salinity waterflooding

Simulations have been performed for three different cases. The first case involves only seawater injection, the second case involves injection of LS1 brine and LS2 brine is injected in the third case. The three cases are known as SW, LS1 and LS2, respectively. In all three cases, 10 PV are flooded with the respective fluids. The results of oil recovery and ion exchange equivalent fractions are presented in figs. 6.1 and 6.2, respectively. A summary of the results is given in table 6.1.

Table 6.1: Oil recovery comparison for secondary mode low salinity waterflooding

Injection scheme	Oil Recovery (% OOIP)	
	Coreflood 1	Coreflood 2
SW	55.67	48.54
LS1	62.35	56.20
LS2	62.35	56.20

(a) Coreflood 1　　　　　　　　　　**(b)** Coreflood 2
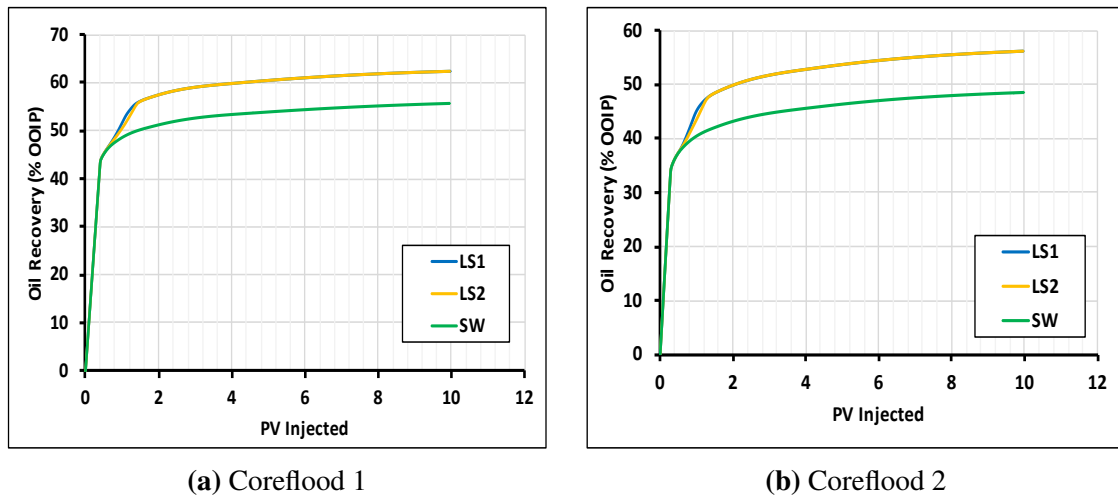
Figure 6.1: Oil recovery comparison for secondary mode LSWF and SW flooding
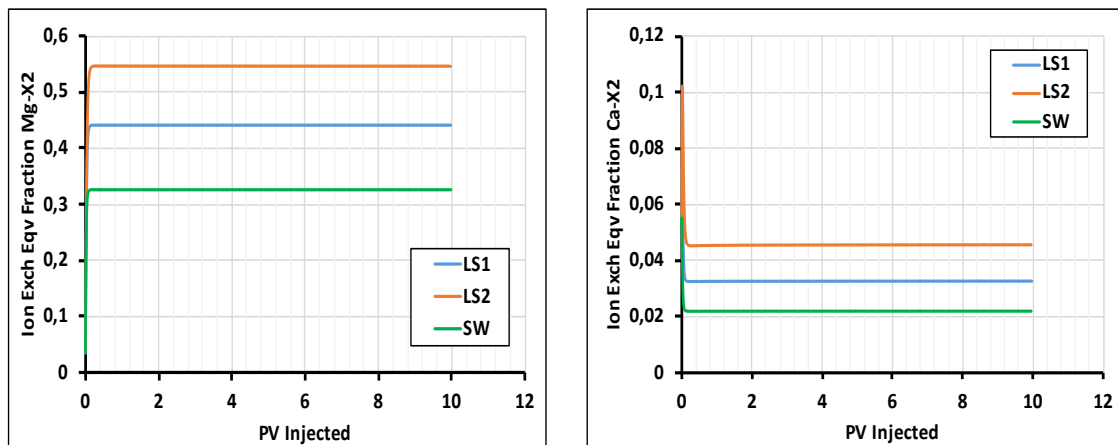
Figure 6.2: Ion exchange equivalent fraction of Mg^{2+} and Ca^{2+}, Block 1,1,1

Tertiary-mode low salinity waterflooding

Injecting low salinity water in secondary mode might lead to undesirable project economics
due to equipment and operational costs, which makes implementing LSWF in tertiary
mode more reasonable. The effect of injection interval size of high salinity waterflooding
and low salinity waterflooding has been investigated and the results are discussed in this
section. Three different interval sizes have been selected, where the cores are first flooded
with seawater and then with low salinity water. The simulations were done in such a way
that a total of 15 PV were flooded in each case. Six different scenarios have been simulated
for each of the corefloods, with three involving seawater and LS1 brine, and the other three
involving seawater and LS2 brine. The six cases are known as cases 1-6. In case 1, 10
PV are injected with SW followed by 5 PV of LS1 brine, similar to the experimental
procedure. Case 2 involves 7 PV of SW injection and 8 PV of LS1 injection. 5 PV and
10 PV are flooded with SW and LS1 brine in case 3, respectively. The same interval sizes
are used accordingly for cases 4 to 6. However, LS2 brine is injected instead of LS1 brine
after SW injection. Figures 6.3 and 6.4 show the oil and ion exchange equivalent fractions
obtained from the simulations. The results are summarized in table 6.2.

(a) Coreflood 1 SW-LS1

(b) Coreflood 2 SW-LS1

(c) Coreflood 1 SW-LS2

(d) Coreflood 2 SW-LS2
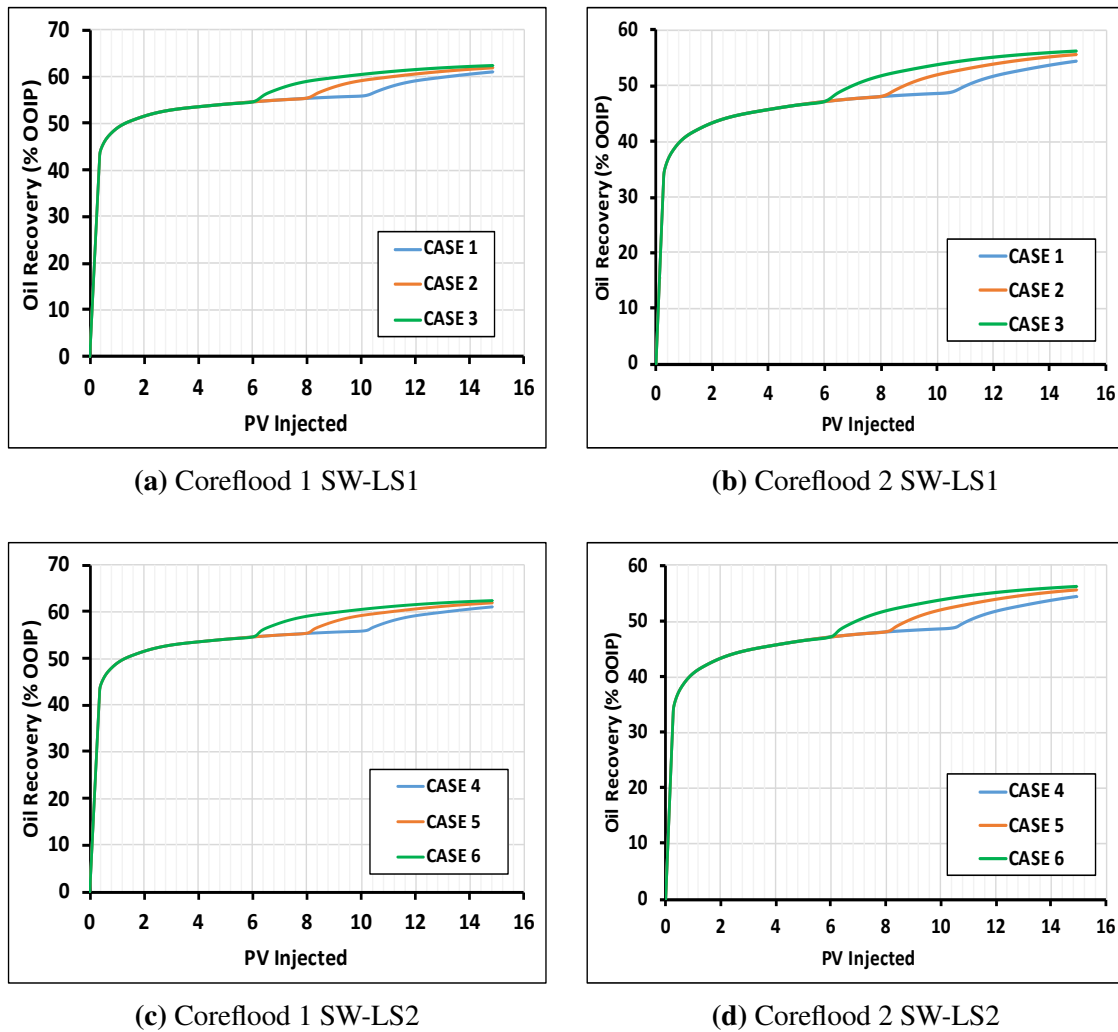
Figure 6.3: Oil recovery as a function of interval size of high salinity (seawater) and low salinity water injection.

Table 6.2: Oil recovery results for the three different HS-LS injection interval sizes studies

Injection scheme	Oil Recovery (% OOIP)	
	Coreflood 1	Coreflood 2
CASE 1 (10PV SW - 5PV LS1)	60.06	54.44
CASE 2 (7PV SW - 8PV LS1)	61.93	55.62
CASE 3 (5PV SW - 10PV LS1)	62.41	56.24
CASE 4 (10PV SW - 5PV LS2)	61.08	54.47
CASE 5 (7PV SW - 8PV LS2)	61.94	55.64
CASE 6 (5PV SW - 10PV LS2)	62.41	56.25

(a) SW-LS1

(b) SW-LS1

(c) SW-LS2

(d) SW-LS2
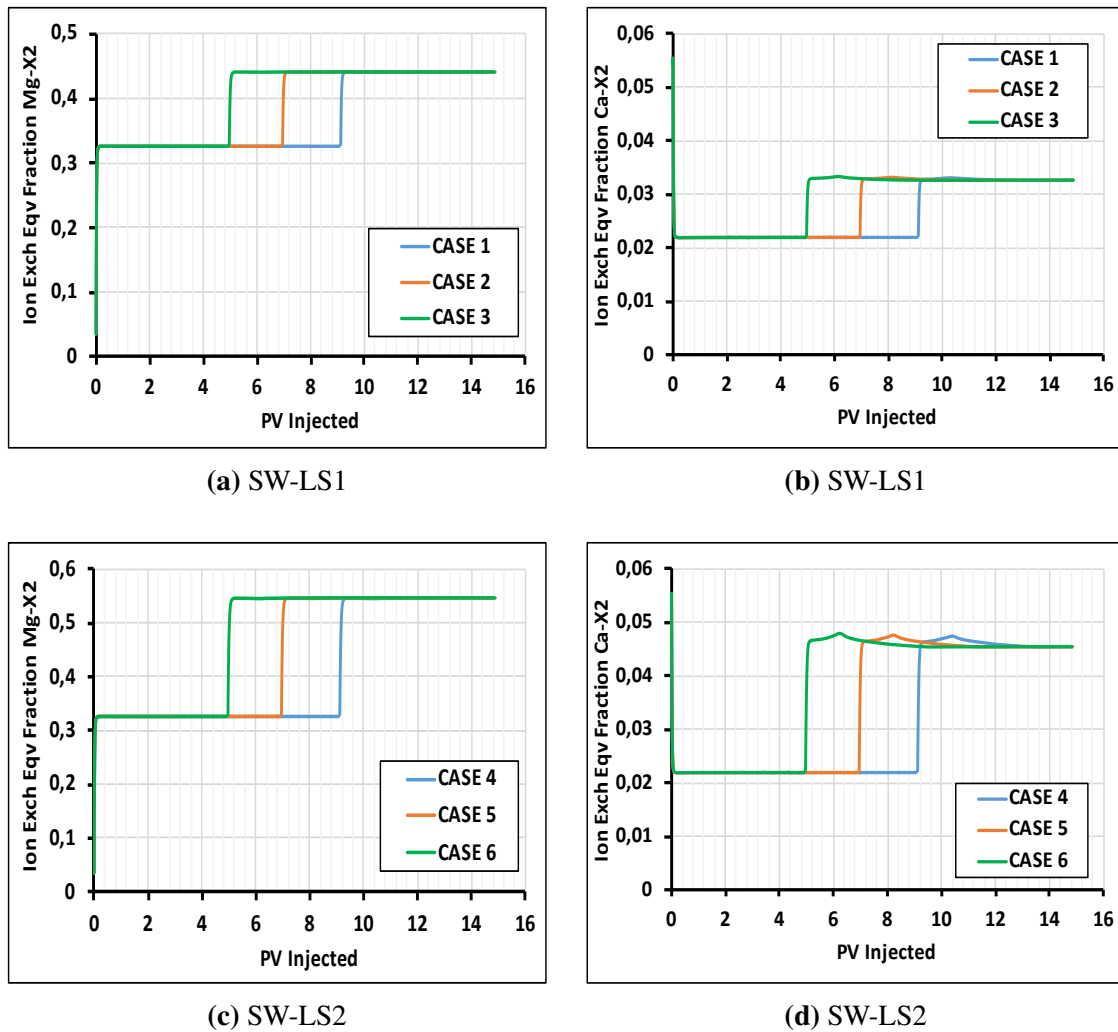
Figure 6.4: Ion exchange equivalent fraction of Mg^{2+} and Ca^{2+}, Block 1,1,1

Both figs. 6.1 and 6.3 show that the earlier the onset of low salinity waterflooding, the higher the final oil recovery. When low salinity water is injected at earlier time, it has more time to interact with the reservoir rock and the fluids present. The salinity gradient that exists when low salinity water is injected into a high saline environment causes a disruption of the thermodynamic equilibrium within the reservoir, and triggers the exchange of ionic species such as SO_4^{2-}, Mg^{2+} and Ca^{2+} between the injected brine and the COBR system. This eventually leads to wettability alteration and higher oil recovery[1,91,92]. Figure 6.4 shows the ion exchange equivalent fractions of Mg^{2+} and Ca^{2+} for the different cases of tertiary-mode LSWF.

It should be noted the increase in oil recovery is substantially higher when LSWF is implemented in secondary mode compared to tertiary, which is in line with the observations of Shiran and Skauge[75]. In addition, fig. 6.3 and table 6.2 show that LSWF with LS2 brine yields almost the same recovery as LSWF with LS1 brine both in secondary and tertiary modes. However, the water beakthrough time (BT) for the two cases differ, with BT occurring slightly earlier for LS2 brine injection. It is worth pointing out that these investigations have been done at core scale, and the increase at reservoir scale would

probably be much less. Taking into account that the timing of low salinity waterflooding might lead to higher costs, a thorough economic analysis is needed to compare the costs and benefits before a decision is made on when to implement low salinity waterflooding.

6.1.2. Injection rate

Low salinity waterflooding yields benefits from both physical and chemical displacement processes, unlike conventional high salinity waterflooding where the benefits is mostly from physical displacement[80]. Physical displacement occurs immediately as the process of water injection begins whereas it takes some time for chemical displacement to begin, due to the time taken for the ions in the brine to react with the rock surface. The injection rate is therefore a crucial parameter in optimizing the low salinity process. In this thesis, the effect of injection rate on oil recovery has been investigated using three injection rates. The three injection rates include: 0.1 (base case), 0.045 and 0.5; all in ml/min.

Figure 6.5 shows that the higher the injection rate, the higher the oil recovery. At low injection rates, chemical displacement dominates while at high/moderate injection rates, both physical and chemical displacements are favored, resulting in higher recovery. The effect of the injection rate on the ion exchange equivalent fractions of Mg^{2+} and Ca^{2+} is shown in fig. 6.6. This figure shows that changing the injection rate has little effect on the geochemical interactions, thus implying that the change in oil recovery with injection rate is most likely due to a change in the contribution from physical displacement. Although not investigated in this thesis, it is expected that at very high injection rates, only physical displacement will dominate because the ions in the injected brine would not have enough time to interact with the rock surface, and the recovery from the process would also be less than at moderate injection rates[80]. The oil recovery results are summarized in table 6.3.

(a) Coreflood 1   **(b)** Coreflood 2
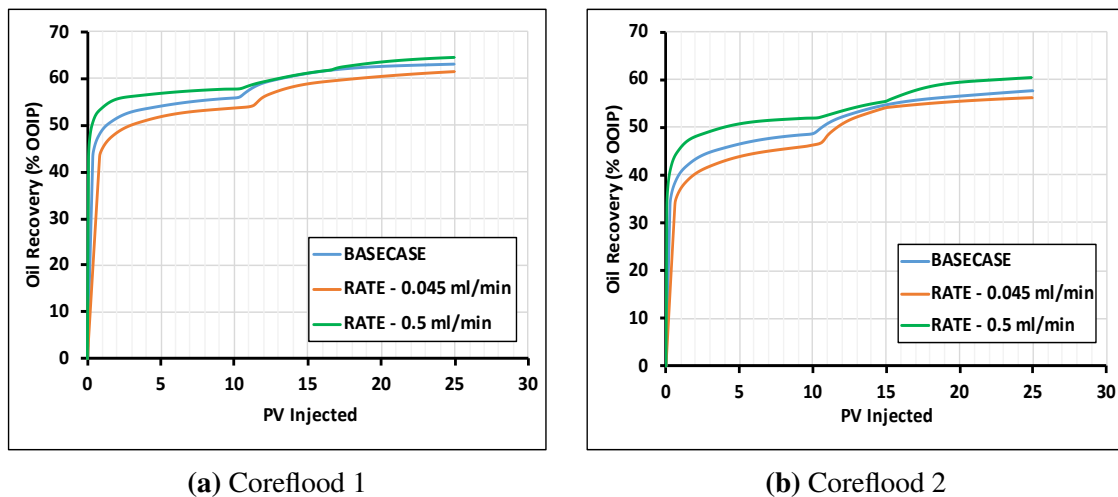
Figure 6.5: Oil recovery as a function of injection rate

Figure 6.6: Ion exchange equivalent fractions of Mg^{2+} and Ca^{2+}, Block 1,1,1

Table 6.3: Oil recovery results for the three different injection rates

Injection rate (ml/min)	Oil Recovery (% OOIP)	
	Coreflood 1	Coreflood 2
0.1 (Base Case)	63.10	57.69
0.045 (Low)	61.49	56.23
0.5 (High)	64.54	60.45

6.1.3. Injection temperature

The effect of temperature on low salinity waterflooding was also investigated. In GEM™, temperature effects are activated by turning on the thermal option, using the THERMAL ON keyword, and then supplying an injection temperature using the keyword INJ-TEMP 'INJ'. The THERMAL ON keyword is placed after the SOLUBILITY keyword in the fluid section of the data file while the INJ-TEMP 'INJ' keyword comes after the OPERATE keyword in the well and recurrent data section. 'INJ' is the name of the injector well in this case. In this thesis, three different injection temperatures were used to investigate the effect of temperature on low salinity waterflooding. The first case is the base case, where the injection temperature is the same as the reservoir temperature (90.6°C). In the second case, the injection temperature (70°C) is less than the reservoir temperature and finally, the injection temperature (110°C) is higher than the reservoir temperature in the last case.

Figure 6.7 shows that there is very little change in the oil recovery as the injection temperature changes. This is because the oil recovery is primarily a function of the relative permeability interpolation, and no changes have been made to the relative permeability interpolation in all three cases. However, differences can be seen in the ion exchange equivalent fractions of Mg^{2+} and Ca^{2+}, mineral behavior and pH (figs. 6.8 to 6.10). Figure 6.8 shows that the injection temperature has a greater effect on the exchange of Mg^{2+} between the injected brine and the carbonate surface than on the exchange of Ca^{2+}. This is probably because Mg^{2+} is the main cation responsible for the observed low salinity effects (LSE). Figure 6.9 also shows that the injection temperature has a significant effect

on mineral dissolution/precipitation. At low injection temperature, the changes in the moles of calcite and dolomite are very small compared to when the injection temperature is high. This is because at low temperatures, the reaction rates are small. The low reaction rates also slow down the ion exchange process, and no effect of LSWF on oil recovery is seen as shown in figs. 6.7a and 6.7b. Figure 6.10 shows that temperature also has a huge effect on the pH, and this is due to its effect on mineral reactions. The results are summarized in table 6.4.

(a) Coreflood 1   **(b)** Coreflood 2
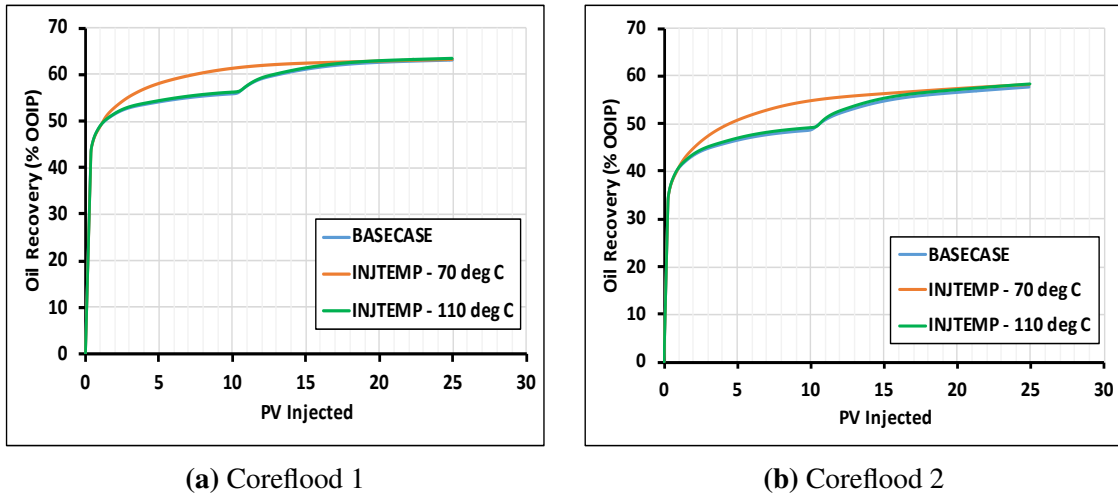
Figure 6.7: Oil recovery as a function of injection temperature
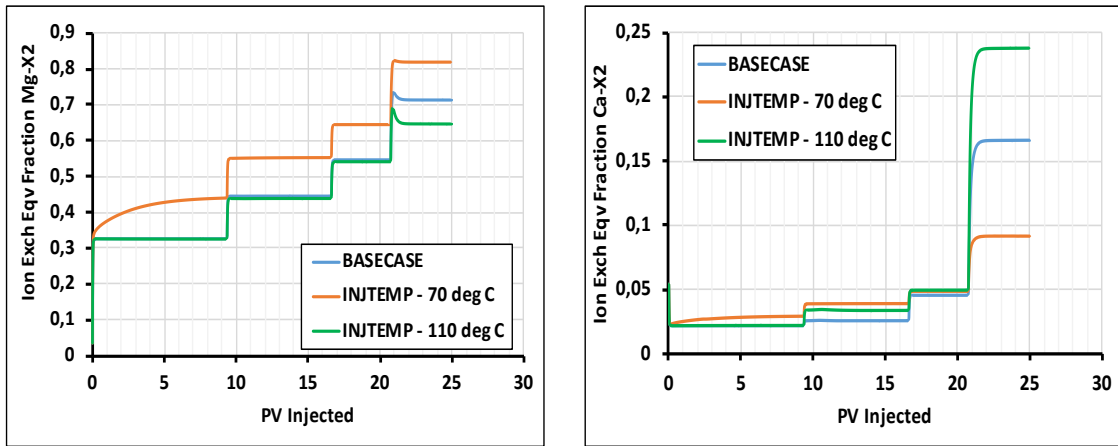
Figure 6.8: Ion exchange equivalent fraction of Mg^{2+} and Ca^{2+}, Block 1,1,1
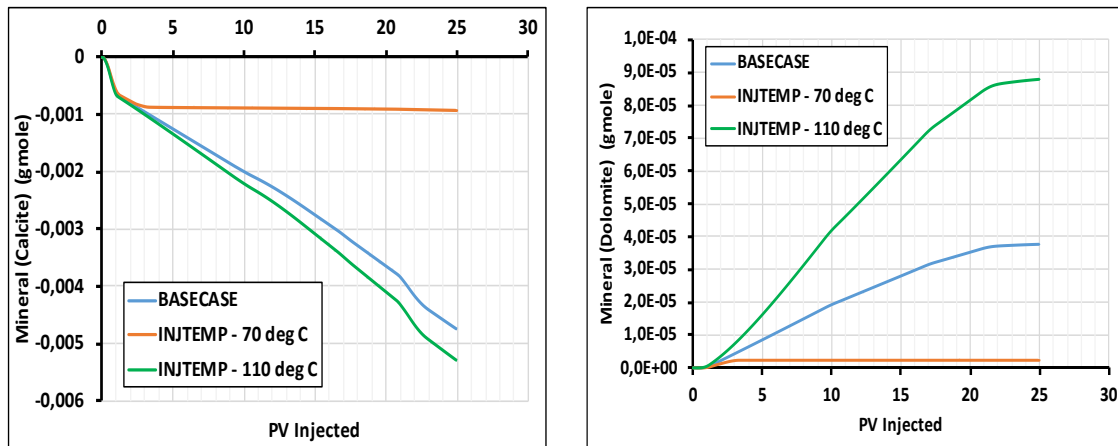
Figure 6.9: Changes in mineral moles of Calcite and Dolomite
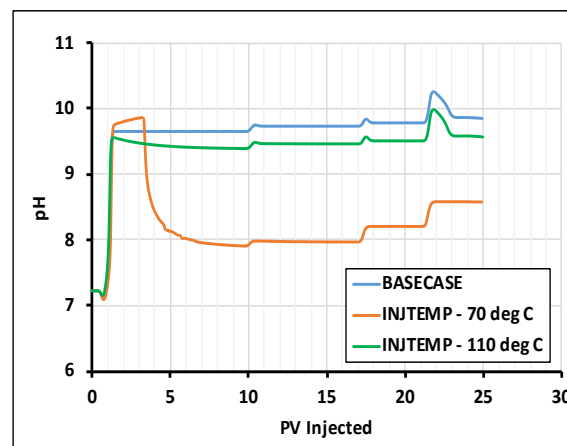
Figure 6.10: Effluent pH

Table 6.4: Oil recovery results for the three different injection temperatures

Injection Temperature (°C)	Oil Recovery (% OOIP)	
	Coreflood 1	Coreflood 2
90.6 (Base Case)	63.10	57.69
70	63.24	58.21
110	63.44	58.32

6.1.4. Injection concentration

The concentration of Ca^{2+} and Mg^{2+} in each of the injection brines was varied by increasing and decreasing the concentrations of Ca^{2+} and Mg^{2+} by a factor of three in all the low salinity brines compared to the base case. The concentration of the two ions were changed by the same factor to ensure that the ionic strength of the solutions remains the same as that in the base case, respectively. Figure 6.11 shows the oil recovery for the two coreflood

simulations. No LSWF effect is seen when the Mg^{2+} concentration in the injection brines is three times less and Ca^{2+} concentration is three times more. This is because the amount of Mg^{2+} and Ca^{2+} adsorbed onto the carbonate surface are almost the same, as shown in fig. 6.12. In such a case, the interpolant needs to be changed to obtain the desired results. A summary of the results is given in table 6.5.

(a) Coreflood 1   **(b)** Coreflood 2
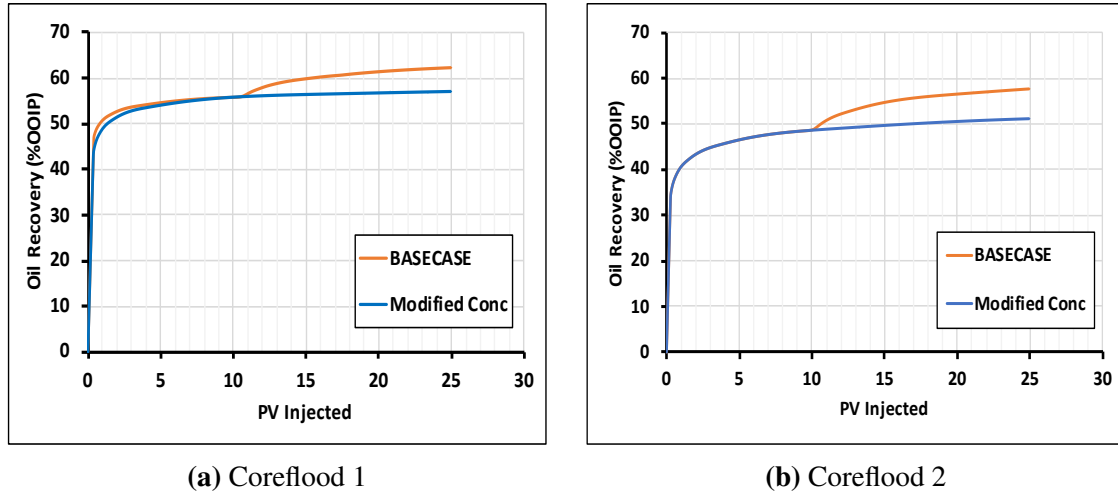
Figure 6.11: Oil recovery as a function of the concentration of Ca^{2+} and Mg^{2+} in the injection brines
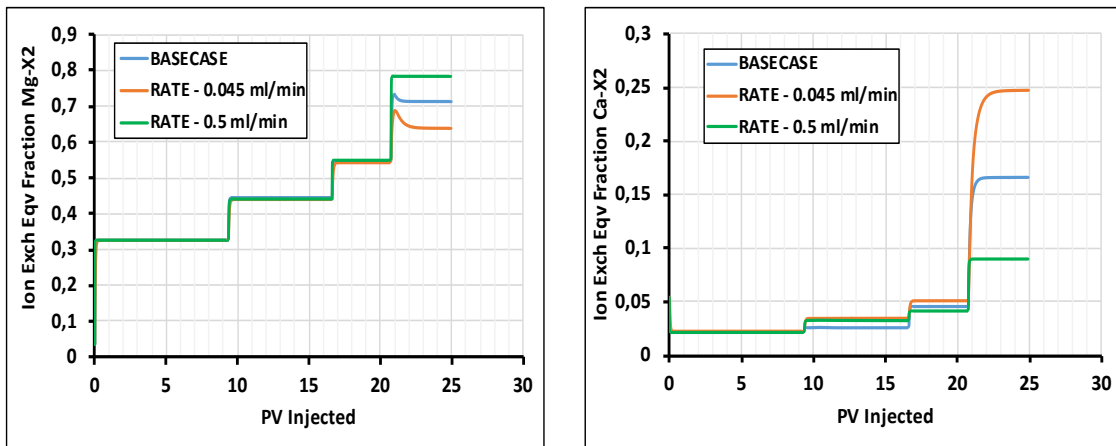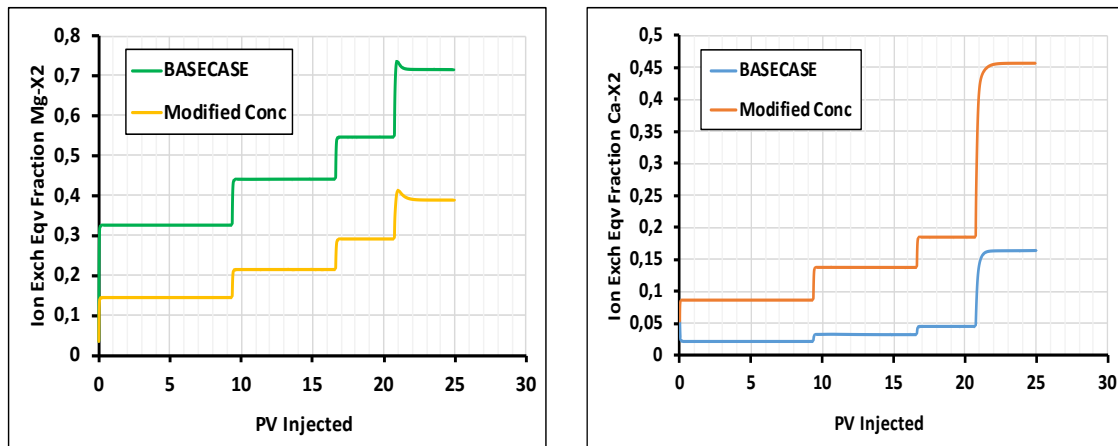

Figure 6.12: Ion exchange equivalent fraction of Mg^{2+} and Ca^{2+}, Block 1,1,1

Table 6.5: Oil recovery results for different injection concentrations of Ca^{2+} and Mg^{2+}

Injection Concentration	Oil Recovery (% OOIP)	
	Coreflood 1	Coreflood 2
Base Case	63.10	57.69
Modified Conc	57.05	51.15

6.1.5. Interpolation routines

Two additional mechanistic modeling methods have been used to investigate the ability of the different methods to model the same process. The two additional methods involve relative permeability interpolations that are based on the anion exchange occurring between the sulfate ion in the brine and the carboxylic ion in the oil, and the concentration of the sulfate ion in the aqueous phase. The two different approaches are implemented in the ROCKFLUID section. In the case of anion exchange, the equivalent fraction (EQVFRIEX) of SO_4^{2-} was used as the relative permeability interpolation parameter whereas the aqueous concentration of sulfate ion was used in the other case, and this is activated using the INTCOMP AQUEOUS $'SO_4^{2-}'$ keyword. The anion exchange reaction between the injected brine and the exchanger on the carbonate rock surface is given below:

$$SO_4{}^{2-} + 2\,CH_3COO{-}X \longleftrightarrow 2\,CH_3COO^- + SO_4{-}X_2 \tag{R2}$$
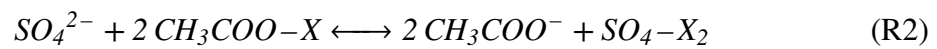
The oil recovery for the three different cases is shown in fig. 6.13. This figure shows that the oil recovery profile is very sensitive to the interpolant used in modeling the process. When the equivalent fraction of sulfate ion is used as the interpolant, no LSE is observed during LSWF. This is because all the anion exchange between sulfate ion and carboxylic ion occurs within the first five pore volumes of the injection process. That is, during SW injection as shown in fig. 6.14. When the different low salinity brines are injected, only the adsorption of divalent cations (Mg^{2+} and Ca^{2+}) is taking place. Since the equivalent fraction of SO_4^{2-} is constant during LSWF, no change in oil recovery is observed during LSWF. On the other hand, although LSE is observed when the aqueous concentration of sulfate ion is used, the required oil recovery profile that matches the experimental data is not obtained. The best match is obtained when the equivalent fraction of Mg^{2+} is used as the interpolant. The final oil recovery from the three methods are however close to each other. Table 6.6 provides a summary of the results.

(a) Coreflood 1   **(b)** Coreflood 2
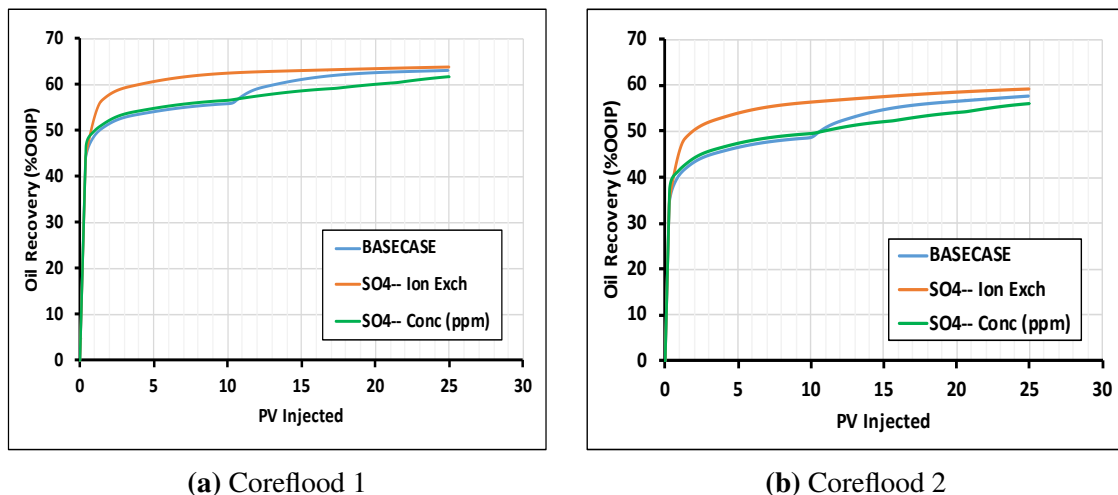
Figure 6.13: Oil recovery as a function of the mechanistic modeling method
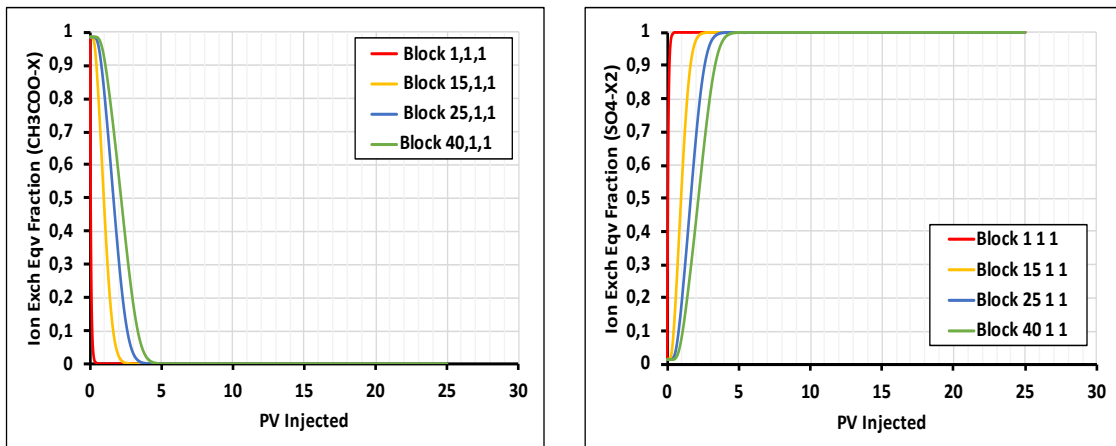
Figure 6.14: Ion exchange equivalent fraction of sulfate and carboxylic ions for different gridblocks

Table 6.6: Oil recovery results using different interpolants

Interpolant	Oil Recovery (% OOIP)	
	Coreflood 1	Coreflood 2
EQVFRIEX Mg^{2+} (Base Case)	63.10	57.69
EQVFRIEX SO_4^{2-}	63.83	59.22
SO_4^{2-} Concentration (ppm)	61.74	56.05

6.2.   Surfactant Flooding

6.2.1.   Interfacial tension

A sensitivity study was done on the interfacial tension to investigate its effect on oil recovery. This was however done only for coreflood 2; where the effect of surfactant was visible. The table of IFT values used in study are presented in table 6.7. Figure 6.15 shows the oil recovery recovery and pressure drop obtained from the simulation. A significant increase in the oil recovery is observed when the IFT is decreased, due to an increase in viscous forces (capillary number). The oil recovery increases from 48.66% after seawater flooding to 65.58% after surfactant flooding; an increase of 16.92% compared to the 2.51% increase with the original IFT values. A corresponding increase in pressure drop is also observed with the increase in oil recovery. Since the salinity and adsorption values are kept constant, the two-phase flow of oil and water ahead of the surfactant slug as proposed by Tavassoli et al.[84] could be the reason for the increase in the pressure drop. The pressure drop profile also shows that some numerical dispersion might be occurring during surfactant flooding.
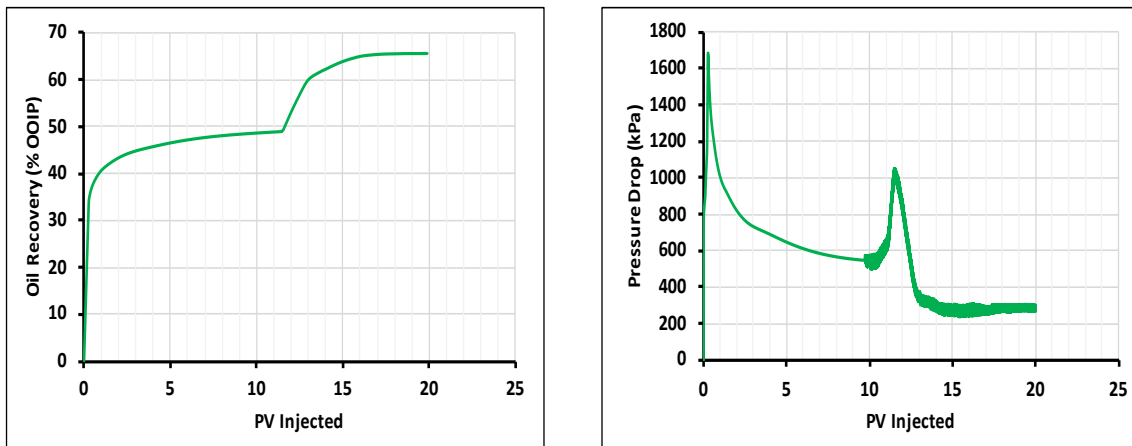
Figure 6.15: Oil recovery and pressure drop

Table 6.7: Oil-water IFT table used for sensitivity study

cift	sigft
0	20.75
0.00004224	0.5
0.00021121	0.1

$cift$ is the surfactant mole fraction, $sigft$ is the oil-water IFT.

6.2.2. Adsorption

Similarly, the effect of adsorption on oil recovery was investigated. The adsorption was decreased by a factor of 10 compared to the base case. A comparison of the oil recovery and pressure drop is shown in fig. 6.16. When surfactant adsorption is low, the effect of surfactant on oil recovery is observed much earlier after the surfactant is injected, compared to when the adsorption is higher. The lower adsorption also corresponds to less increase in pressure drop, which confirms that adsorption also contributes to the increase in pressure drop during surfactant flooding. The final recovery factor for the two cases is however still the same. The oil recovery is mainly given by the relative permeability interpolation, and in this case, the interpolation is based on the capillary number, which depends mainly on the IFT. Since the IFT values are kept constant, there is no change in the relative permeability and the same recovery is obtained for both cases. A comparison of the adsorption for the two cases is shown in fig. 6.17.
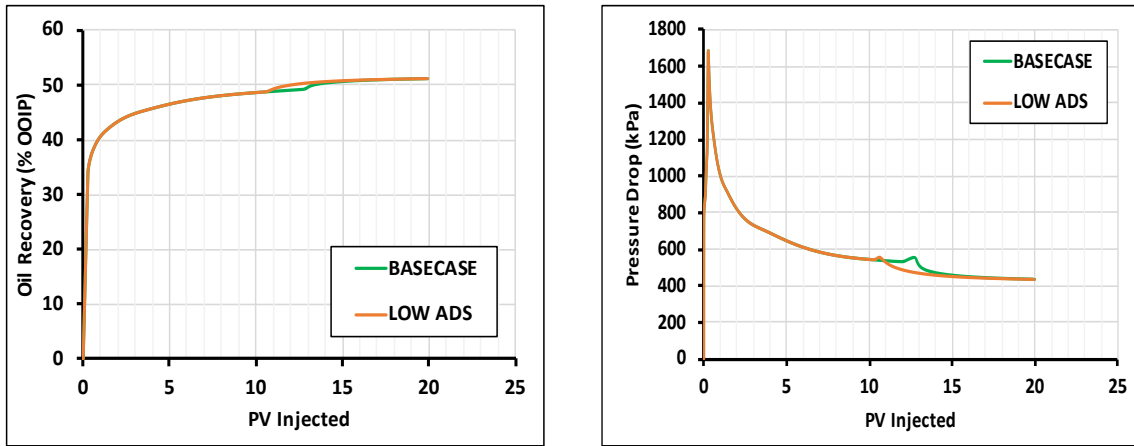
Figure 6.16: Oil recovery and pressure drop
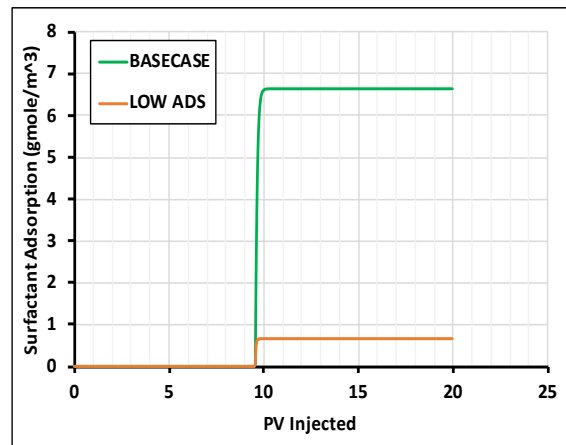
Figure 6.17: Surfactant adsorption, Block 1,1,1

6.3.   Chapter Summary

This chapter presents and discusses the results of sensitivity studies done on many key parameters that could affect the LSWF process, and simulation results. Simulation results show that the timing of low salinity waterflooding, injection rate, injection temperature and composition have significant effect on LSWF. The earlier the onset of LSWF, the higher the increase in oil recovery because the injected brine has more time to interact with the reservoir rock and fluids. At medium injection rates, both physical and chemical displacements are favored leading to a higher increase in oil recovery than at low or high injection rates where only chemical and physical displacements dominate, respectively. Injection temperature has a significant effect on the intra-aqueous, mineral and ion exchange reactions, and thus affects the oil recovery.

The simulation results are also strongly affected by the mechanistic modeling method used to model the process. When LSWF was modeled based on anion exchange between SO_4^{2-} and CH_3COO^-; using the ion exchange equivalent fraction of sulfate ion as the interpolant, no LSE was observed during LSWF. When the interpolant was changed to the concentration of sulfate ion in the aqueous phase, an increase in oil recovery was observed during LSWF. However, the oil recovery profile was different from the experimental results. A closer match between experimental and simulation results was obtained when the ion exchange equivalent fraction of Mg^{2+} was used as the interpolant.

Surfactant adsorption and IFT have a significant effect on the success of any surfactant flooding project. The lower the adsorption, the earlier the effect of the surfactant is observed, and the lower the concentration of surfactant that would be required to attain the same results as when surfactant adsorption is high. In addition, the greater the ability of the surfactant to reduce IFT, the higher the oil recovery.

7.   Conclusions

This thesis has investigated the geochemical modeling of low salinity waterflooding and surfactant flooding. A history match of laboratory data from coreflood experiments done on heterogeneous low permeability carbonate cores has been performed using the EOS compositional simulator GEM™ by CMG. Sensitivity analysis has been done on some key parameters to investigate their effects on the results obtained.

Based on the history matching and sensitivity analysis, the following conclusions have been drawn:

- GEM™ has the ability to model both low salinity waterflooding and surfactant flooding. However, the academic versions of GEM™ cannot currently model a hybrid EOR process such as low salinity surfactant flooding, because it lacks the ability to interpolate between rock regions. In the modeling of LSWF, many different mechanistic methods can be used to history match laboratory data, using detailed geochemistry. The method selected should be based on the reservoir properties and the experimental workflow and results.

- A mechanistic modeling method that incorporates multicomponent ion exchange, intra-aqueous and mineral reactions, and wettability alteration has been used to model low salinity waterflooding. An increase in oil recovery of about 7% and 9% was observed during low salinity waterflooding for the two coreflood experiments, respectively. Multicomponent ion exchange involving the exchange of SO_4^{2-}, CH_3COO^-, Ca^{2+} and Mg^{2+} between the injected brine and the carbonate rock surface has been identified as the main mechanism responsible for wettability alteration, and the observed increase in oil recovery during low salinity waterflooding for both coreflood simulations. Other contributing mechanisms include mineral dissolution/precipitation, and pH increase. Capillary pressure has a significant effect on history matching of experimental pressure drop during low salinity waterflooding, and should also be included in the modeling.

- The timing of low salinity waterflooding has a significant effect on oil recovery. The earlier the onset of low salinity waterflooding, the more the oil recovery is enhanced because the low salinity brine has more time to interact with the reservoir rock and fluids. An increase in oil recovery of about 7% and 8% was observed when low salinity water was implemented in secondary mode compared to seawater injection, respectively. In tertiary mode, the highest recoveries were obtained when low salinity waterflooding was implemented at the earliest time. However, the recoveries from the three different implementation times in tertiary mode were similar. Due to the additional costs associated with implementing low salinity waterflooding in secondary mode or at an earlier time in tertiary mode, a comprehensive economic analysis is required to determine the optimal start-up time for low salinity waterflooding.

- Benefits from low salinity waterflooding are from a combination of both physical and chemical displacement processes, which makes the injection rate a very important parameter in the process. At low rates, chemical displacement dominates whereas

both physical and chemical displacements dominate at moderate rates. At high rates, physical displacement dominates leaving behind a lot of unswept oil. Determining the optimal injection rate is therefore a crucial part of any low salinity waterflooding project. Temperature effects on mineral and ion exchange reactions can also be significant and should be included when modeling the process.

- In carbonate reservoirs where low salinity waterflooding is implemented in tertiary mode, the relative permeability interpolation should be based on either the ion exchange equivalent fraction of Ca^{2+} or Mg^{2+}, or the aqueous concentration of one of the potential determining ions (SO_4^{2-}, Ca^{2+} and Mg^{2+}). The ion exchange equivalent fraction of SO_4^{2-} should not be used as the interpolant because all the anion exchange between SO_4^{2-} and CH_3COO^- occurs during seawater injection, and thus no low salinity effects would be observed. If the reservoir temperature is greater than 90°C, the equivalent fraction of Mg^{2+} should be used as the relative permeability interpolation parameter. On the other hand, the equivalent fraction of Ca^{2+} would be a more appropriate interpolant if the reservoir temperature is less than 90°C. Additionally, the concentrations of Ca^{2+} and Mg^{2+} in the injected fluids should be taken into consideration when deciding which interpolant to use.

- Detailed and robust geochemistry should be included when modeling surfactant flooding. The potential of surfactants to enhance oil recovery after high salinity (seawater) waterflooding has been tested and compared to the experimental results of when surfactants are injected after low salinity waterflooding. Increase in oil recovery of 0.82% and 2.51% compared to 3.5% and 4.8%, respectively, shows that a low salinity environment is beneficial for surfactants. Adsorption or retention of surfactants is a crucial part of any surfactant flooding project and should be included in the modeling of such a process. The ability of a surfactant to reduce the IFT is also key to the effectiveness of the surfactant to mobilize trapped oil. Although anionic surfactants have low adsorption in carbonates, they are ineffective at reducing the IFT, and should therefore be used as a cosurfactant during surfactant flooding.

- The potential of a hybrid low salinity water and surfactant flooding process has been tested for one of the coreflood simulations and indicates that the combined process gave a higher final recovery than the individual low salinity waterflooding and surfactant flooding processes. Surfactants are able to enhance oil recovery by reducing the oil-water interfacial tension, and thus increasing the microscopic sweep efficiency. Surfactant phase behavior is improved while adsorption is reduced in a low salinity environment, thus enabling the surfactants to be more effective at enhancing oil recovery.

- Although the modeling done in this thesis is for two cores from the same carbonate reservoir, the same workflow can be followed to model coreflood experimental results of low salinity waterflooding, surfactant flooding and low salinity surfactant flooding for cores from different carbonate reservoirs.

8. Recommendations for Future Work

The modeling studies done in this thesis reveal that the academic versions of GEM™ have the ability to model low salinity waterflooding and surfactant flooding using robust geochemistry, but currently has the limitation of interpolating between rock regions when modeling a hybrid enhanced oil recovery process. Based on the results and observations from the modeling studies, the following recommendations for future work have been put forward:

- Further research on how to overcome the current limitation of GEM™ being unable to interpolate between rock regions for hybrid EOR processes is required.

- Upscaling of the simulation models used in this thesis to evaluate the behavior of the process at reservoir scale would be interesting. This would provide a way to evaluate the impact of important properties such as wettability and reservoir heterogeneity.

- The use of different mechanistic modeling methods revealed that the experimental results and reservoir properties are important parameters to consider when deciding which method to use. It would however be also interesting to use even more methods to model the same coreflood experiments than the three used in this thesis.

- In-situ generation of surfactant has been observed, and might contribute to the improved oil recovery during low salinity surfactant flooding. Further research into the conditions such as pH at which this occurs would reveal even more interesting findings and provide a way of enhancing oil recovery from the process even further.

9. Bibliography

Adegbite, J. O., Al-Shalabi, E. W., and Ghosh, B. (2018). Geochemical modeling of engineered water injection effect on oil recovery from carbonate cores. *Journal of Petroleum Science and Engineering*, 170:696–711.

Agbalaka, C., Y, A., Dandekar, Patil, S. L., and Khataniar, S. (2008). An investigation of the effects of wettability on the recovery of oil by water flooding. In *Proceedings of the 2008 SPE Asia Pacific Oil and Gas Conference*, pages 1–13, Perth, Australia. Society of Petroleum Engineers.

Ahmed, T. (2010). Fundamentals of Rock Properties. In *Reservoir Engineering Handbook*, chapter 4, pages 189–287. Gulf Professional Publishing, 30 Corporate Drive, Suite 400, Burlington, MA 01803, USA, 4 edition.

Akbar, M. and Alghamdi, A. H. (2000). A snapshot of carbonate reservoir evaluation. *Oilfield Review*, pages 20–22.

Al-Attar, H. H., Mahmoud, M. Y., Zekri, A. Y., Almehaideb, R., and Ghannam, M. (2013). Low-salinity flooding in a selected carbonate reservoir: experimental approach. *Journal of Exploration and Production Technology*, 3:139–149.

Al-Shalabi, E., Sepehrnoori, K., and Delshad, M. (2013). Does the Double Layer Expansion Mechanism Contribute to the LSWI Effect on Hydrocarbon Recovery from Carbonate Rocks. In *Proceedings of the SPE Reservoir Characterization and Simulation Conference and Exhibition*, pages 1–17, Abu Dhabi, UAE. Society of Petroleum Engineers.

Aladasani, A., Bai, B., and Wu, Y.-S. (2012). Investigating Low Salinity Waterflooding Recovery Mechanisms in Carbonate Reservoirs. In *Proceedings of the SPE EOR Conference at Oil and Gas West Asia*, pages 1–21, Berlin. Society of Petroleum Engineers.

Alagic, E. and Skauge, A. (2010). Combined Low Salinity Brine Injection and Surfactant Flooding in Mixed-Wet Sandstone Cores. *Energy Fuels*, 24:3551–3559.

Alameri, W., Teklu, T. W., Kazemi, H., and AlSumaiti, A. M. (2015). Low-salinity Water-alternate-surfactant in Low-permeability Carbonate Reservoirs. In *Proceedings of the 18th European Symposium on Improved Oil Recovery*, pages 1–16.

Altahir, M., Yu, M., and Hussain, F. (2017). Low salinity water flooding in carbonate rocks – dissolution effect. In *Proceedings of the 2017 International Symposium of the Society of Core Analysts*, pages 1–8, Vienna, Austria.

Amott, E. (1959). Observations relating to the wettability of porous rock. *Petroleum Transactions, AIME*, 216:156–162.

Anderson, W. G. (1987a). Wettability Literature Survey-Part 4: Effects of Wettability on Capillary Pressure. *Journal of Petroleum Technology*, 39:1283–1300.

Anderson, W. G. (1987b). Wettability Literature Survey-Part 5: Effects of Wettability on Relative Permeability. *Journal of Petroleum Technology*, 39:1453–1468.

Appelo, C. and Postma, D. (2005). *Geochemistry, Groundwater and Pollution*. A.A. Balkema Publishers, Amsterdam, the Netherlands, 2 edition.

Arri, L. E., Yee, D., Morgan, W. D., and Jeansonne, M. (1992). Modeling Coal bed Methane Production With Binary Gas Sorption. In *Proceedings of the SPE Rocky Mountain Regional Meeting*, SPE 24363, pages 459–472, Casper, Wyoming. Society of Petroleum Engineers.

Austad, T., Shariatpanahi, S. F., Strand, S., Black, C. J. J., and Webb, K. J. (2011). Conditions for a Low-Salinity Enhanced Oil Recovery (EOR) Effect in Carbonate Oil Reservoirs. *Energy Fuels*, 26:569–575.

Austad, T., Strand, S., Høgnesen, E. J., and Zhang, P. (2005). Seawater as IOR fluid in Fractured Chalk. In *Proceedings of the 2005 SPE International Symposium on Oilfield Chemistry*, pages 1–10, The Woodlands, Texas, USA. Society of Petroleum Engineers.

Awolayo, A. N., Sarma, H. K., and long X. Nghiem (2017). A Comprehensive Geochemical-Based Approach at Modeling and Interpreting Brine Dilution in Carbonate Reservoirs. In *SPE Reservoir Simulation Conference*, pages 1–27, Montgomery, TX, USA. Society of Petroleum Engineers.

Bernard, G. G. (1967). Effect of waterflood Salinity on Recovery of Oil from Cores Containing Clays. In *Proceedings of the 38th SPE Annual California Regional Meeting*, SPE 1725, pages 1–8. Society of Petroleum Engineers.

Bethke, C. M. (1996). *Geochemical Reaction Modeling: Concepts and Applications*. Oxford University Press, New York.

Blunt, M. J. (2017). *Multiphase flow in Permeable Media: A Pore Scale Perspective*. Cambridge University Press, Cambridge.

British Geological Survey (2006). Limestone. *Mineral Planning Factsheet*, pages 1–9.

Brooks, R. H. and Corey, A. T. (1964). Hydraulic properties of porous media. *Hydrology Papers*, pages 1–37.

Callegaro, C., Bartosek, M., Franco Masserano, M. N., Parracello, V. P., Pizzinelli, C. S., and Caschili, A. (2013). Opportunity of Enhanced Oil Recovery Low salinity Water Injection: From Experimental Work to Simulation Study up to Field proposal. In *Proceedings of the EAGE Annual Conference & Exhibition*, pages 1–13, London, United Kingdom. Society of Petroleum Engineers.

Chandrasekhar, S. and Mohanty, K. (2013). Wettability Alteration with Brine Composition in High Temperature Carbonate Reservoirs. In *Proceedings of the SPE Annual Technical Conference and Exhibition*, pages 1–17, New Orleans, Louisiana, USA. Society of Petroleum Engineers.

Computer Modelling Group Ltd. (2018). GEM : Compositional and Unconventional Simulator.

Craig Jr., F. F. (1971). *The Reservoir Engineering Aspects of Waterflooding: SPE Monograph Series, Vol. 3*. American Institute of Mining, Metallurgical and Petroleum engineers, Inc, Richardson, Texas.

Dang, C., Nghiem, L., Nguyen, N., Chen, Z., and Nguyen, Q. (2015). Modeling and Optimization of Low Salinity Waterflood. In *Proceedings of the SPE Reservoir Simulation Symposium*, pages 1–19, Houston, Texas, USA. Society of Petroleum Engineers.

Dang, C., Nghiem, L., Nguyen, N., Chen, Z., and Nguyen, Q. (2016). Mechanistic modeling of low salinity water flooding. *Journal of Petroleum Science and Engineering*, 146:191–209.

Dang, C. T. Q. (2015). *Mechanistic Modeling, Design, and Optimization of Low Salinity Waterflooding*. Doctoral thesis, University of Calgary.

Delaney, J. M. and Lundeen, S. R. (1990). The Lawrence Livermore National Laboratory Thermodynamic Database. In *Lawrence Livermore National Report UCRL-21658*.

Derkani, M. H., Fletcher, A. J., Abdallah, W., Sauerer, B., Anderson, J., and Zhang, Z. J. (2018). Low Salinity Waterflooding in Carbonate Reservoirs : Review of Interfacial Mechanisms. *Colloids and Interfaces*, 2:1–43.

Donaldson, E. C., Thomas, R. D., and Lorenz, P. B. (1969). Wettability Determination and Its Effect on Recovery Efficiency. *Society of Petroleum Engineers Journal*, 9:13–20.

Enge, I. B. (2014). The effect of brine composition and rock type on oil recovery by the use of combined low-salinity waterflooding and surfactant flooding. Master's thesis, Norwegian University of Science and Technology.

Farad, S., Mugisa, J., Alahdal, H. A., Idris, A. K., Kisiki, N. H., and Kabenge, I. (2016). Effect of wettability on oil recovery and breakthrough time for immiscible gas flooding. *Petroleum Science and Technology*, 34:1705–1711.

Feng, Q., Zhou, J., Chen, Z., Wang, X., Ni, F., and Yang, H. (2002). Study on EOR Mechanisms by Microbial Flooding. In *Proceedings of the 26th Annual SPE International Technical Conference and Exhibition in Abuja, Nigeria*, pages 1–11. Society of Petroleum Engineers.

Ginsburg, R. N. and James, N. P. (1974). Holocene carbonate sediments of continental shelves. In Burk, C. and Drake, C., editors, *The Geology of Continental Margins*, pages 137–155. Springer, Berlin, Heidelberg.

Glover, P. W. J. Porosity. In *Petrophysics MSc Course Notes*, chapter 2, pages 10–20.

Hall, F. E., Zhou, C., Gasem, K. A. M., Robinson Jr., R., and Yee, D. (1994). Adsorption of Pure Methane, Nitrogen, and Carbon Dioxide and Their Binary Mixtures on Wet Fruitland Coal. In *Proceedings of the 1994 Eastern Regional Conference & Exhibition*, SPE 29194, pages 329–344, Charleston, West Virginia. Society of Petroleum Engineers.

Hallenbeck, L., Sylte, J., Ebbs, D., and Thomas, L. (1991). Implementation of the Ekofisk Field Waterflood. *SPE Formation Evaluation*, 6:284–290.

Hamouda, A. A. and Gupta, S. (2017). Enhancing oil recovery from chalk reservoirs by a low-salinity water flooding mechanism and fluid/rock interactions. *Energies*, 10:1–16.

Hiorth, A., Cathles, L. M., Kolnes, J., Vikane, O., Lohne, A., Korsnes, R. I., and Madland, M. V. (2008). A chemical model for the Seawater-CO_2-Carbonate system – Aqueous and Surface Chemistry. In *Proceedings of the 2008 International Symposium of the Society of Core Analysts*, pages 1–12, Abu Dhabi, UAE.

Honarpour, M., Koederitz, L., and Harvey, A. H. (1986). *Relative Permeability of Petroleum Reservoirs*. CRC Press, Inc., Boca Raton, Florida.

Iglauer, S., Pentland, C. H., and Busch, A. (2015). CO_2 wettability of seal and reservoir rocks and the implications for carbon geo-sequestration. *Water Resources Research*, 51:729–774.

Jahanbani G., A. and Torsaeter, O. (2018). Numerical Simulation Of Low Salinity Water Flooding: Wettability Alteration Considerations. In *Proceedings of the 16th European Conference on the Mathematics of Oil Recovery*, ECMOR XVI 2018, pages 1–15, Barcelona, Spain. EAGE.

Jerauld, G. R., Lin, C. Y., Webb, K. J., and Seccombe, J. C. (2008a). Modeling Low-Salinity Waterflooding. *SPE Reservoir Evaluation & Engineering*, 11:1000–1012.

Jerauld, G. R., Webb, K. J., Lin, C. Y., and Seccombe, J. C. (2008b). Modeling Low-Salinity Waterflooding. In *Proceedings of the 2006 SPE Annual Technical Conference and Exhibition*, pages 1–13, San Antonio, Texas, USA. Society of Petroleum Engineers.

Johannesen, E. B. and Graue, A. (2007). Mobilization of Remaining Oil - Emphasis on Capillary Number and Wettability. In *Proceedings of the 2007 International Oil Conference and Exhibition*, pages 1–6, Veracruz, Mexico. Society of Petroleum Engineers.

Kantzas, A., Bryan, J., and Taheri, S. The Porous Medium. In *Fundamentals of Flow in Porous Media*, chapter 2, pages 15–170.

Kennedy, H. T., Burja, E. O., and Boykin, R. S. (1955). An investigation of the effects of wettability on the recovery of oil by water flooding. *Journal of Physical Chemistry*, 59:867–869.

Khanamiri, H. H. (2016). *Enhanced Oil Recovery by Low Salinity Surfactant: Effect of Ions on Core and Pore Scales*. Doctoral thesis, Norwegian University of Science and Technology, Trondheim, Norway.

Kharaka, Y. K., Gunter, W. D., Aggarwal, P. K., Perkins, E. H., and DeBraal, J. D. (1989). SOLMINEQ.88: A Computer Program for Geochemical Modelling of Water-Rock Reactions. In *US Geological Survey Water-Resources Investigations Report 88-4227*.

KRÜSS GmbH. Critical micelle concentration (cmc) and surfactant concentration. `https://www.kruss-scientific.com/services/education-theory/glossary/critical-micelle-concentration-cmc-and-surfactant-concentration/`. Accessed March, 28 2019.

Lager, A., Webb, K. J., Black, C. J. J., Singleton, M., and Sorbie, K. S. (2006). Low Salinity Oil Recovery - An Experimental Investigation. In *Proceedings of the International Symposium of the Society of Core Analysts*, SCA2006-36, pages 1–12, Trondheim, Norway.

Lager, A., Webb, K. J., Black, C. J. J., Singleton, M., and Sorbie, K. S. (2008). Low Salinity Oil Recovery - An Experimental Investigation. *Petrophysics*, 49:28–35.

Lake, L. W. (1989). *Enhanced Oil Recovery*. Englewood Cliffs, N.J.: Prentice Hall.

Masalmeh, S. K. (2012). Impact of capillary forces on residual oil saturation and flooding experiments for mixed to oil-wet carbonate reservoirs. In *Proceedings of the International Symposium of the Society of Core Analysts*, SCA2012-11, pages 1–14, Aberdeen, Scotland.

Meng, W., Haroun, M. R., Sarma, H. K., Adeoye, J. T., Aras, P., Punjabi, S., Rahman, M. M., and Kobaisi, M. A. (2015). A Novel Approach of Using phosphate-spiked Smart Brines to Alter Wettability in Mixed Oil-wet Carbonate Reservoirs. In *Proceedings of the Abu Dhabi International Petroleum Exhibition and conference*, pages 1–16, Abu Dhabi, UAE. Society of Petroleum Engineers.

Morrow, N. R. (1990). Wettability and Its Effect on Oil Recovery. *Journal of Petroleum Technology*, 42:1476–1484.

Morrow, N. R., Tang, G., Valat, M., and Xie, X. (1998). Prospects of improved oil recovery related to wettability and brine composition. *Journal of Petroleum Science and Engineering*, 20:267–276.

Nasralla, R. A., Mahani, H., van der Linde, H. A., Marcelis, F. H., Masalmeh, S. K., Sergienko, E., Brussee, N. J., Pieterse, S. G., and Basu, S. (2018). Low salinity waterflooding for a carbonate reservoir: Experimental evaluation and numerical interpretation. *Journal of Petroleum Science and Engineering*, 164:640–654.

Nerbøvik, S. M. (2018). Modelling of low salinity surfactant polymer coreflood experiments. Master's thesis, Universitas Bergensis.

Nghiem, L., Sammon, P., Grabenstetter, J., and Ohkuma, H. (2004). Modeling CO_2 Storage in Aquifers with a Fully-Coupled Geochemical EOS Compositional Simulator. In *Proceedings of the SPE/DOE 14th Symposium on Improved Oil Recovery*, SPE 89474, pages 1–16, Tulsa, Oklahoma, U.S.A. Society of Petroleum Engineers.

Non-Newtonian Fluid Dynamics Research Group, Massachusetts Institute of Technology. *Interfacial tension*. `http://web.mit.edu/nnf/education/wettability/interfacial.html`. Accessed on Feb 11, 2019.

Norwegian Petroleum Directorate (2017). Resource report 2017. `http://ressursrapport2017.npd.no/en/resurssrapporten-2017/`.

Norwegian Petroleum Directorate (2019). Carbonate and chalk reservoirs. `https://www.npd.no/en/force/improved-oil-and-gas-recovery/carbonate-and-chalk-reservoirs/`. Accessed May 04, 2019.

Pedersen, V. L. (2018). Low salinity waterflooding in combination with surfactant/polymer. Master's thesis, Universitas Bergensis.

Ravari, R. R. (2011). *Water-Based EOR in Limestone by Smart Water*. Doctoral thesis, University of Stavanger.

Raza, S., Treiber, L., and Archer, D. (1968). Wettability of reservoir rocks and its evaluation. *Prod. monthly*, 32:2–7.

RezaeiDoust, A., Puntervold, T., Strand, S., and Austad, T. (2009). Smart Water as Wettability Modifier in Carbonate and Sandstone: A Discussion of Similarities/Differences in the Chemical Mechanisms. *Energy Fuels*, 23:4479–4485.

Schlumberger. *Carbonate reservoirs*. `https://www.slb.com/services/technical_challenges/carbonates.aspx`. Accessed May 03, 2019.

Shalabi, E. W. A., Sepehrnoori, K., and Delshad, M. (2014). Mechanisms behind low salinity water injection in carbonate reservoirs. *Fuel*, 121:11–19.

Shehata, A., Alotaibi, M. B., and Nasr-El-Din, H. (2014). Waterflooding in Carbonate Reservoirs: Does Salinity Really Matter? *SPE Reservoir Evaluation & Engineering*, 17:304–313.

Sheng, J. J. (2011). *Modern Chemical Enhanced Oil Recovery:Theory and Practice*. Gulf Professional Publishing.

Shiran, B. S. and Skauge, A. (2013). Enhanced Oil Recovery (EOR) by Combined Low Salinity Water/Polymer Flooding. *Energy Fuels*, 27:1223–1235.

Skjaeveland, S., Siqveland, L., Kjosavik, A., Thomas, W. H., and Virnovsky, G. (2000). Capillary Pressure Correlation for Mixed-Wet Reservoirs. *SPE Reservoir Evaluation & Engineering*, 3:60–67.

Sohal, M. A., Thyne, G., , and Søgaard, E. G. (2016). Review of Recovery Mechanisms of Ionically Modified Waterflood in Carbonate Reservoirs. *Energy Fuels*, 30:1904–1914.

Sohrabi, M., Mahzari, P., Farzaneh, S. A., Mills, J. R., Tsolis, P., and Ireland, S. (2017). Novel Insights Into Mechanisms of Oil Recovery by Use of Low-Salinity-Water Injection. *SPE Journal*, 22:407–416.

Spildo, K., Sun, L., Djurhuus, K., and Skauge, A. (2014). A strategy forlow cost,effective surfactant injection. *Journal of Petroleum Science and Engineering*, 117:8–14.

Srisuriyachai, F., Panthuvichien, S., Phomsuwansiri, T., and Katekaew, W. (2016). Effects of Injection Rate of Low Salinity Brine on Oil Recovery Mechanisms and Relative Permeability Curves. In *Proceedings of the 78th EAGE Conference and Exhibition 2016*. EAGE.

Strand, S., Austad, T., Puntervold, T., Høgnesen, E. J., Olsen, M., and Barstad, S. M. F. (2008). "Smart Water" for Oil Recovery from Fractured Limestone: A Preliminary Study. *Energy Fuels*, 22:3126–3133.

Sun, S. Q. and Sloan, R. (2003). Quantification of uncertainty in recovery efficiency predictions: Lessons learned from 250 mature carbonate fields. In *Proceedings of the SPE Annual Technical Conference and Exhibition*, pages 1–15. Society of Petroleum Engineers.

Sylte, J., Hallenbeck, L., and Thomas, L. (1988). Ekofisk Formation Pilot Waterflood. In *Proceedings of the 63rd Annual Technical Conference and Exhibition*, pages 1–16, Houston, Texas. Society of Petroleum Engineers.

Tavassoli, S., Korrani, A. K. N., Pope, G. A., and Sepehrnoori, K. (2016). Low-Salinity Surfactant Flooding—A Multimechanistic Enhanced-Oil-Recovery Method. *Society of Petroleum Engineers Journal*, 21:744–760.

Teklu, T. W., Alameri, W., Kazemi, H., Graves, R. M., and AlSumaiti, A. M. (2017). Low salinity water-Surfactant-CO_2 EOR. *Petroleum*, 3:309–320.

US Department of Energy. *Enhanced oil recovery*. `https://www.energy.gov/fe/science-innovation/oil-gas-research/enhanced-oil-recovery`. Accessed Feb 26, 2019.

US Energy Information Administration (2017). *Today in Energy*. `https://www.eia.gov/todayinenergy/detail.php?id=32912`. Accessed May 03, 2019.

Wheaton, R. (2016). Basic rock and fluid properties. In *Fundamentals of Applied Reservoir Engineering*, chapter 2, pages 6–57. Gulf Professional Publishing, 50 Hampshire Street, 5th Floor, Cambridge, MA 02139, USA.

Yousef, A. A., Al-Saleh, S., and Al-Jawfi, M. (2012). Improved/Enhanced Oil Recovery from Carbonate Reservoirs by Tuning Injection Water Salinity and Ionic Content. In *Proceedings of the 18th SPE Improved Oil Recovery Symposium*, pages 1–18. Society of Petroleum Engineers.

Yousef, A. A., Al-Saleh, S., Al-Kaabi, A., and Al-Jawfi, M. (2011). Laboratory Investigation of the Impact of Injection-Water Salinity and Ionic Content on Oil recovery From Carbonate Reservoirs. *SPE Reservoir Evaluation & Engineering*, 14:578–593.

Zhang, P., Tweheyo, M. T., and Austad, T. (2006). Wettability Alteration and Improved Oil Recovery in Chalk: The Effect of Calcium in the Presence of Sulfate. *Energy Fuels*, 20:2056–2062.

Zhang, P., Tweheyo, M. T., and Austad, T. (2007). Wettability alteration and improved oil recovery by spontaneous imbibition of seawater into chalk: Impact of the potential determining ions Ca^{2+}, Mg^{2+}, and SO_4^{2-}. *Colloids and Surfaces A*, 301:199–208.

Zhang, Y. and Morrow, N. (2006). Comparison of Secondary and Tertiary Recovery With Change in Injection Brine Composition doe Crude Oil/Sandstone Combinations. In *Proceedings of the 2006 SPE/DOE Symposium on Improved Oil Recovery*, SPE 99757, pages 1–14. Society of Petroleum Engineers.

Appendix A.   Experimental Data

A.1.   Oil Recovery and Pressure Drop
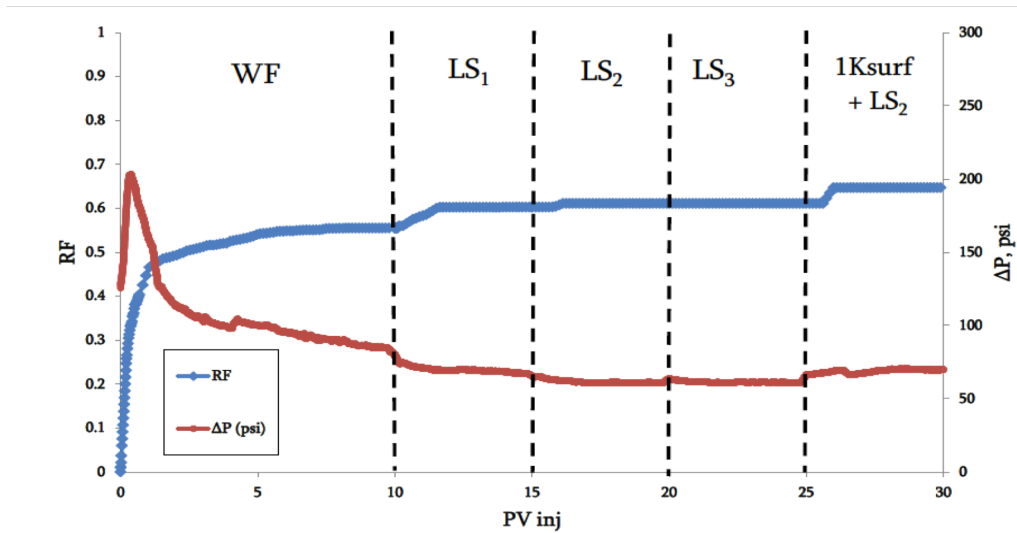
Figure A.1: Oil recovery factor (RF) and pressure drop as a function of injected pore volume of Facies-5 composite core[9].
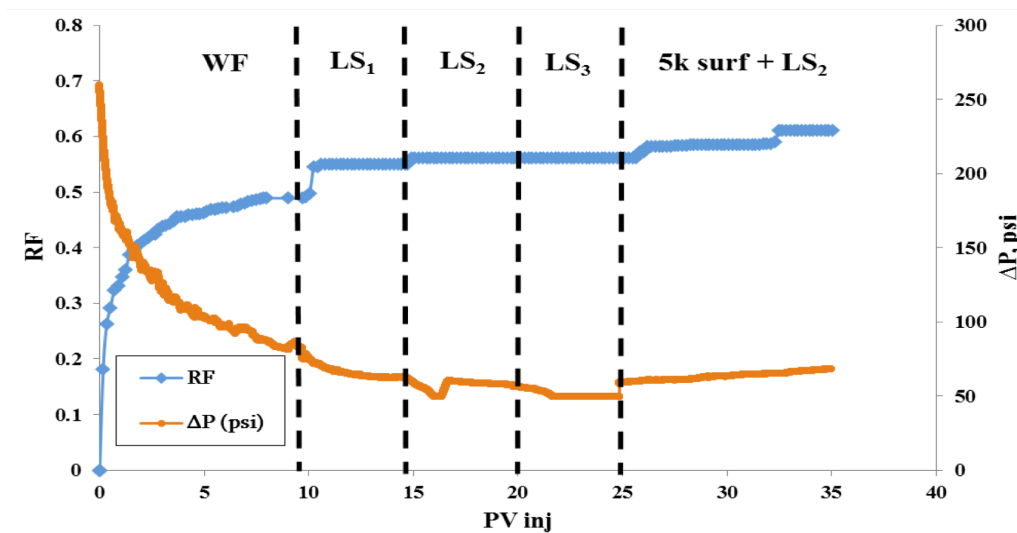
Figure A.2: Oil recovery factor (RF) and pressure drop as a function of injected pore volume of Facies-6 composite core[9].

NB: 1Ksurf + LS_2 and 5k surf + LS_2 represent 1000 ppm and 5000 ppm of surfactant dissolved in LS2 brine, respectively.

A.2. Fluid Properties and Brine Compositions

Table A.1: Fluid properties used in the simulations (Adapted from Alameri et al. [9])

Fluid	Viscosity (@195°F)	°API	pH
Oil	3	32	–
FW	0.535	–	7.17
SW	0.535	–	6.6
LS1	0.535	–	6.53
LS2	0.535	–	6.31
LS3	0.535	–	6.00

Table A.2: Compositions of brines used in the simulations (Adapted from Teklu et al. [85])

Brine/Conc. (ppm)	Na^+	Ca^{2+}	Mg^{2+}	Cl^-	SO_4^{2-}	TDS
FW	32439.52	6118.10	1229.72	65202.00	869.56	107013.8
SW	12986.10	691.54	3458.98	30110.59	4098.80	51346.0
LS1	6495.10	345.95	1729.49	15058.65	2049.82	25679.0
LS2	3247.55	172.97	864.87	7529.70	1024.91	12840.0
LS3	259.83	13.72	69.18	602.14	82.13	1027.0

Appendix B.   Draft of Paper for Submission

Geochemical modeling of low salinity waterflooding in heterogeneous
low-permeability carbonate cores

Daniel Isong Otu Egbe, Ashkan Jahanbani Ghahfarokhi*, Ole Torsaeter

Department of Geoscience and Petroleum, Norwegian University of Science and Technology

Abstract

Waterflooding has been the most widely used technique to improve recovery from oil reservoirs worldwide through pressure support. Recently, there has been growing interest in the chemistry and ionic composition of the injected water. Low salinity waterflooding (LSWF) is a relatively recent enhanced oil recovery (EOR) technique that has the ability to alter the crude oil/brine/rock (COBR) interactions, and improve oil recovery in both clastics and carbonates. Many laboratory studies and a few field studies have confirmed the potential of low salinity waterflooding to improve oil recovery. Despite the growing interest in this EOR technique, there is still no consensus on the mechanisms responsible for the increase in oil recovery. Wettability alteration is widely accepted to be the main mechanism although the mechanism for wettability alteration is still a subject of debate. This paper investigates multicomponent ionic exchange (MIE) as a mechanism for wettability alteration during low salinity waterflooding in heterogeneous low-permeability carbonate cores.

In this paper, the increase in the oil recovery during low salinity waterflooding has been modeled based on the exchange of divalent cations (Ca^{2+} and Mg^{2+}) between the aqueous phase and the carbonate rock surface. Numerical simulations have been performed using laboratory coreflood data, and oil recovery and pressure drop from experimental work have been successfully history matched. The ion exchange equivalent fractions, effluent ions concentrations, changes in mineral moles, and pH have also been examined. The results show that wettability alteration is responsible for the increase in oil recovery during low salinity waterflooding, as reflected by the shift in the crossover points of the relative permeability curves. A sensitivity study done on many key parameters such as timing of low salinity water injection, injection rate and temperature, and the mechanistic modeling method revealed that they all have huge effects on the process.

Keywords: Low salinity waterflooding (LSWF), wettability alteration, multicomponent ion exchange (MIE), low salinity effects (LSE), geochemical modeling of LSWF.

1. Introduction

Carbonate reservoirs are estimated to hold about 60% and 40% of the world's oil and gas reserves respectively [28]. Despite the significant amount of oil and gas in carbonates reservoirs, they have been very challenging to understand and develop due to their heterogeneous nature that results from the combination of depositional geometry and diagenesis. This, coupled with the fact that about 90% of carbonate rocks are either neutral or oil-wet has resulted in much lower primary recoveries (average of 30%) compared to sandstones [1,33].

Waterflooding has been and is currently the most widely used method to increase production from oil reservoirs worldwide because it is economical, easily accessible and reliable [14,11]. It is a secondary recovery mechanism that helps to increase and maintain reservoir pressure. Initially, less attention was dedicated to the effects of the chemistry and ionic composition of injected brine. However, it has recently been reported by many researchers that modifying the chemistry of the injected brine either by changing the ionic composition or the salinity by dilution can lead to significant increases in the oil recovery both in sandstones and carbonates, compared to conventional high salinity waterflooding. This is known as low salinity waterflooding (LSWF). Other names such as smart waterflooding, advanced ion

management, engineered water injection, designer waterflood, and LoSal are also used in literature.

Many laboratory studies[2,24,17,25] have reported an increase in oil recovery in carbonates from LSWF as well as a few field studies[35]. Despite the growing interest in the process, there is currently no consensus on the mechanisms responsible for the increase in oil recovery, and it is believed that a combination of mechanisms contribute to the observed low salinity effects (LSE). Moreover, the LSWF process is even less understood in carbonates compared to sandstones because carbonates are very heterogeneous in nature, lack clay minerals and due to the high bonding energy that exists between the surface of the carbonate rocks and the polar components in crude oil[16,23,27]. However, wettability alteration is widely accepted to be the primary mechanism.

The proposed wettability alteration mechanisms include: multicomponent ionic exchange (MIE), expansion of the electrical double layer (EDL), rock dissolution, fines migration, interfacial tension decrease, pH increase, and formation of micro-dispersions. A review of the different mechanisms is presented below.

Zhang et al.[36,37] proposed an MIE mechanism that involves an ion exchange process that takes place between the potential determining ions, PDIs (Mg^{2+}, Ca^{2+}, and SO_4^{2-}) in the injected brine and the carbonate rock surface. The SO_4^{2-} ions are adsorbed unto the positively charged carbonate surface, reducing the electrostatic repulsion. Ca^{2+} ions are then adsorbed and they react with the carboxylic group bonded to the carbonate rock surface. This results in the release of some carboxylic materials from the rock surface, a change in wettability, and an increase in oil recovery. They also investigated the effect of temperature on the process and observed that the adsorption of SO_4^{2-} and co-adsorption of Ca^{2+} increases with temperature as well as the substitution of Ca^{2+} by Mg^{2+} at the rock surface.

Hiorth et al.[18] proposed the dissolution of calcite as the main wettability alteration mechanism. A geochemical model was developed and tested using experimental results. They believed that if a change in surface potential was responsible for low salinity effects, then the change should be observed at both high and low temperatures. This was however not the case based on the results from their model. In addition, they suggested that the adsorption of oil components onto the carbonate rock surface is a strong and irreversibly process, and therefore the equilibrium between the rock surface and oil should not be affected by a change in water chemistry. Based on the observations, they proposed rock dissolution as a mechanism for wettability alteration in carbonates.

Altahir et al.[5] developed an innovative approach to investigate dissolution and dissolution induced fines migration using a heterogeneous limestone core. Scanning electron microscope (SEM) images were taken before and after coreflood experiments, to investigate the potential of dissolution to alter the rock geometry, and for comparison purposes. Ionic chromatography was also used to quantify the concentrations of anions and cations produced in the effluent. Fines migration was observed in all the images, and they proposed dissolution as the mechanism for fines migration. Also, no pressure drop was observed and this was attributed to the coexistence of both dissolution and fines migration. Finally, an increase in pH was observed, which they believed is further confirmation of the dissolution of calcite.

The role of COBR interactions and the formation of micelles was investigated by Sohrabi et al.[31]. Significant additional oil recovery was observed in clay-free porous medium, which they believed was due to the formation of micelles[31]. It is believed that micro-dispersions are formed in the oil-phase when low salinity water comes in contact with crude oil, and the micro-dispersions deplete the surface-active components at the oil/brine interface. This changes the balance of forces at the rock/brine and oil/brine interfaces and results in wettability alteration.

2. Numerical modeling

Reservoir modeling is a very valuable tool for the verification and validation of experimental results, and also for predictions at conditions beyond the scope of experimental work[16]. However, the number of modeling studies on low salinity waterflooding in carbonates are relatively fewer than in sandstones. This is because more time has been dedicated to understanding the mechanisms responsible for the incremental oil recovery in carbonates through laboratory studies. In addition, modeling based on the geochemical reactions that occur between the carbonate rock surface and the aqueous phases was further delayed by the complex nature of the COBR interactions and heterogeneity in carbonates[1].

Jerauld et al.[20,21] presented one of the earliest models on LSWF; which considered salt as an additional component lumped in the aqueous phase. Relative permeability, capillary pressure, and aqueous phase density and viscosity were all modeled as functions of salinity. In the model however, residual oil saturation was assumed to be linearly dependent on salinity. The model equations for relative permeability and capillary pressure are presented below:

2

$$k_{rw} = \theta k_{rw}^{HS}(S^*) + (1 - \theta)k_{rw}^{LS}(S^*) \qquad (1)$$

$$k_{row} = \theta k_{row}^{HS}(S^*) + (1 - \theta)k_{row}^{LS}(S^*) \qquad (2)$$

$$P_{cow} = \theta P_{cow}^{HS}(S^*) + (1 - \theta)P_{cow}^{LS}(S^*) \qquad (3)$$

$$\theta = (S_{orw} - S_{orw}^{LS})/(S_{orw}^{HS} - S_{orw}^{LS}) \qquad (4)$$

$$S^* = (S_o - S_{orw})/(1 - S_{wr} - S_{orw}) \qquad (5)$$

Although the same scaling factor proposed by Jerauld et al. is currently used by most LSWF models, Al-Shalabi et al.[3] pointed out the need to use different scaling parameters for handling the relative permeability and capillary pressure of oil and water respectively. They used UTCHEM; an in-house simulator at the University of Texas at Austin to simulate and history match coreflood experiments done on composite carbonate cores. It was observed that LSWF had negligible effect on the endpoint water relative permeability and corey water exponent[3]. They also highlighted the need for geochemical modeling of LSWF to investigate the change in surface charge and expansion of the EDL.

Dang et al.[13] developed a comprehensive ion exchange model that captures the geochemical reactions occurring during LSWF. The model was coupled with the compositional simulator; GEM™ from CMG and was validated with the ion exchange model of PHREEQC and two coreflood experiments; for a North Sea reservoir and a heterogeneous sandstone Texas reservoir. The geochemistry model was also used to evaluate LSWF optimization through well placement, and they investigated the potential of a hybrid EOR process that involved combining LSWF and CO_2 injection in a miscible WAG process[12,14].

A geochemical model that uses the equivalent fraction of divalent cations (Ca^{2+} and Mg^{2+}) was proposed by Awolayo et al.[7]. The model was used to history match several carbonate coreflood experiments. Based on the simulation results, they concluded that the interplay between surface charge alteration and mineral dissolution was key to the improved oil recovery at core-scale.

3. Experimental data

Two coreflood experiments were performed by Alameri et al.[4] on heterogeneous low permeability carbonate cores. The carbonate cores used for the experiments were from two facies; Facies 5 and 6 of a Middle Eastern carbonate reservoir. The experiments were aimed at investigating the viability of a hybrid of low salinity water-surfactant EOR process. This paper was however focused just on the low salinity waterflooding parts of the experiments.

The cores were first flooded with formation water at a rate of 0.1 ml/min so that the core is initially 100% saturated with brine. Oil was then injected into the cores at the same flow rate until irreducible water saturation was reached (S_{wi}). The carbonate cores were then aged for eight weeks at reservoir temperature (195°F) and pressure, for restoration of the wettability. After ageing, the cores were flooded with synthetic seawater at a flow rate of 0.1 ml/min until residual oil saturation. Brines of different salinities (LS1, LS2 and LS3) were then injected to study the effect of low salinity brine on wettability alteration and oil recovery[4]. LS1, LS2 and LS3 brines were made by diluting SW twice, four times and fifty times respectively. 5 pore volumes (PV) were injected for each set of low salinity water. Oil recovery and pressure drop for all the flooding experiments were measured and recorded. More information about the experimental work can be found in Alameri et al.[4], Teklu et al.[34].

4. Geochemistry

During low salinity waterflooding, the initial thermodynamic equilibrium of the system is disrupted through the geochemical reactions that occur at the rock/brine interface[12,19,1]. The geochemical reactions can be divided into homogeneous and heterogeneous reactions. The homogeneous reactions occur between the aqueous phase components, and are also known as intra-aqueous reactions whereas the heterogeneous reactions occur between the aqueous components and mineral species such as mineral dissolution/precipitation and ion exchange reactions[10]. The two types of reactions are typically represented as chemical equilibrium reactions and rate-dependent reactions respectively because the intra-aqueous reactions are relatively faster than the mineral dissolution/precipitation reactions.

4.1. Intra-aqueous reactions

According to Bethke[8], equilibrium constants are used in modeling chemical equilibrium reactions. For a chemical reaction to be in thermodynamic equilibrium, the rate of the forward and backward reactions must be equal; implying that the activity product of the reaction must be equal to its equilibrium constant. This concept gives rise to the governing equations for chemical equilibrium

3

reactions:

$$Q_\alpha - K_{eq,\alpha} = 0, \qquad \alpha = 1, ..., R_{aq} \qquad (6)$$

$$Q_\alpha = \prod_{i=1}^{n_{aq}} a_i^{v_{i\alpha}} \qquad (7)$$

where $K_{eq,\alpha}$ is the equilibrium constant for aqueous reaction α, R_{aq} is the number of aqueous phase reactions, Q_α is the activity product, and a_i and $v_{i\alpha}$ are the activity of component k and the stoichiometry coefficients respectively. The aqueous phase components consists of both components that only exist in the aqueous phase (n_a components) and gaseous components that are soluble in the aqueous phase, n_c. The total number of components in the aqueous phase, n_{aq} is the sum of the two. The aqueous species can also be divided into independent (primary) and dependent (secondary) aqueous species.

Tables of values of the equilibrium constants for many reactions as a function of temperature can be found in the works by Delany and Lundeen[15] and Kharaka et al.[22]. The relationship between the activities of a species i, a_i and its molality, m_i is given in eq. (8). The molality of a species is its moles per kilogram (kg) of water, and is expressed in units molal (M).

$$a_i = \gamma_i m_i, \qquad i = 1, ..., n_{aq} \qquad (8)$$

γ_i in the above equation is the activity coefficient. The activity of an ideal solution is equal to its molality because $\gamma_i = 1$. However, most solutions are non-ideal and a value other than one is required for γ_i. Many models exists for calculating the activity coefficients of electrolytic solutions such as the Debye-Hückel equation, the Davies equation and the B-Dot model[8]. An activity coefficient model describes the relation between a species' activity coefficient and the ionic strength (I) of the solution. The Davies and B-Dot models are variants of the Debye-Hückel equation developed by Debye and Hückel in 1923[8]. In GEM™, computations of the ionic activity coefficients are done using the B-Dot model. The model is widely applied in many geochemical models because it can accurately predict the activity coefficients of species over a wide range of temperature (0-300°C) and molality (up to 3M ionic strength of a solution with NaCl as the dominant solute), compared to the other models[8]. The expressions for the B-Dot equation and ionic strength are given in eqs. (9) and (10).

$$log \gamma_i = -\frac{A_\gamma z_i^2 \sqrt{I}}{1 + \mathring{a}_i B_\gamma \sqrt{I}} + \dot{B} \qquad (9)$$

$$I = \frac{1}{2} \sum_{i=1}^{n_{aq}} m_i z_i^2 \qquad (10)$$

A_γ, B_γ and $\dot{B}$ are temperature dependent coefficients, $\mathring{a}_i$ is the ion size parameter (constant), z_i is the valence number of species i, and m_i is its molality[8,10].

4.2. Mineral Dissolution/Precipitation Reactions

Reactions involving minerals and aqueous species are slower than aqueous reactions, and are modeled using kinetic rate laws[8,10]. The expression for the rate law for mineral dissolution and precipitation is given in eq. (11):

$$r_\beta = \hat{A}_\beta k_\beta \left(1 - \frac{Q_\beta}{K_{eq,\beta}}\right), \qquad \beta = 1, ...R_{mn} \qquad (11)$$

where r_β is the reaction rate, $\hat{A}_\beta$ is the reactive surface area for mineral β, and k_β, $K_{eq,\beta}$ and Q_β are the rate constant, equilibrium constant and activity product for mineral reaction β respectively. Q_β is similar to the activity product for aqueous chemical equilibrium reactions given in eq. (7):

$$Q_\beta = \prod_{i=1}^{n_{aq}} a_i^{v_{i\alpha}} \qquad (12)$$

The activities of minerals are equal to unity and are therefore not included in the above equation. The ratio ($Q_\beta/K_{eq,\beta}$) in eq. (11) is called the saturation index. Mineral dissolution occurs if log ($Q_\beta/K_{eq,\beta}$)<0 while mineral precipitation occurs if log ($Q_\beta/K_{eq,\beta}$)>0. If log ($Q_\beta/K_{eq,\beta}$)=0, the mineral is in equilibrium with the aqueous phase and no reaction occurs ($r_\beta = 0$). Equation (11) applies to minerals only. The rate of formation/-consumption of different aqueous species is obtained by multiplying r$_\beta$ by the respective stoichiometry coefficient[26,10]:

$$r_{k\beta} = v_{k\beta} \cdot r_\beta \qquad (13)$$

Reaction rate constant for different reactions are normally reported in literature at a reference temperature, T_0 (usually 298.15K or 25°C). The temperature of petroleum reservoirs is typically higher than T_0. To calculate the rate constant at a different temperature T, eq. (14) is used.

$$k_\beta = k_{0\beta} \exp\left[-\frac{E_{a\beta}}{R}\left(\frac{1}{T} - \frac{1}{T_0}\right)\right] \qquad (14)$$

where $E_{a\beta}$ and $k_{0\beta}$ are the activation energy for reaction β (J/mol) and the rate constant for reaction β at the reference temperature, T_0, R is the universal gas constant

4

(8.314J/mol-K). Both T and T_0 are in Kelvin (K). The activation energy (E_a) needed for the chemical reactions that result in wettability modification during LSWF is very important because if the reaction rate is slow, no new equilibrium would be established during the LSWF interval and thus no LS effects would be observed[27]. The activation energy is related to how strongly the polar oil components are bonded to the mineral surface, the solvency of the polar components in the actual phases and the reactivity of the ions in the injected water. The bonding energy between polar compounds in oil and carbonates is generally higher than that between the oil and clays in sandstones[27].

The equilibrium constants for aqueous and mineral reactions can alternatively be calculated using a fourth order polynomial expression as a function of reservoir temperature, T:

$$\log(K_{eq}) = a_0 + a_1 T + a_2 T^2 + a_3 T^3 + a_4 T^4 \qquad (15)$$

The default values of a_0, a_1, a_2, a_3 and a_4 for the different reactions are specified GEM's internal library and the reservoir temperature, T is 90.6°C. Equation (15) is used to calculate the equilibrium constants for all the aqueous and mineral reactions used in the modeling study.

As mineral dissolution/precipitation occurs, the surface area available for reactions also changes, and therefore the reactive surface area is an important parameter when calculating the reaction rate. The change in the reactive surface area as minerals dissolve/precipitate is calculated using eq. (16)[26,10].

$$\hat{A}_\beta = \hat{A}_\beta^0 \cdot \frac{N_\beta}{N_\beta^0} \qquad (16)$$

where $\hat{A}_\beta^0$ and N_β^0 are the reactive surface area and the number of moles of mineral β per unit gridblock bulk volume at time 0 and N_β is the number of moles of mineral β per unit gridblock bulk volume at current time.

In addition, both the void volume (porosity) and permeability of the porous medium are altered as a result of mineral dissolution and precipitation. Equations (17) and (18) are expressions for calculating the change in porosity.

$$\hat{\phi}^* = \phi^* - \sum_{\beta=1}^{n_m} \left(\frac{N_\beta}{\rho_\beta} - \frac{N_\beta^0}{\rho_\beta} \right) \qquad (17)$$

$$\phi = \hat{\phi}^*[1 + c_\phi(p - p*)] \qquad (18)$$

where ϕ is the new porosity, ϕ^* is the reference porosity with no mineral dissolution/precipitation, $\hat{\phi}^*$ is the porosity with dissolution/precipitation, ρ_β is the mineral's molar density, c_ϕ is the rock compressibility, p and p^* are respectively the current and reference pressures.

To calculate the change in permeability, the Kozeny-Carman equation is used:

$$\frac{k}{k^0} = \left(\frac{\phi}{\phi^0} \right)^3 \cdot \left(\frac{1 - \phi^0}{1 - \phi} \right)^2 \qquad (19)$$

where k^0 is the initial permeability and ϕ^0 is the initial porosity.

4.3. Ion exchange reactions

When water with a different ionic composition to the formation water is injected, multiple ion exchange and geochemical reactions occur between the ions in the aqueous phase and the rock surface. The exchange reactions are fast and homogeneous, and are therefore modeled as chemical equilibrium reactions[7,10]. The multiple ion exchange and geochemical reactions are key to the increase in oil recovery during LSWF. However, they differ with the reservoir rock type. Sulfate ions are adsorbed from the aqueous phase during LSWF in carbonates, which reduces the surface charge allowing the adsorption of cations from the aqueous phase.

In this study, multicomponent ion exchange and the resulting wettability alteration during low salinity waterflooding is modeled using the exchange of divalent cations; Ca^{2+} and Mg^{2+}. The ion exchange reactions are shown in table 2. The X in the reactions represents the ion exchanger on the carbonate rock surface. During low salinity waterflooding, Ca^{2+} and Mg^{2+} are taken up by the exchanger, while Na^+ is released. The reverse process occurs during high salinity waterflooding[10]. Ion exchange reactions are characterized by equilibrium constants, like chemical equilibrium reactions:

$$K_{Na/Ca} = \frac{[a(Ca^{2+})]^{1/2} a(Na - X)}{a(Na^+)[a(Ca - X_2)]^{1/2}} \qquad (20)$$

$$K_{Na/Mg} = \frac{[a(Mg^{2+})]^{1/2} a(Na - X)}{a(Na^+)[a(Mg - X_2)]^{1/2}} \qquad (21)$$

where a is the activity. It is however difficult to evaluate the activity coefficients of Na-X, Ca-X$_2$ and Mg-X$_2$, and thus, selectivity coefficients are used in the place of equilibrium constants according to the Thomas-Gaines convention[6]. Rewriting eqs. (20) and (21) in terms of the selectivity coefficients results in the expressions in eqs. (22) and (23).

5

$$K'_{Na/Ca} = \frac{\zeta(Na-X)[m(Ca^{2+})]^{0.5}}{[\zeta(Ca-X_2)]^{0.5}m(Na^+)} \cdot \frac{[\gamma(Ca^{2+})]^{0.5}}{\gamma(Na^+)} \quad (22)$$

$$K'_{Na/Mg} = \frac{\zeta(Na-X)[m(Mg^{2+})]^{0.5}}{[\zeta(Mg-X_2)]^{0.5}m(Na^+)} \cdot \frac{[\gamma(Mg^{2+})]^{0.5}}{\gamma(Na^+)} \quad (23)$$

where $\zeta[i - X_a]$ (i = Na$^+$, Ca^{2+} or Mg^{2+} and a is the valency) is the ion exchange equivalent fraction on the exchanger, m is the molality and γ is the activity coefficient. An important property of the exchanger is its cation exchanger capacity (CEC), which describes the amount of ions that can be adsorbed on its surface. The moles of all components in GEM™ are expressed as moles per gridblock bulk volume, N. Thus, if V is the bulk volume of the rock, the total moles of the exchangeable species (Na-X, Mg-X$_2$ and Ca-X$_2$) would be $VN_{(i-X_a)}$. Equation (24) must therefore be satisfied for a given value of CEC in the gridblock:

$$VN_{Na-X_2} + 2VN_{Ca-X_2} + 2VN_{Mg-X_2} = V\phi(CEC) \quad (24)$$

Table 1 shows the various species used in the simulations while all the intra-aqueous, mineral and ion-exchange reactions used in the modeling of low salinity waterflooding are provided in table 2.

Table 1: List of the aqueous, solid and exchange species used in coreflood simulations

Species	Elements
Independent aqueous species	H$^+$, OH$^-$, HCO$_3^-$, Ca^{2+}, Cl$^-$, CH$_3$COO$^-$, SO$_4^{2-}$, Mg^{2+}, Na$^+$
Dependent aqueous species	CaSO$_4$, MgSO$_4$, NaCl, H$_2$O, CaCH$_3$COO$^+$, CO$_2$
Solid species	CaCO$_3$, CaMg(CO$_3$)$_2$
Exchange species	Na$^+$, Ca^{2+}, Mg^{2+}

4.4. Relative permeability and capillary pressure

Relative permeability is a very important parameter for history matching of both experimental and field production data. The Brooks-Corey relative permeability correlation was used to obtain all the relative permeability curves used in the modeling studies[9]:

$$k_{rw}(s_w) = k_{rw}^o s_{wn}^{n_w} \quad (25)$$

$$k_{ro}(s_w) = k_{ro}^o (1 - s_{wn})^{n_o} \quad (26)$$

$$s_{wn} = \frac{s_w - s_{wir}}{1 - s_{wir} - s_{or}} \quad (27)$$

where k_{ro}^o and k_{rw}^o are the end-point relative permeabilities, s_{wn} is the normalized water saturation, s_{wir} is the irreducible water saturation, s_{or} is the residual oil saturation and n_o and n_w are respectively the power law parameters for oil and water; known as Corey exponents.

The effect of capillary pressure on the simulation results and history matching of coreflood data was also taken into account for low salinity waterflooding. Initially, a constant pressure and saturation is defined for all gridblocks. As the different fluids are injected, both the pressure and saturation change. The Skjaeveland capillary pressure correlation was used to model capillary pressure effects on the history match results[30]. The correlation is given in eqs. (28) and (29) for oil-wet and mixed-wet conditions respectively.

$$P_c = \frac{C_o}{\left(\frac{S_o - S_{oR}}{1 - S_{oR}}\right)^{a_o}} \quad (28)$$

$$P_c = \frac{c_w}{\left(\frac{S_w - S_{wR}}{1 - S_{wR}}\right)^{a_w}} + \frac{c_o}{\left(\frac{S_o - S_{oR}}{1 - S_{oR}}\right)^{a_o}} \quad (29)$$

where c_w, c_o, a_w and a_o are all constants for water and oil. c_w and c_o represent the entry pressures whereas a_w and a_o account for the pore size distribution. S_{wR} and S_{oR} are the irreducible water and residual oil saturations respectively.

4.5. Wettability alteration modeling

The change in wettability from more oil-wet to intermediate wet during low salinity waterflooding was proposed as the reason behind the observed increase in oil recovery from the coreflood experiments. Wettability alteration is modeled in terms of a change in the relative permeability where two separate relative permeability curves are defined; one for seawater (high salinity) and the other for low salinity water. In the modeling study, multicomponent ion exchange was assumed to be the main mechanism responsible for the change in wettability, and is modeled using the ion exchange equivalent fraction of Mg^{2+} (ζ[Mg-X$_2$]) as the interpolant for the relative permeability curves. ζ[Mg-X$_2$] represents the amount of Mg^{2+} that is adsorbed on the carbonate surface during the process.

It is assumed that the adsorption of divalent cations such as Mg^{2+} and Ca^{2+} from the injected brine onto the carbonate surface; resulting from the adsorption of SO$_4^{2-}$ during seawater injection causes the change in wettability from more oil wet to less oil wet during LSWF and thus, increase in oil recovery. Zhang et al.[36,37] reported that there is a high tendency of Mg^{2+} to substitute Ca^{2+} on the rock surface at high temperatures (usually 90°C-110°C). Since the reservoir temperature is greater

6

Table 2: List of aqueous, mineral and ion exchange reactions used in simulations

Aqueous Reactions	Equilibrium constants
$CO_2 + H_2O \longleftrightarrow H^+ + HCO_3^-$	$K_1^{eq} = 10^{-6.39}$
$H^+ + OH^- \longleftrightarrow H_2O$	$K_2^{eq} = 10^{12.39}$
$CaCH_3COO^+ \longleftrightarrow CH_3COO^- + Ca^{2+}$	$K_3^{eq} = 10^{0.38}$
$CaHCO^{3+} \longleftrightarrow Ca^{2+} + HCO_3^-$	$K_4^{eq} = 10^{-1.51}$
$CaSO_4 \longleftrightarrow Ca^{2+} + SO_4^{2-}$	$K_5^{eq} = 10^{-2.69}$
$MgSO_4 \longleftrightarrow Mg^{2+} + SO_4^{2-}$	$K_6^{eq} = 10^{-2.54}$
$HSO_4^- \longleftrightarrow H^+ + SO_4^{2-}$	$K_7^{eq} = 10^{-3.06}$
$NaCl \longleftrightarrow Cl^- + Na^+$	$K_8^{eq} = 10^{1.06}$
Mineral Reactions	**Solubility Product**
$(CaCO_3) + H^+ \longleftrightarrow Ca^{2+} + HCO_3^-$	$K_1^{sp} = 10^{6.41}$
$(CaMg(CO_3)_2) + 2H^+ \longleftrightarrow Ca^{2+} + Mg^{2+} + 2HCO_3^-$	$K_2^{sp} = 10^{2.53}$
Ion Exchange Reactions	**Selectivity Coefficient**
$Na^+ + \frac{1}{2}Ca-X_2 \longleftrightarrow \frac{1}{2}Ca^{2+} + Na-X$	$K_1^\zeta = 10^{0.67}$
$Na^+ + \frac{1}{2}Mg-X_2 \longleftrightarrow \frac{1}{2}Mg^{2+} + Na-X$	$K_2^\zeta = 10^{0.58}$

than 90°C, the ion exchange equivalent fraction of Mg^{2+} was used as the interpolant. In the modeling studies, if $\zeta[Mg-X_2]$ is less than or equal to 0.33, the oil-wet relative permeability curves are used whereas the less oil-wet curves are used when $\zeta[Mg-X_2]$ is greater than or equal to 0.43. For $\zeta[Mg-X_2]$ values between 0.33 and 0.43, interpolation is done between the two curves. The relative permeability and capillary pressure curves are shown in figs. 1 to 3.

5. Simulation Study

Two one dimensional (1D) Cartesian grid systems consisting of 30 x 1 x 1 and 40 x 1 x 1 gridblocks have been used to model the two coreflood experiments by Alameri

et al.[4]. The composite of four cores from Facies 5 was discretized into 40 gridblocks whereas that from Facies 6 (three composite cores) was discretized into 30 gridblocks. 10 gridblocks were used to represent each part of the composite cores and the dimensions were chosen such that experimental measurements are honored. The 40-gridblock and 30-gridblock models are respectively known as corefloods 1 and 2. Heterogeneity in porosity and permeability is captured by the composite nature of the cores that was used for the experiments. Based on X-Ray Diffraction (XRD), the predominant mineral is calcite, with minor occurrences of dolomite. A volume fraction 95% and 5% was therefore used for calcite and dolomite respectively. The properties of the reservoir cores and simulation models are presented in tables 3

(a) Coreflood 1
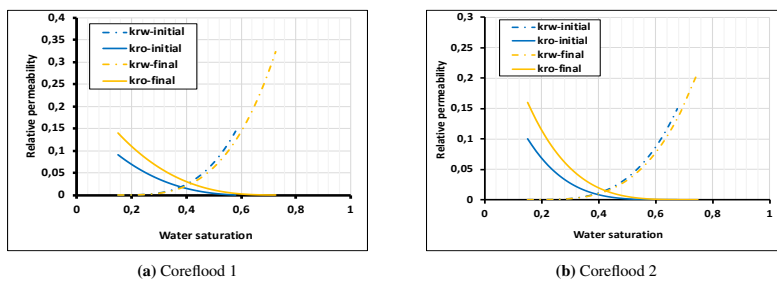
(b) Coreflood 2

Figure 1: oil-water relative permeability curves

7

(a) Initial imbibition capillary pressure curve

(b) Final imbibition capillary pressure curve
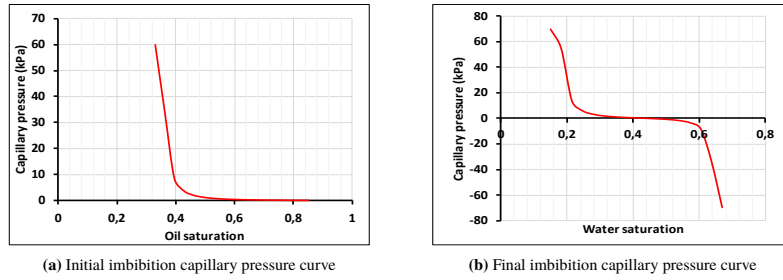
Figure 2: Coreflood 1 imbibition capillary pressure curves

(a) Initial imbibition capillary pressure curve

(b) Final imbibition capillary pressure curve
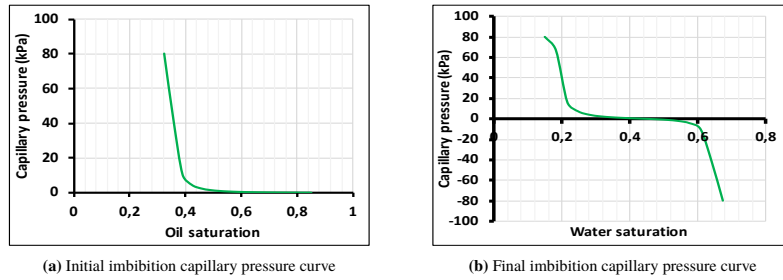
Figure 3: Coreflood 2 Imbibition capillary pressure curves

and 4. The properties and compositions of the fluids are given in tables 5 and 6. Figure 4 shows the porosity and permeability distribution for the two coreflood models.

A horizontal configuration was used for the simulation models, similar to the configurations used in the experiments, with two vertical wells; an injector and a producer. Rate control was used for the injection well and a constant injection rate of 0.1 ml/min (1.44e-4 m^3/min) was set for the injection well in both cases. Based on the dimensions of the cores used in the simulation runs, one PV is equivalent to 0.34 and 0.23 day of injection time for corefloods 1 and 2 respectively. The producer was controlled using a minimum bottomhole pressure, which was set at 1200 kPa. A sensitivity study was done on the number of gridblocks and the maximum and minimum time steps; to ensure that the physics of the process is properly captured. This can be observed from the material balance error reported during the simulation runs.

Table 3: Petrophysical properties of reservoir cores (Adapted from Alameri et al. [4])

Core properties	Facies-5 cores	Facies-6 cores
Length, L (in)	1.643 3.255 1.82 1.896	1.95 1.81 1.51
Diameter, D (cm)	3.81	
Cross-sectional Area (cm^3)	11.401	

Note: The diameter, D and cross-sectional area, A are the same for both cases

Table 5: Fluid properties used in the simulations (Adapted from Alameri et al. [4])

Fluid	Viscosity (@195°F)	°API	pH
Oil	3	32	–
FW	0.535	–	7.17
SW	0.535	–	6.6
LS1	0.535	–	6.53
LS2	0.535	–	6.31
LS3	0.535	–	6.00

8

(a) Permeability distribution for model 1

(b) Porosity distribution for model 1

(c) Permeability distribution for model 2

(d) Porosity distribution for model 2
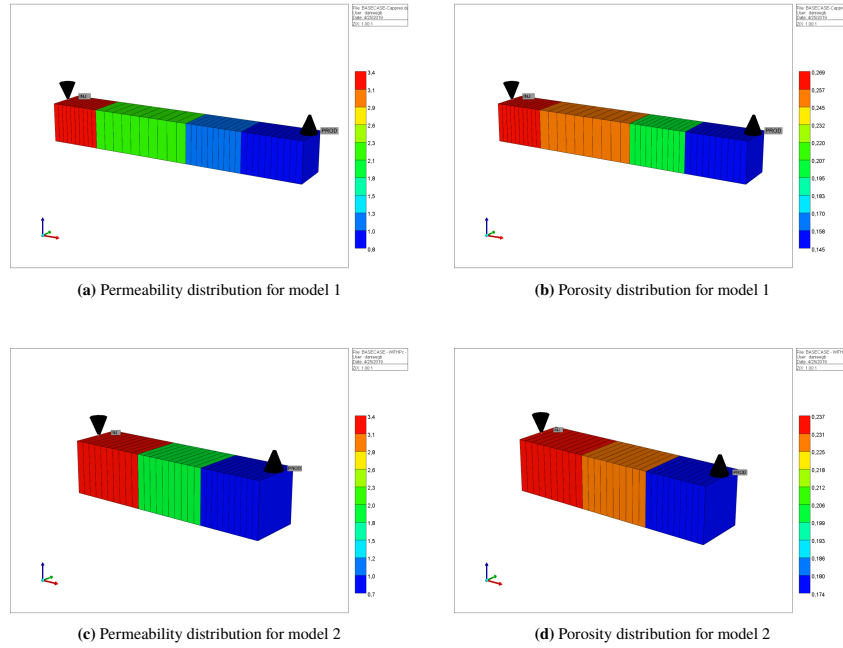
Figure 4: Simulation models with heterogeneous porosity and permeability

6. Results and discussion

Several modeling cases (data files) were built, and simulations were performed to history match the experimental results of oil recovery and pressure drop from the two coreflood experiments. The relative permeability and capillary pressure curves shown in figs. 1 to 3 depict a change a wettability from oil-wet during seawater injection to intermediate wet after low salinity waterflooding.The crossover point changes from 0.39 during seawater injection to 0.44 and 0.43 for corefloods 1 and 2, respectively.

Figures 5 and 6 show the results of the best history match obtained for oil recovery and pressure drop for the two coreflood simulations. It can be seen that the simulations results are in very good agreement with the experimental results, especially when capillary pressure is included in the model. The figures also show that cap-

illary pressure has a greater effect on the pressure drop than the oil recovery, which is in line with the observations of Adegbite et al.[1]. The history match parameters for relative permeability and capillary pressure are given in table 7 whereas the geochemical history match parameters are summarized in table 8.

Table 7: Relative permeability parameters used for history matching

Relative permeability	Coreflood 1	Coreflood 2
k_{rw}^*	0.27	0.15
k_{rO}^*	0.092	0.1
n_w	3.3	3.5
n_o	2.7	3.9
Capillary pressure		
C_w	0.08	0.1
C_O	-0.08	-0.1
$a_w = a_o$	2	2

9

Table 4: Properties of simulation models

Model Description	Coreflood 1	Coreflood 2
Model Dimensions (1D)	40 x 1 x 1	30 x 1 x 1
Gridblock sizes	Δx_1=0.0041732m Δx_2=0.0082677m Δx_3=0.0046228m Δx_4=0.0048158m Δy=Δz=0.03195m	Δx_1=0.004953m Δx_3=0.004597m Δx_3=0.003835m Δy=Δz=0.03355m
Pore Volume (cm^3)	49.3163	32.4875
Porosity (ϕ)	ϕ_1 = 0.2694 ϕ_2 = 0.246 ϕ_3 = 0.207 ϕ_4 = 0.1454	ϕ_1 = 0.2375 ϕ_2 = 0.2271 ϕ_3 = 0.1736
Permeability (K_x=K_y=K_z), mD	K_{x1} = 3.38 K_{x2} = 2.25 K_{x3} = 1.16 K_{x4} = 0.696	K_{x1} = 3.38 K_{x2} = 1.81 K_{x3} = 0.696
Initial water saturation	0.18	0.20
Reservoir Temperature ($°C$)	90.6	90.6
Initial pressure (kPa)	1200	1200
Mineral volume fraction	75% Calcite 5% Dolomite	75% Calcite 5% Dolomite

Table 6: Compositions of brines used in the simulations (Adapted from Teklu et al. [34])

Brine/Conc (ppm)	Na^+	Ca^{2+}	Mg^{2+}	Cl^-	SO_4^{2-}	TDS
FW	32439.52	6118.10	1229.72	65202.00	869.56	107013.80
SW	12986.10	691.54	3458.98	30110.59	4098.80	51346.00
LS1	6495.10	345.95	1729.49	15058.65	2049.82	25679.00
LS2	3247.55	172.97	864.87	7529.70	1024.91	12840.00
LS3	259.83	13.72	69.18	602.14	82.13	1027.00

Table 8: Geochemistry parameters used for history matching

Exchange reactions parameters	
CEC	80
$K'_{Na/Ca}$	0.67
$K'_{Na/Mg}$	0.58
Interpolation parameter 1	0.33
Interpolation parameter 2	0.43
Mineral reactions	
Reactive surface area (m^2/m^3)	100
Activation Energy (J/mol)	41870
Reaction rate Calcite (mol/m^2s)	-6.8
Reaction rate Dolomite (mol/m^2s)	-10.8

As shown in table 6, the concentration of SO_4^{2-} in SW is about 5 times its concentration in the initial formation water (FW). The higher concentration increased the amount of SO_4^{2-} adsorbed on the exchanger on the carbonate surface during SW injection , and this resulted in the desorption of oil from the rock surface. This also increased the cation exchange capacity (CEC) of the rock and subsequently led to the co-adsorption of Mg^{2+} as shown in fig. 7. Mg^{2+} was exchanged during SW injection until equilibrium was reached. That is, when the ion exchange equivalent fraction of Mg^{2+} remained constant. During LSWF, no further adsorption of SO_4^{2-} occured because of the high SO_4^{2-} adsorption that had previously occured during SW injection. However, the carbonate surface site was still open to more cation exchange, and thus the exchange of Mg^{2+} and Ca^{2+} continued until equilibrium was reached at each injection stage.

The ion exchange equivalent fractions for different gridblocks are shown in fig. 7. This figure shows that the amount of Mg^{2+} exchanged on the surface site is higher than that of Ca^{2+}, and this could be the reason for the improved recovery. Additionally, it can also be seen that as LS3 brine is injected, further adsorption of Mg^{2+} occurs only in the gridblock where the injection well is located. In the other gridblocks, the desorption of Mg^{2+} from carbonate surface takes place. On the other hand,

10

(a) Oil recovery with no Pc

(b) Pressure drop with no Pc

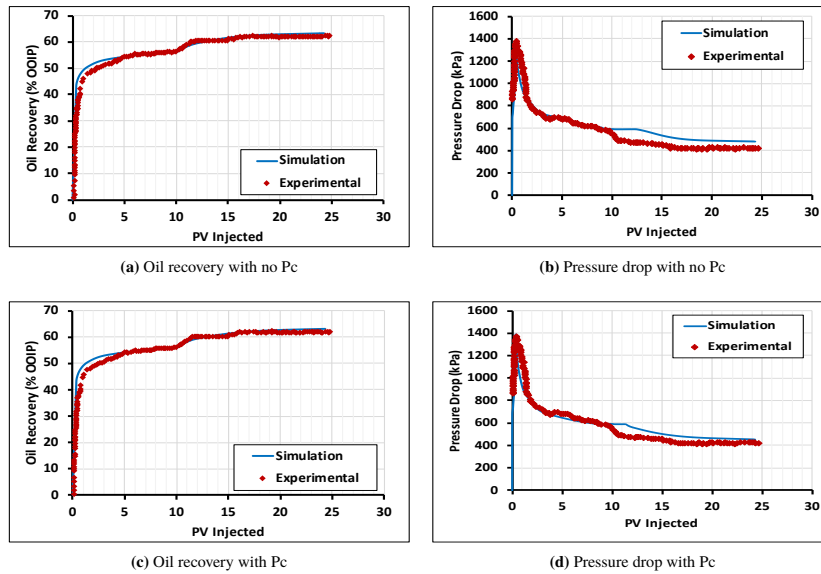**(c)** Oil recovery with Pc

(d) Pressure drop with Pc

Figure 5: History match of oil recovery and pressure drop for coreflood 1, with and without capillary pressure

there is high adsorption of Ca^{2+} for all the gridblocks. This desorption of Mg^{2+}, and adsorption of Ca^{2+} is most likely the reason why no further increase in oil recovery was observed from the experiments, after the injection of LS3 brine.

The adsorption of Mg^{2+} and Ca^{2+} decreases the amounts of the ions present in the aqueous phase and this results in the dissolution of calcite. The dissolution of calcite increases the amount of Ca^{2+} in solution, and causes the precipitation of dolomite as shown in fig. 8. However, it can be seen that calcite dissolution is about one order of magnitude higher than dolomite precipitation. A decrease in the effluent concentrations of Mg^{2+}, Ca^{2+}, SO_4^{2-}, Na^+ and Cl^- was reported from the experimental work, and the same trend was observed from the simulations as shown in fig. 9. The increase in the effluent concentration of Ca^{2+} towards the end of the injection cycle is because of an increase in Ca^{2+} adsorption during the period of LS3 brine flooding as previously discussed. The increase in Ca^{2+} adsorption increases the rate of calcite dissolution, resulting in an increase in the effluent concentration of Ca^{2+}. The ef-

fluent concentration of Mg^{2+} also increased towards the end because of a decrease in dolomite precipitation.

It is also worth noting that Na^+ and Cl^- are considered as non-active ions and are not expected to play a role in the process[7]. Since Na^+ and Cl^- were neither present in seawater nor in any of the low salinity brines, the Na^+ and Cl^- in the effluent is from the formation water. The small dips at the start of each injection stage is because of the ion exchange taking place between the injected brine and exchanger on the carbonate surface. Figure 10 shows an increase in pH during the process. There is a sharp rise in the pH at the start of LS3 brine injection, after which the pH decreases to an equilibrium value. This is due to the increased Ca^{2+} adsorption, and calcite dissolution during LS3 brine injection.

7. Sensitivity Study

Sensitivity analysis is a crucial part of every modeling study. It is aimed at investigating how results and conclusions change when some of the model's parameters and assumptions are changed. In this study, sensitiv-

11

(a) Oil recovery with no Pc

(b) Pressure drop with no Pc

(c) Oil recovery with Pc

(d) Pressure drop with Pc
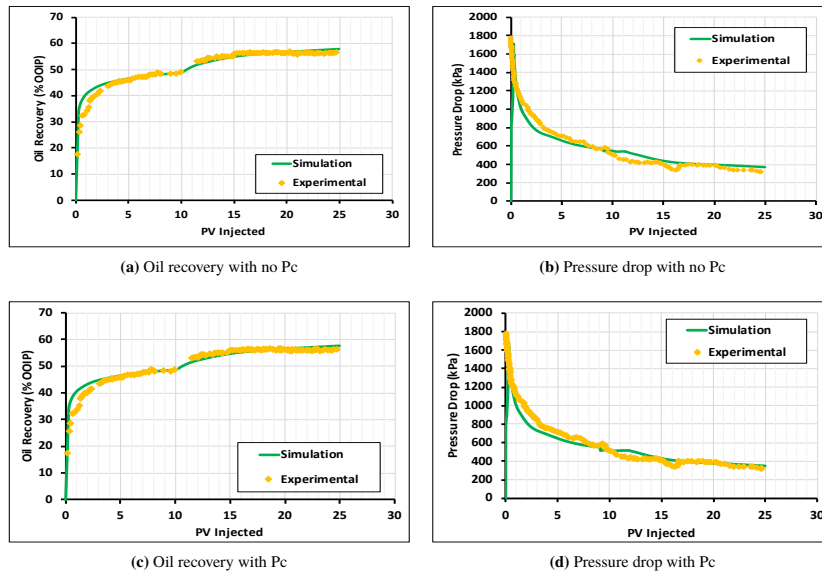
Figure 6: History match of oil recovery and pressure drop for coreflood 2, with and without capillary pressure
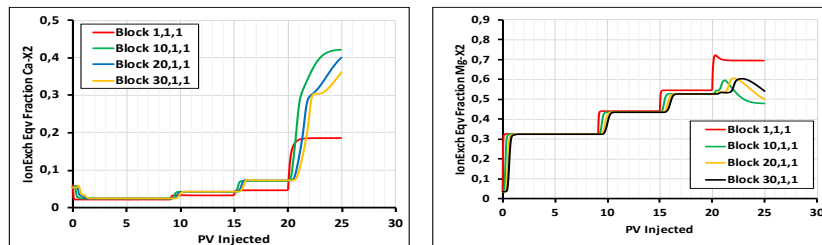
Figure 7: Ion exchange equivalent fractions for different gridblocks

ity analysis has been done on many key parameters and the results are discussed in this section, in terms of oil recovery and ion exchange equivalent fractions.

7.1. Timing of low salinity water injection

The effect of injecting low salinity water in secondary mode compared to seawater injection has been inves-tigated by some researchers[29,38]. A comparison of oil recovery from LSWF in secondary and tertiary modes was done by Zhang and Morrow[38], based on their ex-periments done on Berea sandstone cores. They con-cluded that improvement in oil recovery by LSWF is usually observed for both secondary or tertiary modes, but sometimes only for one or the other. Shiran and

12
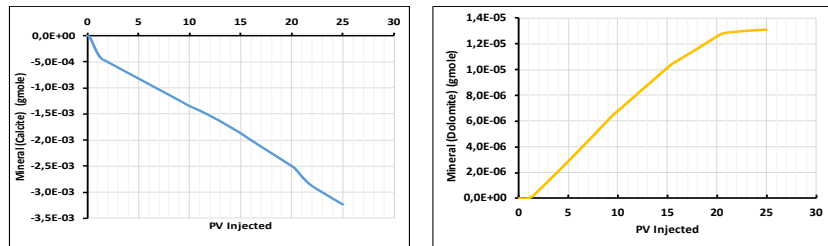
Figure 8: Changes in mineral moles of calcite and dolomite
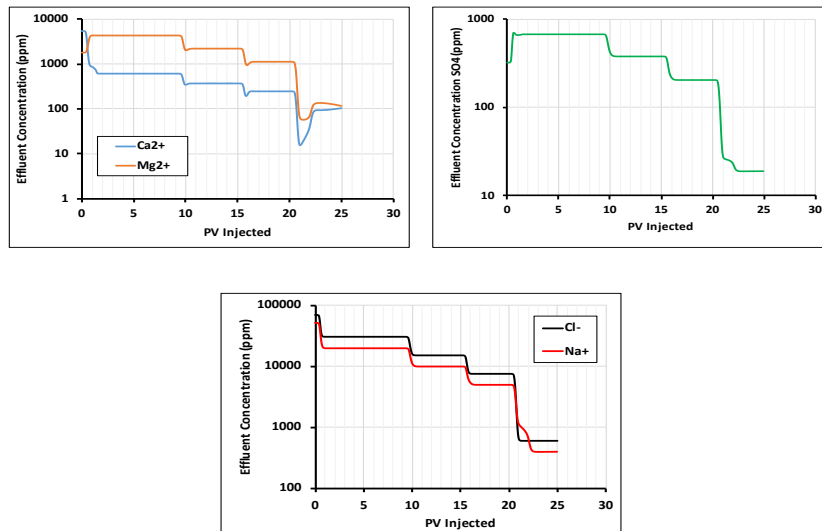
Figure 9: Effluent ions concentration

Skauge[29] also reported a positive response from injecting low salinity water in secondary mode for water-wet and intermediate-wet Berea sandstone cores. They suggested that the high oil recovery observed in secondary mode compared to tertiary mode by LSWF might be a result of effective trapping. The injection of low salinity water at an early time might lead to more effective mobilization of oil by maintaining a continuous oil phase[29].

In this thesis, the effect of injecting low salinity water in secondary and tertiary modes has been investigated and the results are discussed.

7.1.1. Secondary-mode low salinity waterflooding

Simulations have been performed for three different cases. The first case involves only seawater injection,

13

(a) Coreflood 1

(b) Coreflood 1.85

Figure 10: Effluent pH

the second case involves injection of LS1 brine and LS2 brine is injected in the third case. The three cases are known as SW, LS1 and LS2, respectively. In all three cases, 10 PV are flooded with the respective fluids. The results of oil recovery and ion exchange equivalent fractions are presented in figs. 11 and 12, respectively. A summary of the results is given in table 9.

Table 9: Oil recovery comparison for secondary mode low salinity waterflooding

Injection scheme	Oil Recovery (% OOIP)	
	Coreflood 1	Coreflood 2
SW	55.67	48.54
LS1	625	56.20
LS2	625	56.20

7.1.2. Tertiary-mode low salinity waterflooding

Injecting low salinity water in secondary mode might lead to undesirable project economics due to equipment and operational costs, which makes implementing LSWF in tertiary mode more reasonable. The effect of injection interval size of high salinity waterflooding and low salinity waterflooding has been investigated and the results are discussed in this section. Three different interval sizes have been selected, where the cores are first flooded with seawater and then with low salinity water. The simulations were done in such a way that a total of 15 PV were flooded in each case. Six different scenarios have been simulated for each of the corefloods, with three involving seawater and LS1 brine, and the other three involving seawater and LS2 brine. The six cases are known as cases 1-6. In case 1, 10 PV are injected with SW followed by 5 PV of LS1 brine, similar to the experimental procedure. Case 2 involves 7 PV of SW

(a) Coreflood 1

(b) Coreflood 2

Figure 11: Oil recovery comparison for secondary mode LSWF and SW flooding

14
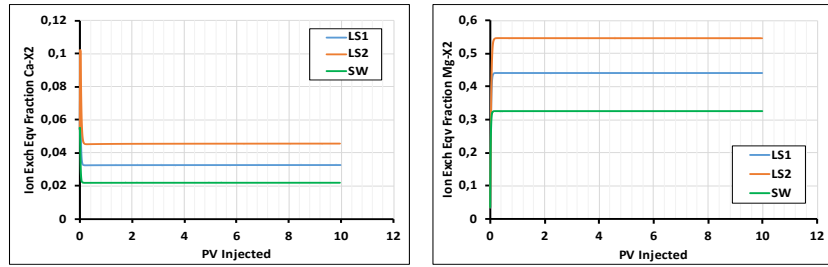
Figure 12: Ion exchange equivalent fraction of Ca^{2+} and Mg^{2+}, Block 1,1,1

injection and 8 PV of LS1 injection. 5 PV and 10 PV are flooded with SW and LS1 brine in case 3, respectively. The same interval sizes are used accordingly for cases 4 to 6. However, LS2 brine is injected instead of LS1 brine after SW injection. Figures 13 and 14 show the oil and ion exchange equivalent fractions obtained from the simulations. The results are summarized in table 10.

Table 10: Oil recovery results for the three different HS-LS injection interval sizes studies

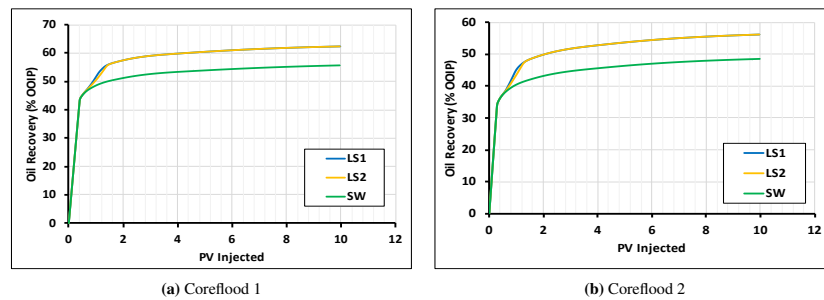| Injection scheme	Oil Recovery (% OOIP)	
	Coreflood 1	Coreflood 2
CASE 1	60.06	54.44
CASE 2	61.93	55.62
CASE 3	62.41	56.24
CASE 4	61.08	54.47
CASE 5	61.94	55.64
CASE 6	62.41	56.25

Both figs. 11 and 13 show that the earlier the onset of low salinity waterflooding, the higher the final oil recovery. When low salinity water is injected at earlier time, it has more time to interact with the reservoir rock and the fluids present. The salinity gradient that exists when low salinity water is injected into a high saline environment causes a disruption of the thermodynamic equilibrium within the reservoir, and triggers the exchange of ionic species such as SO_4^{2-}, Mg^{2+} and Ca^{2+} between the injected brine and the COBR system. This eventually leads to wettability alteration and higher oil recovery[1,36,37]. Figure 14 shows the ion exchange equivalent fractions of Mg^{2+} and Ca^{2+} for the different cases of tertiary-mode LSWF.

It should be noted the increase in oil recovery is substantially higher when LSWF is implemented in secondary mode compared to tertiary, which is in line with the observations of Shiran and Skauge[29]. In addition, fig. 13 and table 10 show that LSWF with LS2 brine yields almost the same recovery as LSWF with LS1 brine both in secondary and tertiary modes. However, the water breakthrough time (BT) for the two cases differ, with BT occurring slightly earlier for LS2 brine injection. It is worth pointing out that these investigations have been done at core scale, and the increase at reservoir scale would probably be much less. Taking into account that the timing of low salinity waterflooding might lead to higher costs, a thorough economic analysis is needed to compare the costs and benefits before a decision is made on when to implement low salinity waterflooding.

7.2. Injection rate

Low salinity waterflooding yields benefits from both physical and chemical displacement processes, unlike conventional high salinity waterflooding where the benefits is mostly from physical displacement[32]. Physical displacement occurs immediately as the process of water injection begins whereas it takes some time for chemical displacement to begin, due to the time taken for the ions in the brine to react with the rock surface. The injection rate is therefore a crucial parameter in optimizing the low salinity process. In this thesis, the effect of injection rate on oil recovery has been investigated using three injection rates. The three injection rates include: 0.1 (base case), 0.045 and 0.5; all in ml/min.

Figure 15 shows that the higher the injection rate, the higher the oil recovery. At low injection rates, chemical displacement dominates while at high/moderate injection rates, both physical and chemical displacements are favored, resulting in higher recovery. The effect of the

15

(a) Coreflood 1 SW-LS1

(b) Coreflood 2 SW-LS1

(c) Coreflood 1 SW-LS2

(d) Coreflood 2 SW-LS2
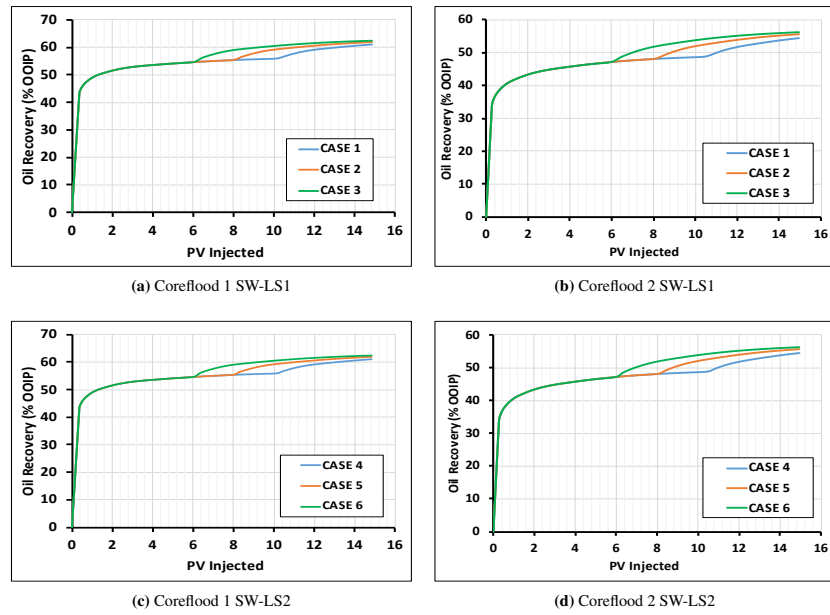
Figure 13: Oil recovery as a function of interval size of high salinity (seawater) and low salinity water injection.

injection rate on the ion exchange equivalent fractions of Mg^{2+} and Ca^{2+} is shown in fig. 16. This figure shows that changing the injection rate has little effect on the geochemical interactions, thus implying that the change in oil recovery with injection rate is most likely due to a change in the contribution from physical displacement. Although not investigated in this thesis, it is expected that at very high injection rates, only physical displacement will dominate because the ions in the injected brine would not have enough time to interact with the rock surface, and the recovery from the process would also be less than at moderate injection rates [32]. The oil recovery results are summarized in table 11.

Table 11: Oil recovery results for the three different injection rates

| Injection rate (ml/min) | Oil Recovery (% OOIP) | |
	Coreflood 1	Coreflood 2
0.1-Base case	63.10	57.69
0.045	61.49	56.23
0.5	64.54	60.45

7.3. Injection temperature

The effect of temperature on low salinity waterflooding was also investigated; using three different injection temperatures. The first case is the base case, where the injection temperature is the same as the reservoir temperature (90.6°C). In the second case, the injection temperature (70°C) is less than the reservoir temperature and finally, the injection temperature (110°C) is higher than the reservoir temperature in the last case.

Figure 17 shows that there is very little change in the oil recovery as the injection temperature changes. This

16

(a) SW-LS1

(b) SW-LS1

(c) SW-LS2

(d) SW-LS2
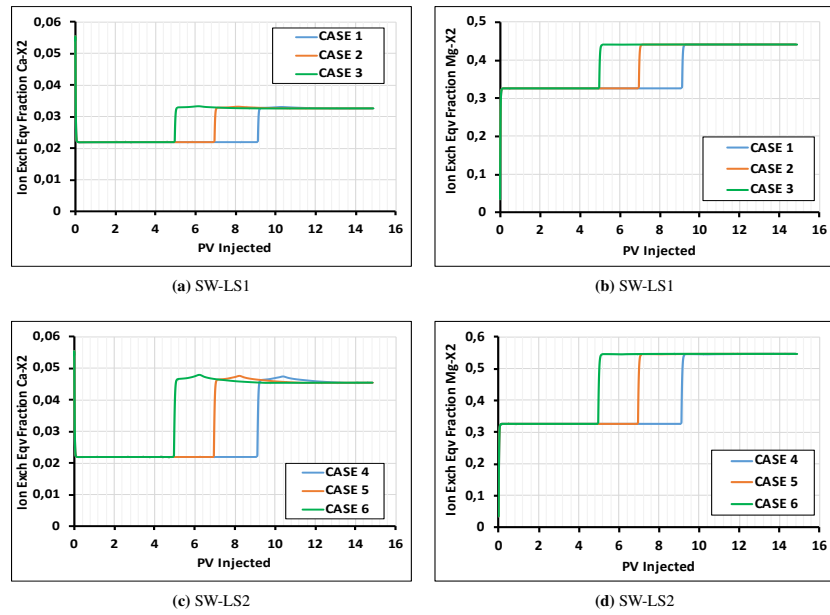
Figure 14: Ion exchange equivalent fraction of Ca^{2+} and Mg^{2+}, Block 1,1,1

is because the oil recovery is primarily a function of the relative permeability interpolation, and no changes have been made to the relative permeability interpola-tion in all three cases. However, differences can be seen in the ion exchange equivalent fractions of Mg^{2+} and Ca^{2+}, mineral behavior and pH (figs. 18 to 20). Fig-

(a) Coreflood 1

(b) Coreflood 2
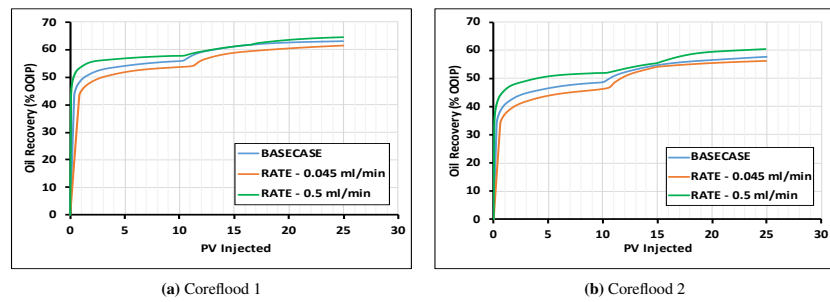
Figure 15: Oil recovery as a function of injection rate

17
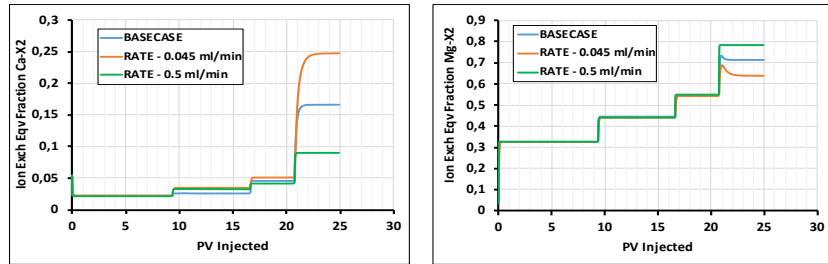
Figure 16: Ion exchange equivalent fractions of Ca^{2+} and Mg^{2+}, Block 1,1,1

(a) Coreflood 1

(b) Coreflood 2
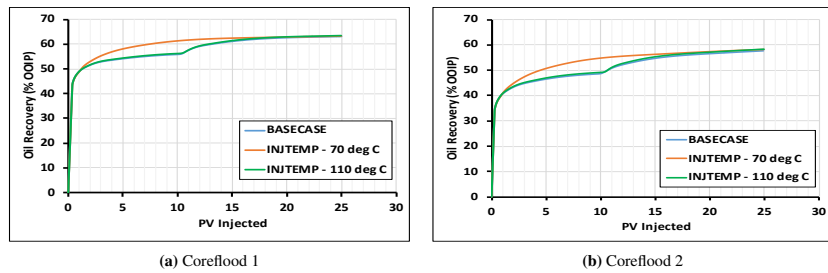
Figure 17: Oil recovery as a function of injection temperature

ure 18 shows that the injection temperature has a greater effect on the exchange of Mg^{2+} between the injected brine and the carbonate surface than on the exchange of Ca^{2+}. This is probably because Mg^{2+} is the main cation responsible for the observed low salinity effects (LSE). Figure 19 also shows that the injection temperature has a significant effect on mineral dissolution/precipitation. At low injection temperature, the changes in the moles of calcite and dolomite are very small compared to when the injection temperature is high. This is because at low temperatures, the reaction rates are small. The low reaction rates also slow down the ion exchange process, and no effect of LSWF on oil recovery is seen as shown in figs. 17a and 17b. Figure 20 shows that temperature also has a huge effect on the pH, and this is due to its effect on mineral reactions. The results are summarized in table 12.
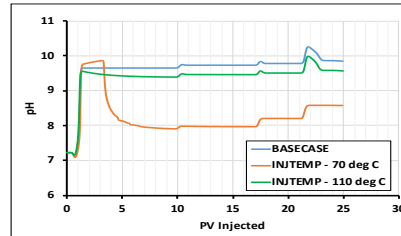
Figure 20: Effluent pH
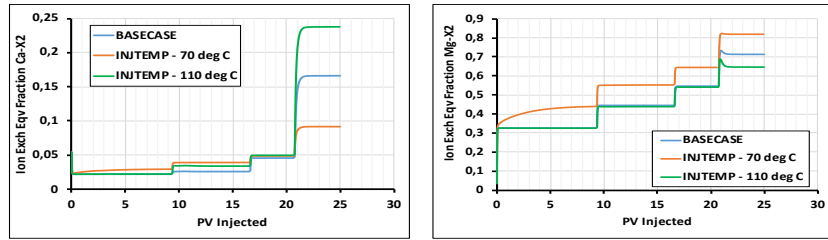
Figure 18: Ion exchange equivalent fraction of Ca^{2+} and Mg^{2+}, Block 1,1,1
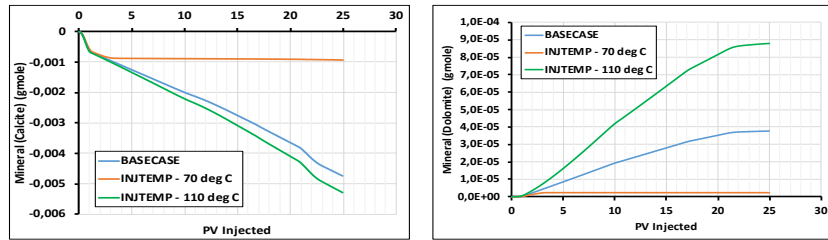
Figure 19: Changes in mineral moles of calcite and dolomite

Table 12: Oil recovery results for the three different injection temperatures

Injection Temp (°C)	Oil Recovery (% OOIP)	
	Coreflood 1	Coreflood 2
90.6 (Base Case)	63.10	57.69
70	63.24	58.21
110	63.44	58.32

7.4. Interpolation routines

Two additional mechanistic modeling methods have been used to investigate the ability of the different methods to model the same process. The two additional methods involve relative permeability interpolations that are based on the anion exchange occurring between the sulfate ion in the brine and the carboxylic ion in the oil, and the concentration of the sulfate ion in the aqueous phase. The anion exchange reaction between the injected brine and the exchanger on the carbonate rock surface is given below:

$$SO_4^{2-} + 2\,CH_3COO{-}X \longleftrightarrow 2\,CH_3COO^- + SO_4{-}X_2$$
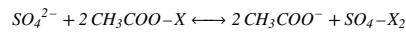
The oil recovery for the three different cases is shown in fig. 21. This figure shows that the oil recovery profile is very sensitive to the interpolant used in modeling the process. When the equivalent fraction of sulfate ion is used as the interpolant, no LSE is observed during LSWF. This is because all the anion exchange between sulfate ion and carboxylic ion occurs within the first five pore volumes of the injection process. That is, during SW injection as shown in fig. 22. When the different low salinity brines are injected, only the adsorption of divalent cations (Mg^{2+} and Ca^{2+}) is taking place. Since the equivalent fraction of SO_4^{2-} is constant during LSWF, no change in oil recovery is observed during LSWF. On the other hand, although LSE is observed when the aqueous concentration of sulfate ion is used, the required oil recovery profile that matches the experimental data is not obtained. The best match is obtained when the equivalent fraction of Mg^{2+} is used as the interpolant. The final oil recovery from the three methods are however close to each other. Table 13 provides a summary of the results.

19

(a) Coreflood 1   **(b)** Coreflood 2
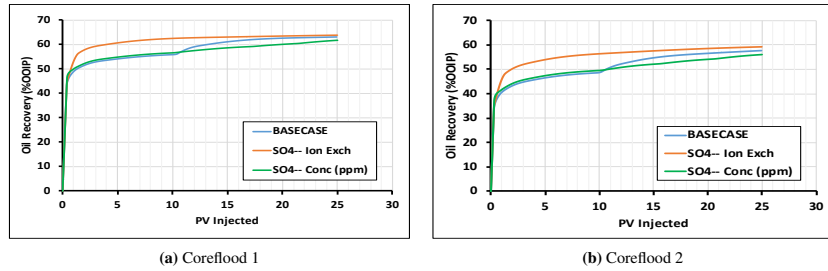
Figure 21: Oil recovery as a function of the mechanistic modeling method
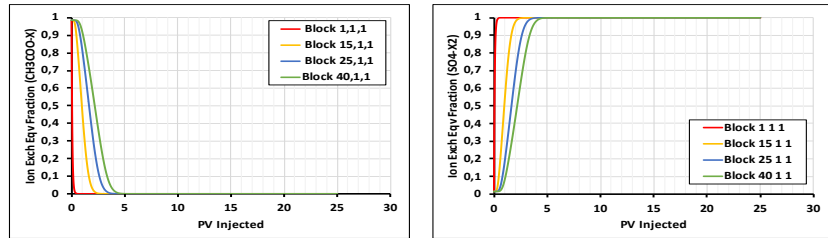
Figure 22: Ion exchange equivalent fraction of sulfate and carboxylic ions for different gridblocks

Table 13: Oil recovery results using different interpolants

Interpolant	Oil Recovery (% OOIP)	
	Coreflood 1	Coreflood 2
Base Case	63.10	57.69
Anion Exch	63.83	59.22
SO_4^{2-} Conc	61.74	56.05

8. Conclusions

This study has investigated the geochemical modeling of low salinity waterflooding. A history match of laboratory data from coreflood experiments done on heterogeneous low permeability carbonate cores has been performed using the EOS compositional simulator GEM™ by CMG. Sensitivity analysis has been done on some key parameters to investigate their effects on the results obtained. Based on the history matching and sensitivity analysis, the following conclusions have been drawn:

- GEM™ has the ability to model low salinity waterflooding based on the geochemical interactions

occurring during the process. In the modeling of LSWF, many different mechanistic methods can be used to history match laboratory data, using detailed geochemistry. The method selected should be based on the reservoir properties and the experimental workflow and results.

- Multicomponent ion exchange involving the exchange of SO_4^{2-}, CH_3COO^-, Ca^{2+} and Mg^{2+} between the injected brine and the carbonate rock surface has been identified as the main mechanism responsible for wettability alteration, and the observed increase in oil recovery during low salinity waterflooding for both coreflood simulations. Capillary pressure has a significant effect on history matching of experimental pressure drop during low salinity waterflooding, and should also be included in the modeling.

- The timing of low salinity waterflooding has a significant effect on oil recovery. The earlier the onset of low salinity waterflooding, the more the oil re-

20

covery is enhanced because the low salinity brine has more time to interact with the reservoir rock and fluids.

- Benefits from low salinity waterflooding are from a combination of both physical and chemical displacement processes, which makes the injection rate a very important parameter in the process. Temperature effects on mineral and ion exchange reactions can also be significant and should be included when modeling the process.

- Temperature, water composition and concentration, injection rate and time, rock mineralogy, and oil type all affect the improvement of oil recovery in carbonates by low salinity waterflooding.

Nomenclature

Abbreviations

LWSF	Low salinity waterflooding
EDL	Electrical Double Layer
WAG	Water Alternating Gas
MIE	Multicomponent ion exchange
CMG	Computer Modeling Group
SEM	Scanning Electron Microscope
COBR	Crude oil/brine/rock
Ca^{2+}	Calcium ion
Mg^{2+}	Magnesium ion
SO_4^{2-}	Sulfate ion
CO_2	Carbon dioxide
PDI	Potential determining ions
LSE	Low Salinity Effect
CEC	Cation Exchange Capacity
OOIP	Oil originally in place
EOR	Enhanced Oil Recovery
PV	Pore Volume
SW	Seawater
TDS	Total Dissolved Solids
Exch	Exchange
Eqv	Equivalent
Conc	Concentration

Symbols

k	Relative permeability
P_c	Capillary pressure
θ	Scaling factor
a	Activity
γ	Activity coefficient
m	Molality
Q	Activity product
K_{eq}	Equilibrium constant
v	Stoichiometry coefficient
$\mathring{a}$	Ion size
z	Valence number
I	Ionic strength
r	Reaction rate
$\hat{A}$	Reactive surface area
E_a	Activation Energy
R	Universal gas constant
T	Temperature
ϕ	Porosity
N	Number of moles
c_ϕ	Rock compressibility

804	ρ	Molar density
805	K'	Selectivity coefficient
806	ζ	Ion exchange equivalent fraction
807	V	Volume
808	p	Pressure

Subscripts/Superscripts

810	i	Component (phase)
811	aq	Aqueous
812	β	Mineral reaction
813	a	Valence number
814	o	Oil
815	w	Water
816	r	Residual
817	ir	Irreducible
818	LS	Low Salinity
819	HS	High Salinity

Acknowledgements

References

[1] Adegbite, J. O., Al-Shalabi, E. W., and Ghosh, B. (2018). Geochemical modeling of engineered water injection effect on oil recovery from carbonate cores. *Journal of Petroleum Science and Engineering*, 170:696–711.

[2] Al-Attar, H. H., Mahmoud, M. Y., Zekri, A. Y., Almehaideb, R., and Ghannam, M. (2013). Low-salinity flooding in a selected carbonate reservoir: experimental approach. *Journal of Exploration and Production Technology*, 3:139–149.

[3] Al-Shalabi, E., Sepehrnoori, K., and Delshad, M. (2013). Does the Double Layer Expansion Mechanism Contribute to the LSWI Effect on Hydrocarbon Recovery from Carbonate Rocks. In *Proceedings of the SPE Reservoir Characterization and Simulation Conference and Exhibition*, pages 1–17, Abu Dhabi, UAE. Society of Petroleum Engineers.

[4] Alameri, W., Teklu, T. W., Kazemi, H., and AlSumaiti, A. M. (2015). Low-salinity Water-alternate-surfactant in Low-permeability Carbonate Reservoirs. In *Proceedings of the 18th European Symposium on Improved Oil Recovery*, pages 1–16.

[5] Altahir, M., Yu, M., and Hussain, F. (2017). Low salinity water flooding in carbonate rocks âĂŞ dissolution effect. In *Proceedings of the 2017 International Symposium of the Society of Core Analysts*, pages 1–8, Vienna, Austria.

[6] Appelo, C. and Postma, D. (2005). *Geochemistry, Groundwater and Pollution*. A.A. Balkema Publishers, Amsterdam, the Netherlands, 2 edition.

[7] Awolayo, A. N., Sarma, H. K., and long X. Nghiem (2017). A Comprehensive Geochemical-Based Approach at Modeling and Interpreting Brine Dilution in Carbonate Reservoirs. In *SPE Reservoir Simulation Conference*, pages 1–27, Montgomery, TX, USA. Society of Petroleum Engineers.

[8] Bethke, C. M. (1996). *Geochemical Reaction Modeling: Concepts and Applications*. Oxford University Press, New York.

[9] Brooks, R. H. and Corey, A. T. (1964). Hydraulic properties of porous media. *Hydrology Papers*, pages 1–37.

[10] Computer Modelling Group Ltd. (2018). GEM : Compositional and Unconventional Simulator.

[11] Craig Jr., F. F. (1971). *The Reservoir Engineering Aspects of Waterflooding: SPE Monograph Series, Vol. 3*. American Institute of Mining, Metallurgical and Petroleum engineers, Inc, Richardson, Texas.

[12] Dang, C., Nghiem, L., Nguyen, N., Chen, Z., and Nguyen, Q. (2015). Modeling and Optimization of Low Salinity Waterflood. In *Proceedings of the SPE Reservoir Simulation Symposium*, pages 1–19, Houston, Texas, USA. Society of Petroleum Engineers.

[13] Dang, C., Nghiem, L., Nguyen, N., Chen, Z., and Nguyen, Q. (2016). Mechanistic modeling of low salinity water flooding. *Journal of Petroleum Science and Engineering*, 146:191–209.

[14] Dang, C. T. Q. (2015). *Mechanistic Modeling, Design, and Optimization of Low Salinity Waterflooding*. Doctoral thesis, University of Calgary.

[15] Delaney, J. M. and Lundeen, S. R. (1990). The Lawrence Livermore National Laboratory Thermodynamic Database. In *Lawrence Livermore National Report UCRL-21658*.

[16] Derkani, M. H., Fletcher, A. J., Abdallah, W., Sauerer, B., Anderson, J., and Zhang, Z. J. (2018). Low Salinity Waterflooding in Carbonate Reservoirs : Review of Interfacial Mechanisms. *Colloids and Interfaces*, 2:1–43.

[17] Hamouda, A. A. and Gupta, S. (2017). Enhancing oil recovery from chalk reservoirs by a low-salinity water flooding mechanism and fluid/rock interactions. *Energies*, 10:1–16.

[18] Hiorth, A., Cathles, L. M., Kolnes, J., Vikane, O., Lohne, A., Korsnes, R. I., and Madland, M. V. (2008). A chemical model for the Seawater-CO_2-Carbonate system âĂŞ Aqueous and Surface Chemistry. In *Proceedings of the 2008 International Symposium of the Society of Core Analysts*, pages 1–12, Abu Dhabi, UAE.

[19] Jahanbani G., A. and Torsaeter, O. (2018). Numerical Simulation Of Low Salinity Water Flooding: Wettability Alteration Considerations. In *Proceedings of the 16th European Conference on the Mathematics of Oil Recovery*, ECMOR XVI 2018, pages 1–15, Barcelona, Spain. EAGE.

[20] Jerauld, G. R., Lin, C. Y., Webb, K. J., and Seccombe, J. C. (2008a). Modeling Low-Salinity Waterflooding. *SPE Reservoir Evaluation & Engineering*, 11:1000–1012.

[21] Jerauld, G. R., Webb, K. J., Lin, C. Y., and Seccombe, J. C. (2008b). Modeling Low-Salinity Waterflooding. In *Proceedings of the 2006 SPE Annual Technical Conference and Exhibition*, pages 1–13, San Antonio, Texas, USA. Society of Petroleum Engineers.

[22] Kharaka, Y. K., Gunter, W. D., Aggarwal, P. K., Perkins, E. H., and DeBraal, J. D. (1989). SOLMINEQ.88: A Computer Program for Geochemical Modelling of Water-Rock Reactions. In *US Geological Survey Water-Resources Investigations Report 88-4227*.

[23] Lager, A., Webb, K. J., Black, C. J. J., Singleton, M., and Sorbie, K. S. (2006). Low Salinity Oil Recovery - An Experimental Investigation. In *Proceedings of the International Symposium of the Society of Core Analysts*, SCA2006-36, pages 1–12, Trondheim, Norway.

[24] Lager, A., Webb, K. J., Black, C. J. J., Singleton, M., and Sorbie, K. S. (2008). Low Salinity Oil Recovery - An Experimental Investigation. *Petrophysics*, 49:28–35.

[25] Nasralla, R. A., Mahani, H., van der Linde, H. A., Marcelis, F. H.,

22

Masalmeh, S. K., Sergienko, E., Brussee, N. J., Pieterse, S. G., and Basu, S. (2018). Low salinity waterflooding for a carbonate reservoir: Experimental evaluation and numerical interpretation. *Journal of Petroleum Science and Engineering*, 164:640–654.

[26] Nghiem, L., Sammon, P., Grabenstetter, J., and Ohkuma, H. (2004). Modeling CO_2 Storage in Aquifers with a Fully-Coupled Geochemical EOS Compositional Simulator. In *Proceedings of the SPE/DOE 14th Symposium on Improved Oil Recovery*, SPE 89474, pages 1–16, Tulsa, Oklahoma, U.S.A. Society of Petroleum Engineers.

[27] RezaeiDoust, A., Puntervold, T., Strand, S., and Austad, T. (2009). Smart Water as Wettability Modifier in Carbonate and Sandstone: A Discussion of Similarities/Differences in the Chemical Mechanisms. *Energy Fuels*, 23:4479–4485.

[28] Schlumberger. *Carbonate reservoirs.* https://www.slb.com/services/technical_challenges/carbonates.aspx. Accessed May 03, 2019.

[29] Shiran, B. S. and Skauge, A. (2013). Enhanced Oil Recovery (EOR) by Combined Low Salinity Water/Polymer Flooding. *Energy Fuels*, 27:1223–1235.

[30] Skjaeveland, S., Siqveland, L., Kjosavik, A., Thomas, W. H., and Virnovsky, G. (2000). Capillary Pressure Correlation for Mixed-Wet Reservoirs. *SPE Reservoir Evaluation & Engineering*, 3:60–67.

[31] Sohrabi, M., Mahzari, P., Farzaneh, S. A., Mills, J. R., Tsolis, P., and Ireland, S. (2017). Novel Insights Into Mechanisms of Oil Recovery by Use of Low-Salinity-Water Injection. *SPE Journal*, 22:407–416.

[32] Srisuriyachai, F., Panthuvichien, S., Phomsuwansiri, T., and Katekaew, W. (2016). Effects of Injection Rate of Low Salinity Brine on Oil Recovery Mechanisms and Relative Permeability Curves. In *Proceedings of the 78th EAGE Conference and Exhibition 2016*. EAGE.

[33] Sun, S. Q. and Sloan, R. (2003). Quantification of uncertainty in recovery efficiency predictions: Lessons learned from 250 mature carbonate fields. In *Proceedings of the SPE Annual Technical Conference and Exhibition*, pages 1–15. Society of Petroleum Engineers.

[34] Teklu, T. W., Alameri, W., Kazemi, H., Graves, R. M., and AlSumaiti, A. M. (2017). Low salinity water-Surfactant-CO_2 EOR. *Petroleum*, 3:309–320.

[35] Yousef, A. A., Al-Saleh, S., and Al-Jawfi, M. (2012). Improved/Enhanced Oil Recovery from Carbonate Reservoirs by Tuning Injection Water Salinity and Ionic Content. In *Proceedings of the 18th SPE Improved Oil Recovery Symposium*, pages 1–18. Society of Petroleum Engineers.

[36] Zhang, P., Tweheyo, M. T., and Austad, T. (2006). Wettability Alteration and Improved Oil Recovery in Chalk: The Effect of Calcium in the Presence of Sulfate. *Energy Fuels*, 20:2056–2062.

[37] Zhang, P., Tweheyo, M. T., and Austad, T. (2007). Wettability alteration and improved oil recovery by spontaneous imbibition of seawater into chalk: Impact of the potential determining ions Ca^{2+}, Mg^{2+}, and SO_4^{2-}. *Colloids and Surfaces A*, 301:199–208.

[38] Zhang, Y. and Morrow, N. (2006). Comparison of Secondary and Tertiary Recovery With Change in Injection Brine Composition doe Crude Oil/Sandstone Combinations. In *Proceedings of the 2006 SPE/DOE Symposium on Improved Oil Recovery*, SPE 99757, pages 1–14. Society of Petroleum Engineers.

23

Appendix C.   GEM Data Files

C.1.   Low Salinity Waterflooding

```
** 2019-03-08, 10:41:21 AM, danieegb
** 2019-03-08, 11:02:56 AM, danieegb
RESULTS SIMULATOR GEM 201710

INUNIT SI
WSRF WELL 1
WSRF GRID TIME
WRST TIME
OUTSRF GRID ADS 'Ca++' ADS 'Mg++' ADS 'Na+' ADS 'SO4--' DROP EQVFRIEX
'Ca-X2' EQVFRIEX 'Mg-X2' EQVFRIEX 'Na-X' KRW MINERAL 'Calcite' MINERAL
'Dolomite' MOLALITY 'CH3COO-' MOLALITY 'Ca++' MOLALITY 'Cl-' MOLALITY
'Mg++' MOLALITY 'Na+' MOLALITY 'NaCl' MOLALITY 'SO4--' PH PRES SG SO SW
VISO
OUTSRF RES ALL
OUTSRF WELL LAYER ALL
OUTSRF WELL BHP 'INJ' 1 1 1
            DPORMNR 1 1 1
            DPORMNR 40 1 1
            PH 1 1 1
OUTSRF *FLUX_SECTOR *ALL *RC *SUM
OUTSRF WELL DPORMNR 40 1 1
            DPORMNR 1 1 1
            RECO
            SALIN 20 1 1
            SALINWWR 'PROD'
            SOLITCUM
            TGIP
            TOIP
OUTSRF SPECIAL DPORMNR 1 1 1
            DPORMNR 40 1 1
            EQVFRIEX 'Ca-X2' 1 1 1
            EQVFRIEX 'Ca-X2' 15 1 1
            EQVFRIEX 'Ca-X2' 25 1 1
            EQVFRIEX 'Ca-X2' 40 1 1
            PH 1 1 1
            PRES 1 1 1
            PRES 40 1 1
OUTSRF SPECIAL EQVFRIEX 'Mg-X2' 1 1 1
            EQVFRIEX 'Mg-X2' 15 1 1
            EQVFRIEX 'Mg-X2' 25 1 1
            EQVFRIEX 'Mg-X2' 40 1 1
            PH 15 1 1
            PH 25 1 1
            PH 40 1 1
OUTSRF SPECIAL MOLALITY 'Ca++' 40 1 1
            MOLALITY 'Cl-' 40 1 1
            MOLALITY 'Mg++' 40 1 1
            MOLALITY 'Na+' 40 1 1
            MOLALITY 'SO4--' 40 1 1




WPRN GRID 0
OUTPRN GRID NONE
OUTPRN RES NONE
**  Distance units: m
```

```
RESULTS XOFFSET          0.0000
RESULTS YOFFSET          0.0000
RESULTS ROTATION         0.0000  **  (DEGREES)
RESULTS AXES-DIRECTIONS 1.0 -1.0 1.0
**
*****************************************************************************
**
** Definition of fundamental cartesian grid
**
*****************************************************************************
**
GRID VARI 40 1 1


KDIR DOWN
DI IVAR
 10*0.00417322  10*0.0082677  10*0.0046228  10*0.00481584


DJ JVAR
 0.03195
DK ALL
 40*0.03195


DTOP
 40*0.01

PERMI CON        3.38
*MOD
  11:20 1:1 1:1   = 2.25
  21:30 1:1 1:1   = 1.16
  31:40 1:1 1:1   = 0.76
**  0 = null block, 1 = active block
NULL CON           1
POR CON      0.2694
*MOD
  11:20 1:1 1:1   = 0.246
  21:30 1:1 1:1   = 0.207
  31:40 1:1 1:1   = 0.1454
PERMK  EQUALSI
**  0 = pinched block, 1 = active block
PINCHOUTARRAY CON          1
CPOR 3E-6
PERMJ  EQUALSI

** ================== COMPONENT PROPERTIES ===================**
MODEL PR
NC 3 3
COMPNAME 'CO2' 'OIL' 'CO2T'
HCFLAG
0 1 0
TRES 90.6
PVC3 1.2
MW
44.01 233.1 44.01
AC
0.225 0.758769 0.225
```

```
PCRIT
72.8 17.8862 72.8
VCRIT
0.094 0.800354 0.094
TCRIT
304.2 771.885 304.2
PCHOR
78 621.975 78
SG
0.818 0.865 0.818
TB
-78.45 588.697 -78.45
HEATING_VALUES
0 2651.63 0
BIN
0
0 0

VISW 0.535
SOLUBILITY HENRY
TRACE-COMP 3
EQUIL-REACT-RATE ON
CHEM-EQUIL-SET ON
YAQU-RATE-CUTOFF
1.0e-8 1.0 1.0
DER-CHEM-EQUIL NUMERICAL
DER-REACT-RATE NUMERICAL
ACTIVITY-MODEL B-DOT
SALINITY-CALC ON
RF_EXPONENT 3.0
RFCALC POWER
HENRY-MOD1-CO2
BIN-TDEP-CO2
GEOCHEM_V2
NC-AQUEOUS 14
COMPNAME-AQUEOUS
 'H+' 'CH3COO-' 'Ca++' 'SO4--' 'Mg++' 'Cl-' 'Na+' 'HCO3-' 'OH-'
'CaCH3CO*' 'CaSO4' 'MgSO4' 'HSO4-' 'NaCl'
MW-AQUEOUS
 1.0079 59.0445 40.08 96.0576 24.305 35.453 22.9898 61.0171 17.0073
99.1245 136.138 120.363 97.0655 58.4428
ION-SIZE-AQUEOUS
 9 4.5 6 4 8 3 4 4.5 3.5 4 4 4 4 4
CHARGE-AQUEOUS
 1 -1 2 -2 2 -1 1 -1 -1 1 0 0 -1 0
NC-MINERAL 2
COMPNAME-MINERAL
 'Calcite' 'Dolomite'
MW-MINERAL
 100.089 184.403
MASSDENSITY-MINERAL
 2709.95 2864.96
REACTION-CHEM 'CO2' + 'H2O' = 'H+' + 'HCO3-'
LOG-CHEM-EQUIL-COEFS
 -6.54924 0.00900174 -0.000102115 2.76188e-007 -3.56142e-010
REACTION-CHEM 'H+' + 'OH-' = 'H2O'
LOG-CHEM-EQUIL-COEFS
 14.9282 -0.0418762 0.000197367 -5.54951e-007 7.58109e-010
```

```
REACTION-CHEM 'CaCH3CO*' = 'CH3COO-' + 'Ca++'
LOG-CHEM-EQUIL-COEFS
 1.40575 -0.00818671 -5.26125e-005 2.38632e-007 -4.34722e-010
REACTION-CHEM 'CaSO4' = 'Ca++' + 'SO4--'
LOG-CHEM-EQUIL-COEFS
 -2.2673 -0.000966685 -7.21167e-005 4.52585e-007 -1.14535e-009
REACTION-CHEM 'MgSO4' = 'SO4--' + 'Mg++'
LOG-CHEM-EQUIL-COEFS
 -2.17055 -0.00148402 -4.6643e-005 2.61102e-007 -6.82724e-010
REACTION-CHEM 'HSO4-' = 'H+' + 'SO4--'
LOG-CHEM-EQUIL-COEFS
 -1.71758 -0.00854912 -9.98314e-005 4.04202e-007 -7.6584e-010
REACTION-CHEM 'NaCl' = 'Cl-' + 'Na+'
LOG-CHEM-EQUIL-COEFS
 1.8547 -0.0109083 3.21311e-005 -1.14258e-007 1.5583e-010
REACTION-RATE-TST 'H+' + 'Calcite' = 'Ca++' + 'HCO3-'
LOG-CHEM-EQUIL-COEFS
 2.06889 -0.0142668 -6.06096e-006 1.45921e-007 -4.18928e-010
REACTIVE-SURFACE-AREA 100
ACTIVATION-ENERGY 41870
LOG-TST-RATE-CONSTANT -6.8
REF-TEMP-RATE-CONST 25
REACTION-RATE-TST 2 'H+' + 'Dolomite' = 'Ca++' + 'Mg++' + 2 'HCO3-'
LOG-CHEM-EQUIL-COEFS
 3.39441 -0.0355985 1.32613e-005 2.41057e-007 -8.14935e-010
REACTIVE-SURFACE-AREA 100
ACTIVATION-ENERGY 41870
LOG-TST-RATE-CONSTANT -10.8
REF-TEMP-RATE-CONST 25
NC-IEX 4
COMPNAME-IEX
 'H-X' 'Na-X' 'Ca-X2' 'Mg-X2'
AQIONS-IEX
 'H+' 'Na+' 'Ca++' 'Mg++'
REACTION-IEX 'H-X' + 'Na+' = 'Na-X' + 'H+'
**Selectivity cofficents for ion-exchanger 1
SCOEFF-IEX
25 0.01
90 0.4
REACTION-IEX 'Na+' + 0.5 'Ca-X2' = 0.5 'Ca++' + 'Na-X'
**Selectivity cofficents for ion-exchanger 2
SCOEFF-IEX
25 0.01
90 0.67
REACTION-IEX 'Na+' + 0.5 'Mg-X2' = 0.5 'Mg++' + 'Na-X'
**Selectivity cofficents for ion-exchanger 3
SCOEFF-IEX
25 0.01
90 0.58
COMPNAME-SAL 'Na+'

** ===================== ROCK-FLUID DATA=====================**
ROCKFLUID
RPT 1
INTCOMP EQVFRIEX 'Mg-X2'
KRINTRP 1
INTCOMP_VAL 0.33
**         Sw          krw          krow          Pcow
```

```
SWT

      0.15              0         0.092          -0.133
     0.1825   2.86925e-005     0.0772877         -0.151
      0.215   0.000282597      0.0641519         -0.173
     0.2475    0.00107713      0.0525183         -0.201
       0.28    0.00278334       0.042311         -0.236
     0.3125    0.00581258      0.0334522         -0.281
      0.345     0.0106088      0.0258621         -0.340
     0.3775     0.0176438      0.0194589         -0.420
       0.41     0.0274135      0.0141582         -0.531
     0.4425      0.040436     0.00987253         -0.694
      0.475      0.057249     0.00651137         -0.944
     0.5075     0.0784086        0.00398         -1.360
       0.54      0.104488     0.00217884         -2.125
     0.5725      0.136076     0.00100205         -3.778
      0.605      0.173776    0.000335309         -8.500
     0.6375      0.218207    5.16017e-005        -34.00
       0.67          0.27              0         -60.00
**         Sl           krg           krog
SLT

     0.15001     0.999976              0
    0.203134     0.878886     0.000359367
    0.256258     0.765607      0.00143747
    0.309381     0.660141       0.0032343
    0.362505     0.562487      0.00574986
    0.415629     0.472645      0.00898416
    0.468753     0.390616       0.0129372
    0.521876     0.316399        0.017609
       0.575     0.249994       0.0229995
    0.628124     0.191402       0.0291087
    0.681248     0.140622       0.0359367
    0.734371     0.097654       0.0434834
    0.787495    0.0624985       0.0517488
    0.840619    0.0351554       0.0607329
    0.893743    0.0156246       0.0704358
    0.946866   0.00390616       0.0808575
          1            0          0.092
KRINTRP 2
INTCOMP_VAL 0.43
**         Sw           krw           krow          Pcow
SWT

      0.15              0         0.092           70.00
     0.1825   2.86925e-005     0.0772877          54.57
      0.215   0.000282597      0.0641519          13.51
     0.2475    0.00107713      0.0525183           5.88
       0.28    0.00278334       0.042311           3.18
     0.3125    0.00581258      0.0334522           1.91
      0.345     0.0106088      0.0258621           1.18
     0.3775     0.0176438      0.0194589           0.70
       0.41     0.0274135      0.0141582           0.32
     0.4425      0.040436     0.00987253          -0.02
      0.475      0.057249     0.00651137          -0.40
     0.5075     0.0784086        0.00398          -0.91
       0.54      0.104488     0.00217884          -1.74
     0.5725      0.136076     0.00100205          -3.45
```

```
        0.605     0.173776   0.000335309              -8.22
        0.6375    0.218207   5.16017e-005             -33.76
         0.67        0.27             0               -70.00
**        Sl         krg          krog
SLT

     0.15001     0.999976             0
    0.203134     0.878886   0.000359367
    0.256258     0.765607    0.00143747
    0.309381     0.660141     0.0032343
    0.362505     0.562487    0.00574986
    0.415629     0.472645    0.00898416
    0.468753     0.390616     0.0129372
    0.521876     0.316399      0.017609
       0.575     0.249994     0.0229995
    0.628124     0.191402     0.0291087
    0.681248     0.140622     0.0359367
    0.734371     0.097654     0.0434834
    0.787495    0.0624985     0.0517488
    0.840619    0.0351554     0.0607329
    0.893743    0.0156246     0.0704358
    0.946866   0.00390616     0.0808575
           1            0         0.092
TSOIRW 0.274
TSORW 0.274
TKROCW 0.14
TKRWIRO 0.324
INTERP_SCAL ON
CEC-IEX CON            80
ROCKDEN CON         2710

** =================== INITIAL CONDITIONS =====================**
INITIAL

** RPT OILWET
USER_INPUT

MOLALITY-AQUEOUS-PRIMARY
6.76775e-008 0.171075 0.153587 0.00906036 0.0506576 1.96739 1.45835

VOLUMEFRACTION-MINERAL
0.75 0.05

PRES CON        1200
SW CON          0.18
ZGLOBALC 'OIL' CON        0.9885
ZGLOBALC 'CO2T' CON        0.001
ZGLOBALC 'CO2' CON        0.0105
SWINIT CON         0.18

** =================== NUMERICAL CONTROL ====================**
NUMERICAL
DTMAX 0.0001
DTMIN 1e-5
NEWTONCYC 10

** ================ WELL AND RECURRENT DATA===================**
RUN
```

```
TIME 0

**
DTWELL 0.0001

**----------------- Seawater Injection ---------------------**
**
WELL  'INJ'
INJECTOR 'INJ'
INCOMP  AQUEOUS  0.0  0.0  0.0  8.84710793e-006  1.69363785e-013
0.0172659321  0.0428458478  0.142809548  0.87567753  0.572295434  0.0
0.0  0.0  0.0  0.0  0.0  0.0
OPERATE  MAX  STW  0.000144  CONT
**          rad  geofac  wfrac  skin
GEOMETRY  K  0.0025  0.37  1.0  0.0
     PERF     GEOA  'INJ'
** UBA             ff           Status  Connection
    1 1 1          1.0  OPEN    FLOW-FROM  'SURFACE'
**
WELL  'PROD'
PRODUCER 'PROD'
OPERATE  MIN  BHP  1200.0  CONT
**          rad  geofac  wfrac  skin
GEOMETRY  K  0.0025  0.37  1.0  0.0
     PERF     GEOA  'PROD'
** UBA             ff           Status  Connection
   40 1 1          1.0  OPEN    FLOW-TO  'SURFACE'

TIME 3.1215

**---------------- LS1 Injection ---------------------**
**
WELL  'INJ'
INJECTOR 'INJ'
INCOMP  AQUEOUS  0.0  0.0  0.0  1.04177003e-005  1.69363785e-013
0.00663447412  0.0213833199  0.0712810664  0.431243615  0.284367942  0.0
0.0  0.0  0.0  0.0  0.0  0.0
OPERATE  MAX  STW  0.000144  CONT
OPERATE  MAX  BHP  1810.0  CONT

TIME 5.54167

**-------------------- LS2 Injection ---------------------**
**
WELL  'INJ'
INJECTOR 'INJ'
INCOMP  AQUEOUS  0.0  0.0  0.0  1.72636177e-005  1.69363785e-013
0.0043164652  0.0106806907  0.0356149208  0.213985861  0.141720717  0.0
0.0  0.0  0.0  0.0  0.0  0.0
OPERATE  MAX  STW  0.000144  CONT

TIME 6.91667
**-------------------- LS3 Injection ---------------------**
**
WELL  'INJ'
INJECTOR 'INJ'
```

```
INCOMP  AQUEOUS  0.0  0.0  0.0  3.52217494e-005  1.69363785e-013
0.000342320066  0.000855078056  0.00284652484  0.0169944092  0.0113049061
0.0  0.0  0.0  0.0  0.0  0.0  0.0
OPERATE  MAX  STW  0.000144  CONT

TIME 8.33334


STOP
```

C.2.   Surfactant Flooding

```
** 2019-04-12, 12:05:57 PM, danieegb
** 2019-04-12, 12:43:40 PM, danieegb
RESULTS SIMULATOR GEM 201710


INUNIT SI
WSRF WELL 1
WSRF GRID TIME
OUTSRF GRID ADS 'Ca++' ADS 'Mg++' ADS 'Na+' ADS 'SO4--' DROP EQVFRIEX
'Ca-X2' EQVFRIEX 'Mg-X2' EQVFRIEX 'Na-X' KRW MINERAL 'Calcite' MINERAL
'Dolomite' MOLALITY 'CH3COO-' MOLALITY 'Ca++' MOLALITY 'Cl-' MOLALITY
'Mg++' MOLALITY 'Na+' MOLALITY 'NaCl' MOLALITY 'SO4--' PH PRES SG SO SW
VISO
OUTSRF RES ALL
OUTSRF WELL LAYER ALL DOWNHOLE
OUTSRF *FLUX_SECTOR *ALL *RC *SUM
OUTSRF SPECIAL DPORMNR 1 1 1
           DPORMNR 1 1 1
           EQVFRIEX 'Ca-X2' 1 1 1
           EQVFRIEX 'Ca-X2' 10 1 1
           EQVFRIEX 'Ca-X2' 20 1 1
           EQVFRIEX 'Ca-X2' 30 1 1
           PH 1 1 1
           PRES 1 1 1
OUTSRF SPECIAL EQVFRIEX 'Mg-X2' 1 1 1
           EQVFRIEX 'Mg-X2' 10 1 1
           EQVFRIEX 'Mg-X2' 20 1 1
           EQVFRIEX 'Mg-X2' 30 1 1
           PH 30 1 1
           PRES 30 1 1

OUTSRF SPECIAL MOLALITY 'Ca++' 30 1 1
           MOLALITY 'Mg++' 30 1 1
           MOLALITY 'SO4--' 30 1 1
           MOLALITY 'Cl-' 30 1 1
           MOLALITY 'Na+' 30 1 1

OUTSRF SPECIAL CAPNOW 1 1 1
           CAPNOW 10 1 1
           CAPNOW 20 1 1
           CAPNOW 30 1 1
           SIGMAOW 1 1 1
           SIGMAOW 10 1 1
           SIGMAOW 20 1 1
           SIGMAOW 30 1 1

OUTSRF SPECIAL ADS 'Surfact' 1 1 1
             ADS 'Surfact' 10 1 1
           ADS 'Surfact' 20 1 1
           ADS 'Surfact' 30 1 1
           MOLALITY 'Surfact' 30 1 1



WPRN GRID 0
OUTPRN GRID NONE
OUTPRN RES NONE
```

```
**  Distance units: m
RESULTS XOFFSET           0.0000
RESULTS YOFFSET           0.0000
RESULTS ROTATION          0.0000  **  (DEGREES)
RESULTS AXES-DIRECTIONS 1.0 -1.0 1.0
**
**************************************************************************
**
** Definition of fundamental cartesian grid
**
**************************************************************************
**
GRID VARI 30 1 1
KDIR DOWN
DI IVAR
 10*0.004953 10*0.0045974 10*0.0038354
DJ JVAR
 0.03355
DK ALL
 30*0.03355
DTOP
 30*0.01
PERMI CON        3.38
*MOD
  11:20 1:1 1:1   = 1.81
  21:30 1:1 1:1   = 0.696
**  0 = null block, 1 = active block
NULL CON          1
POR CON        0.2375
*MOD
  11:20 1:1 1:1   = 0.2271
  21:30 1:1 1:1   = 0.1736
PERMK  EQUALSI
**  0 = pinched block, 1 = active block
PINCHOUTARRAY CON           1
PRPOR 1200
CPOR 3E-6
PERMJ  EQUALSI

** ================== COMPONENT PROPERTIES ==================**
MODEL PR
NC 3 3
COMPNAME 'OIL' 'CO2' 'CO2T'
HCFLAG
1 1 1
TRES 90.6
PVC3 1.2
MW
233.107 44.01 44.01
AC
0.758782 0.225 0.225
PCRIT
17.8852 72.8 72.8
VCRIT
0.800402 0.094 0.094
TCRIT
771.892 304.2 304.2
PCHOR
```

```
621.991 78 78
SG
0.865 0.818 0.818
TB
588.706 -78.45 -78.45
OMEGA
0.457236 0.0 0
OMEGB
0.0777961 0.0 0
VSHIFT
0.0801576 0 0
HEATING_VALUES
2651.71 0 0
SOLUBILITY HENRY
TRACE-COMP 3
EQUIL-REACT-RATE ON
CHEM-EQUIL-SET ON
YAQU-RATE-CUTOFF
1.0 1.0e-8 1.0
DER-CHEM-EQUIL ANALYTICAL
DER-REACT-RATE ANALYTICAL
ACTIVITY-MODEL B-DOT
SALINITY-CALC ON
RF_EXPONENT 3.0
RFCALC POWER
HENRY-MOD1-CO2
BIN-TDEP-CO2
GEOCHEM_V2
NC-AQUEOUS 16
COMPNAME-SURFACTANT 'Surfact'
COMPNAME-AQUEOUS
 'Surfact' 'H+' 'Ca++' 'CH3COO-' 'Mg++' 'SO4--' 'Cl-' 'Na+' 'CaHCO3+'
'OH-' 'CaCH3CO*' 'MgSO4' 'CaSO4' 'HSO4-' 'HCO3-' 'NaCl'
MW-AQUEOUS
 427 1.0079 40.08 59.0445 24.305 96.0576 35.453 22.9898 101.097 17.0073
99.1245 120.363 136.138 97.0655 61.0171 58.4428
ION-SIZE-AQUEOUS
 4 9 6 4.5 8 4 3 4 5.2 3.5 4 4 4 4 4.5 4
CHARGE-AQUEOUS
 0 1 2 -1 2 -2 -1 1 1 -1 1 0 0 -1 -1 0
NC-MINERAL 2
COMPNAME-MINERAL
 'Calcite' 'Dolomite'
MW-MINERAL
 100.089 184.403
MASSDENSITY-MINERAL
 2709.95 2864.96
REACTION-CHEM 'CaHCO3+' = 'Ca++' + 'HCO3-'
LOG-CHEM-EQUIL-COEFS
 -1.18729 0.00164938 -0.000118857 8.57886e-007 -2.04302e-009
REACTION-CHEM 'H+' + 'OH-' = 'H2O'
LOG-CHEM-EQUIL-COEFS
 14.9282 -0.0418762 0.000197367 -5.54951e-007 7.58109e-010
REACTION-CHEM 'CaCH3CO*' = 'Ca++' + 'CH3COO-'
LOG-CHEM-EQUIL-COEFS
 1.40575 -0.00818671 -5.26125e-005 2.38632e-007 -4.34722e-010
REACTION-CHEM 'MgSO4' = 'Mg++' + 'SO4--'
LOG-CHEM-EQUIL-COEFS
```

```
 -2.17055 -0.00148402 -4.6643e-005 2.61102e-007 -6.82724e-010
REACTION-CHEM 'CaSO4' = 'Ca++' + 'SO4--'
LOG-CHEM-EQUIL-COEFS
 -2.2673 -0.000966685 -7.21167e-005 4.52585e-007 -1.14535e-009
REACTION-CHEM 'HSO4-' = 'H+' + 'SO4--'
LOG-CHEM-EQUIL-COEFS
 -1.71758 -0.00854912 -9.98314e-005 4.04202e-007 -7.6584e-010
REACTION-CHEM 'CO2' + 'H2O' = 'H+' + 'HCO3-'
LOG-CHEM-EQUIL-COEFS
 -6.54924 0.00900174 -0.000102115 2.76188e-007 -3.56142e-010
REACTION-CHEM 'NaCl' = 'Cl-' + 'Na+'
LOG-CHEM-EQUIL-COEFS
 1.8547 -0.0109083 3.21311e-005 -1.14258e-007 1.5583e-010
REACTION-RATE-TST 'H+' + 'Calcite' = 'Ca++' + 'HCO3-'
LOG-CHEM-EQUIL-COEFS
 2.06889 -0.0142668 -6.06096e-006 1.45921e-007 -4.18928e-010
REACTIVE-SURFACE-AREA 100
ACTIVATION-ENERGY 41870
LOG-TST-RATE-CONSTANT -6.8
REF-TEMP-RATE-CONST 25
REACTION-RATE-TST 2 'H+' + 'Dolomite' = 'Ca++' + 'Mg++' + 2 'HCO3-'
LOG-CHEM-EQUIL-COEFS
 3.39441 -0.0355985 1.32613e-005 2.41057e-007 -8.14935e-010
REACTIVE-SURFACE-AREA 100
ACTIVATION-ENERGY 41870
LOG-TST-RATE-CONSTANT -10.8
REF-TEMP-RATE-CONST 25
NC-IEX 3
COMPNAME-IEX
 'Na-X' 'Ca-X2' 'Mg-X2'
AQIONS-IEX
'Na+' 'Ca++' 'Mg++'
REACTION-IEX 'Na+' + 0.5 'Ca-X2' = 0.5 'Ca++' + 'Na-X'
**Selectivity cofficents for ion-exchanger 2
SCOEFF-IEX
25 0.01
90 0.67
REACTION-IEX 'Na+' + 0.5 'Mg-X2' = 0.5 'Mg++' + 'Na-X'
**Selectivity cofficents for ion-exchanger 3
SCOEFF-IEX
25 0.01
90 0.58
COMPNAME-SAL 'Na+'

** ===================== ROCK-FLUID DATA=====================**
ROCKFLUID
RPT 1
INTCOMP CAPNOW 'Surfact'
IFTTABLE
**  Composition of component/phase  Interfacial tension
                           1e-007                  16.62
                  4.224186435e-005                  4.54
                     0.00021120932                   0.5

INTLOG
KRINTRP 1
INTCOMP_VAL -5
**        Sw         krw         krow         Pc
```

```
SWT

        0.15                0             0.1           -0.165
    0.182812    9.15527e-006       0.0777478          -0.188
    0.215625      0.00010358       0.0594061          -0.217
    0.248438      0.00042815        0.044495          -0.250
     0.28125      0.00117188       0.0325641          -0.293
    0.314063      0.00255898       0.0231934          -0.350
    0.346875      0.00484396       0.0159931          -0.423
    0.379688      0.00830834       0.0106042          -0.522
      0.4125       0.0132583      0.00669858          -0.661
    0.445313       0.0200226      0.00397937          -0.864
    0.478125       0.0289515      0.00218133          -1.176
    0.510938       0.0404153      0.00107131          -1.693
     0.54375       0.0548032      0.00044871          -2.645
    0.576562       0.0725225     0.000146118          -4.702
    0.609375       0.0939982     3.00572e-005         -10.580
    0.642188        0.119671     2.01341e-006         -42.32
       0.675            0.15               0           -80
**       Sl          krg            krog
SLT

     0.15001        0.999976               0
    0.203134        0.878886     0.000390616
    0.256258        0.765607      0.00156246
    0.309381        0.660141      0.00351554
    0.362505        0.562487      0.00624985
    0.415629        0.472645       0.0097654
    0.468753        0.390616       0.0140622
    0.521876        0.316399       0.0191402
       0.575        0.249994       0.0249994
    0.628124        0.191402       0.0316399
    0.681248        0.140622       0.0390616
    0.734371        0.097654       0.0472645
    0.787495       0.0624985       0.0562487
    0.840619       0.0351554       0.0660141
    0.893743       0.0156246       0.0765607
    0.946866      0.00390616       0.0878886
           1               0             0.1


KRINTRP 2
INTCOMP_VAL -0.5
**       Sw          krw      krow
SWT

        0.15             0             0.1
       0.999          0.15               0
           1          0.15               0
**       Sl          krg            krog
SLT

     0.15001        0.999976               0
    0.203134        0.878886     0.000390616
    0.256258        0.765607      0.00156246
    0.309381        0.660141      0.00351554
    0.362505        0.562487      0.00624985
    0.415629        0.472645       0.0097654
    0.468753        0.390616       0.0140622
```

119

```
    0.521876    0.316399    0.0191402
       0.575    0.249994    0.0249994
    0.628124    0.191402    0.0316399
    0.681248    0.140622    0.0390616
    0.734371    0.097654    0.0472645
    0.787495   0.0624985    0.0562487
    0.840619   0.0351554    0.0660141
    0.893743   0.0156246    0.0765607
    0.946866  0.00390616    0.0878886
           1           0         0.1


ADSORBTMAXA 'Surfact' 0.0067623

ADSTABA 'Surfact'
**     Mole Fraction       Adsorption
                 0                  0
          0.00021120932   0.003220140515


INTERP_SCAL ON

CEC-IEX CON            80
ROCKDEN CON         2710

** =================== INITIAL CONDITIONS =====================**
INITIAL
USER_INPUT

MOLALITY-AQUEOUS-PRIMARY
0 6.76775e-008 0.153587 0.171075 0.0506576 0.00906036 1.96739 1.45835

VOLUMEFRACTION-MINERAL
0.95 0.05
PRES CON          1200
SW CON            0.2
ZGLOBALC 'OIL' CON       0.98849
ZGLOBALC 'CO2T' CON          0.001
ZGLOBALC 'CO2' CON         0.0105
SWINIT CON          0.2

** =================== NUMERICAL CONTROL ====================**
NUMERICAL
MAXSTEPS 1000000
DTMAX 0.0001
DTMIN 0.00001

** =============== WELL AND RECURRENT DATA===================**
RUN
TIME 0
**
DTWELL  0.001
**----------------- Seawater Injection --------------------**
**
WELL  'INJ'
INJECTOR 'INJ'
```

```
INCOMP  AQUEOUS  0.0  0.0  0.0 0.0 8.84710793e-006  0.0172659321
1.69363785e-013  0.142809548  0.0428458478  0.87567753  0.572295434  0.0
0.0  0.0  0.0  0.0  0.0  0.0  0.0
OPERATE  MAX  STW  0.000144  CONT

**          rad  geofac  wfrac  skin
GEOMETRY  K  0.001  0.37  1.0  0.0
      PERF      GEOA  'INJ'
** UBA            ff           Status  Connection
    1 1 1          1.0  OPEN    FLOW-FROM  'SURFACE'

**
WELL  'PROD'
PRODUCER 'PROD'
OPERATE  MIN  BHP  1200.0  CONT
**          rad  geofac  wfrac  skin
GEOMETRY  K  0.001  0.37  1.0  0.0
      PERF      GEOA  'PROD'
** UBA            ff           Status  Connection
    30 1 1         1.0  OPEN    FLOW-TO  'SURFACE'


TIME 2.162500

**---------------- Surfactant Injection ---------------------**

WELL  'INJ'
INJECTOR 'INJ'
INCOMP  AQUEOUS  0.0  0.0  0.0  0.0117684441  1.75764972e-005
0.00439400792  1.72441579e-013  0.0362230188  0.0108629632  0.216243049
0.143826336  0.0  0.0  0.0  0.0  0.0  0.0
OPERATE  MAX  STW  0.000144  CONT

TIME 4.52

STOP
```

Daniel Isong Otu Egbe

Low Salinity Waterflooding, Surfactant Flooding, Heterogeneous Low-Permeability Carbonate Cores

◻ NTNU
Norwegian University of
Science and Technology